Stefano Gazzotti

Polylactic acid: exploring its limits and overcoming its boundaries

Doctorate course in **Industrial Chemistry**

XXXI Cycle – A.Y. 2017/2018

Tutor: Dr. Alessandra Silvani

Coordinator: Prof. Maddalena Pizzotti

Table of contents

Preface

In a world of continuous technological growth, the discovery of plastic materials was warmly welcomed. Indeed, they opened new possibilities and revolutionized industrial manufacture of everyday life goods.

The almost incontrollable growth of polymeric materials industrial production, however, brought along the problem of disposal of end-life plastic objects. The increasing necessity of facing the worrying plastic pollution phenomenon, pushed researchers to find environmentally friendly polymers, in order to replace the commonly-used oil-derived ones. Among all biopolymers, polylactic acid (PLA) was found to be one of the most attractive. In particular, PLA monomer, i.e. lactic acid, can be extracted from natural sources and PLA itself is fully biodegradable to unharmful byproducts. Polylactic acid is also characterized by good processability, but its poor toughness and thermal stability are strong hurdles for its wide industrial applicability.

For this reason, PLA-related research is usually aimed at improving its lacking properties, while preserving its good features. The PhD thesis here presented fits in this field. In particular, two strategies were studied, namely the preparation of bionanocomposites and the use of alternative synthetic methodologies.

From one side, the use of different cellulose-based nanofillers was investigated and resulted in the production of fully biodegradable and biocompatible nanocomposites with improved properties over standard PLA.

On the other hand, O-carboxyanhydrides (OCAs) and 1,3-dioxolane-4-ones (DOX) were studied as alternative monomers for the synthesis of highly functionalized polyester-based materials with tailored properties.

1. General introduction

1.1 Polylactic acid: history and general overview.

Polylactic Acid (PLA) or polylactide is an aliphatic polyester, biobased and biodegradable. The first synthesis of high molecular weight PLA was reported in 1932 by Carothers et al.[1] His work originated from an even older report by Bischoff and Walden who, for the first time ever, attempted the polymerization of lactide and glycolide in 1893. First examples of low molecular weight PLA come from 1845 instead, through polycondensation of lactic acid. Carothers' process was patented in 1954 by DuPont, but initially the focus was only on medical grade applications, due to very high production costs. For this reason, interest around PLA slowly grew during the second half of 1900. The first paper focused on its potential use in surgical implants was published in 1966, by Kulkarni et al.[2] PLA was described as non-toxic, non-tissue reactive, biodegradable and its degradation products to be unharmful *in vivo*. In the following decades, the number of papers containing the keywords "polylactic acid" slowly increased, as shown in **Figure 1**. The great breakthrough in PLA-related research was registered during the 1990-2000 decade. This observation, however, shouldn't be surprising.

In 1997 the newly-born *Cargill Dow Polymers* (that would later become *Natureworks LLC*) started the mass production of polylactic acid, giving a new industrial appeal to this material.

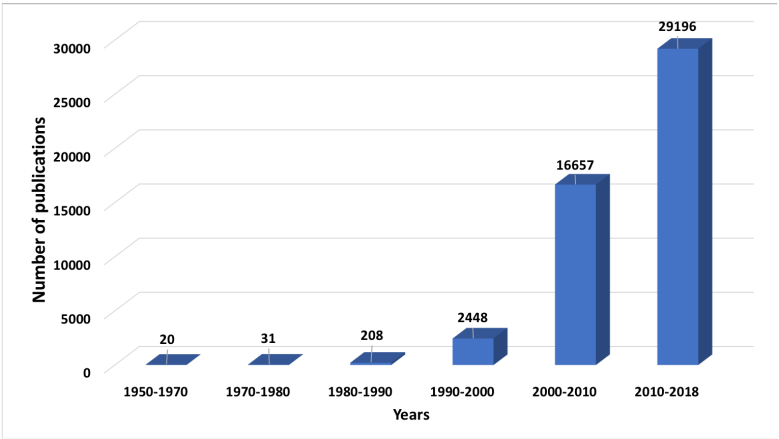

Figure 1: yearly increase of papers with the "polylactic acid" keywords.

From then on, the studies concerning PLA became more and more significant from year to year. The great interest around polylactide gradually widened its field of applicability. Alongside the increasingly advanced medical applications,[3] its use in packaging industry acquired more and more importance.[4, 5] This change of direction was driven not only by the reduction in PLA production costs, but also by an increasing concern regarding plastic pollution.[6] Indeed, since the large-scale production of plastics started (around 1950, after World War II) their use in everyday life commodities became usual. This brought to a massive increase in plastic market: 335 million tons were produced in 2015 and a 2-fold and 4-fold increase is expected over the next 20 years and by 2050 respectively.[7, 8] The main drawback of this great increase of widespread use of plastics is that the biggest part of monomers used comes from fossil hydrocarbons and none of the commonly used plastics are biodegradable. This means that end-life plastic goods tend to accumulate and therefore generate an almost permanent contamination of the environment. It was estimated that nowadays, only the 30% of the total of plastics ever produced is in use, while the 60% has generated waste. Just the 10% was recycled, as shown in **Figure 2**.[8] This quite alarming scenery generated the urge to find more and more green alternatives to replace oil-derived, non-biodegradable plastics. Here's where PLA is shining thanks to a winning combination of good properties and green nature. The great research around polylactic acid is focused on the improvements of its lacking features in order to make it more competitive against the

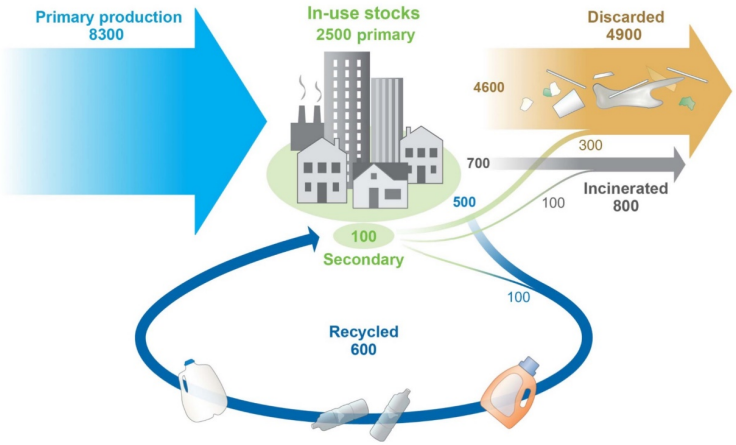

Figure 2: plastics produced, recycled and discarded.

oil-derived counterparts as well as to spread its field of applicability. The project here presented stands within this field and more precisely it was aimed to the development of novel strategies for PLA valorization, based on different chemical approaches.

1.2 Chemistry and properties.

1.2.1 From nature to nature: PLA synthesis and degradation.

As already outlined, PLA is an aliphatic polyester and it is obtained through polymerization of lactic acid. The green and renewable nature of this monomer is one of the key elements for polylactic acid success. Besides chemical synthesis, the main production route of lactic acid is through fermentation processes. To this regard, many different extraction and fermentation methodologies have been developed.[9, 10]

The synthesis of PLA can rely on the use of different kinds of monomers, besides lactic acid, as shown in **Figure 3**. While 1,3-dioxolan-4-ones (DOXs) and O-Carboxyanhydrides (OCAs) polymerizations are very new and still used just at research levels (they will be later discussed in detail), lactic acid and lactide polymerizations are more industrially-sound methodologies. In particular, the two reactions are significantly different one from the other. From one side, starting from lactic acid the polymerization proceeds through polycondensation mechanism, while when lactide is used as monomer, the driving force for the reaction is given by the relief of the ring strain. Since the low monomer cost, starting from lactic acid polycondensation is intriguing from the industrial point of view. However, the very small equilibrium constant for lactic acid condensation reaction makes the process highly inefficient, resulting in low molecular weight products. Either melt-polycondensation reactions

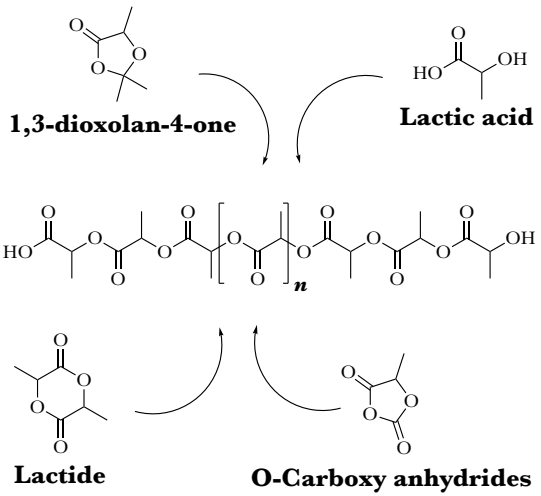

Figure 3: survey of monomers for PLA preparation.

or azeotropic distillation procedures were developed resulting in higher molecular weight products.[11, 12, 13] That said, the use of large solvent volumes and long reaction times make these processes difficult to scale-up. Lactide ring opening polymerization (ROP) allows instead to attain high molecular weight products in short reaction times, making it the strategy of choice for industrial PLA synthesis. Lactide is the cyclic dimer of lactic acid and can exist as L-lactide, L,D-lactide (*meso*) or D-lactide. Its synthesis relies on a multistep reaction, with the first step consisting in an oligomerization of lactic acid, followed by thermal depolymerization catalyzed by zinc oxide.[14] Even if this reaction is pretty efficient, the presence of byproducts such as oligomerization residues or epimerization products still remains. Lactide molecule is characterized by the presence of two planar ester moieties, that confer a skew-boat conformation.[15] The driving force for lactide ROP is given by the relief of the ring strain. Even if the Gibbs free energy for this mechanism is big enough for the reaction to proceed, its value is still modest. This means that lactide polymerization needs high temperatures to start and advance, with a usually metal-based catalyst. In addition, transesterification reaction can take place, both intermolecularly (resulting in chains redistribution) and intramolecularly (resulting in the formation of macrocycles).[16] However, with a proper tuning of polymerization conditions, high levels of conversion and high molecular weight products can be easily obtained.

The second most important feature of PLA from a sustainability aspect is given by its ability to undergo complete degradation.[17] As already outlined PLA can be synthesized starting from both D- or L- configuration monomers. The stereochemistry of the resulting product can affect the biodegradation behavior. In any case polylactic acid is also partially permeable to water and oxygen, making it even more easily degraded, even if compared to other biopolymers. Degradation starts with the hydrolysis of the ester bond, to form both oligomers and free lactic acid. The formation of acidic chain-ends further catalyzes the degradation.[18] This process begins from the external material surface, then it continues in the bulk, taking advantage of permeability as well as pores and cavities.[19] PLA degradation is strongly dependent on both pH and temperature.[20] The possibility to adjust degradation kinetics through modification of environmental parameters makes polylactic acid even more valuable from the biomedical point of view. In particular, regarding *in vivo* applications, the different pH range of different tissues allows for a controlled and targeted degradation within different parts of the body. Alongside chemical degradation, enzymatic depolymerization of PLA to lactic acid was proven to be effective.[21] At the end of its biodegradation process,

polylactide byproducts are excreted by the body either through urine or as carbon dioxide. PLA lifecycle starts from nature and ends in nature: monomer can be extracted from natural sources, polymer can be fully biodegraded and, finally, degradation byproducts are safe for the environment and the living beings.

1.2.2 Polylactic acid properties, strengths and weaknesses.

Aiming at a valuable green alternative to oil-derived plastics, PLA physical and mechanical properties have to be considered alongside its green nature. Synthesis scalability, processability and material's final properties are indeed key elements to take into account in order to fully assess polylactide industrial appeal.[22] First of all, it was estimated that for PLA production the energy requirement is 25 to 55% lower than for oil-based polymers. In addition, it will be possible to decrease this energy demand by an additional 10% in the future.[23] From the processability point of view, polylactide possesses the best thermal processability with respect to other biopolymers and can be processed by injection molding, film extrusion, blow molding, thermoforming, fiber spinning and film forming.[24]

Polylactic acid physical and mechanical properties strongly depend on its crystallinity aspects (i.e. crystallinity degree and/or crystal structure). It is well known that PLA possesses three main crystalline structures, namely α (the most common one, can generate a disordered α' form) β (generated from α under mechanical stresses) and γ (only recently discovered).[25] Changes in polylactide crystallinity bring to changes in its thermal, mechanical, physical and biodegradability properties. On the other hand, crystallinity can be affected by stereochemistry, molecular weight and thermal history.

Regarding PLA stereochemistry, as already said, lactide can exist in three different stereoisomers: L-lactide, D-lactide and D,L-lactide (**Figure 4**). Although L-lactic acid only is produced from natural sources, there's a great interest on both forms, since the synthesis of copolymers with varying ratios of the two isomers results in products with different properties with respect to the stereoregular enantiopure counterparts.[26] For example, pure poly(D-lactide) (PDLA) and poly(L-lactide) (PLLA) are reported to have a melting point (T_m) of 207 °C, which usually lowers in commercial products to 170-180 °C, due to the presence of minor racemization and impurities. That said, a 50:50 mixture of both monomers results in a product with a T_m of 230 °C, which also shows an almost two-fold increase in ultimate tensile strength.[27]

Figure 4: lactide stereoisomers.

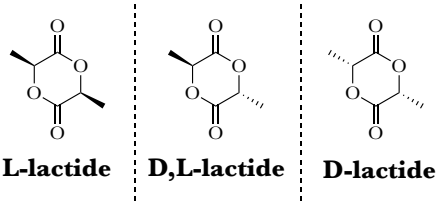

While melting and crystallization behavior are influenced by the stereochemical composition of the polymers, glass transition temperature (T_g) is not and is located around 58 °C. To this regard, a greater influence of molecular weight on T_g is reported instead.[29]

Among all properties influenced by crystallinity, PLA's barrier capabilities are one of the most investigated with the final aim of food packaging applications. In particular, barrier performances against transfer of gases (mainly CO_2 and O_2), water vapor and aroma molecules are the most important for packaging-oriented applications. Shogren compared higher crystallinity and amorphous PLA on water vapor transmission rate (WVTR). The study showed that at 25 °C the latter had a WVTR of 172 g/m^2 with respect to the 82 g/m^2 of the highly crystalline sample.[30] On a general level, the increase in crystallinity degree results in a significant reduction of permeability. This behavior can be attributed to the presence of high-density crystallites that increase the path gas molecules have to travel with respect to a more amorphous material. Even if PLA shows higher permeability than other typical packaging oil-derived plastics (for example PET and oriented polystyrene), it is still suitable for a wide range of applications in packaging industry.[31]

Crystallinity degree also influences PLA mechanical properties. On average, semicrystalline polylactide displays a tensile modulus of 3 GPa, tensile strength of 50-70 MPa, flexural modulus of 5 GPa, flexural strength of 100 MPa and an elongation at break of about 4 %.[32] As expected, PLA mechanical properties are also strongly dependent on molecular weight of the polymer: as the molecular weight increases, so does the mechanical strength of the material.

As already outlined, polylactide can be processed in many different ways. However, many are the challenges that have to be faced in order to avoid bad effects on the material during processing. In particular, PLA thermal degradation starts above 200 °C. Nevertheless, the

presence of oligomers and catalyst residues can increase the degradation rate, bringing to a reduction of the molecular weight of the polymer even at lower temperatures.[33, 34] In addition, given the high (relatively to degradation temperature) T_m (~175 °C), the processing window is very narrow and the temperature sweet spot very difficult to reach without the occurrence of side reactions. Thermal degradation of polylactic acid is a very complex process that involves a great number of different reactions. Both radical and non-radical transesterification reactions can take place, yielding CO, CO_2, macrocycles, acetaldehyde and monomeric species. A full description of all reactions occurring during degradation is nearly impossible, but, still, this lack of thermal stability brings along many obstacles for PLA recycling. The decrease of molecular weight after several high temperature processes is a major drawback that strongly limits the recycling possibilities of this material.

Related to thermal degradation, a lot of different aging processes affect polylactide durability. Alongside the already discussed thermal degradation, photo-oxidation, thermal oxidation, hydrolysis and natural weathering are also known to severely affect PLA properties.[35, 36, 37, 38] To conclude, PLA possesses a lot of key features such as its green and biocompatible character, processability. This successful mix of properties brought polylactide to the top of researchers' interest as potential replacement for oil-derived plastics, especially for packaging-oriented applications. On the other side of the coin, drawbacks such as poor toughness and poor thermal stability reduce the industrial appeal of this material and, thus, its growth in the plastic commodities market. In addition, the scarce monomer scope and the lack of reactive side-chain groups make difficult to operate chemical modifications that could, in principle, be useful for an overall improvement of the properties. For these reasons many different strategies are underway in order to make PLA competitive. Among others, the preparation of nanocomposites and the study of alternative synthetic methodologies will be discussed in detail, as these are the main areas investigated during this PhD.

1.3 Addressing PLA's shortcomings.

In order to successfully implement PLA in many different fields of application, from more specific ones (such as biomedical purposes) to more consumer-oriented ones (for example food packaging applications), improvements of its properties are needed.[39] Given the great potentialities polylactide has, many different strategies have been investigated with the aim of filling its failings while preserving it good features. For example, copolymerization reactions with D-lactide, glycolide, ε-caprolactone and trimethylene carbonate allowed for an appreciable control over PLA crystallization behavior and, thus, properties.[40] Besides copolymerization, blending of polylactide with different plasticizers and polymers is a widely studied approach for the fine tuning of final properties of the material.[41] Another possible strategy involves the surface modification of PLA. Surface-modification methods can have both permanent and non-permanent effects on the material and are useful in order to confer specific properties to the material (such as, for example, hydrophilicity).

Given the great variety of approaches available, we decided to focus mainly on two strategies for PLA's properties improvement: the preparation of PLA-based nanocomposites and the investigation of alternative synthetic methodologies with the final aim of obtaining highly functionalized PLA-based materials.

1.3.1 PLA-based nanocomposites.

The preparation of polymer-based nanocomposites is a research field that has gained more and more attention in recent years. Polymer nanocomposites are referred as multiphase materials in which at least one of the phases, called the nanofiller, is characterized by, at least, one dimension in the nanoscale range (i.e. <100 nm). On a general level, nanocomposites can be prepared by using every polymer. The interest around them arises from the great enhancement in properties that can be achieved even at very low nanofillers concentration. Nanofillers are divided into three main categories, depending on their shape:[42]

1. *Nanoplatelets (1D)*: layered nanofillers with ~1 nm thickness and aspect ratio of at least 25 following the two remaining dimensions.
2. *Nanofibers or whiskers (2D)*: nanofillers with <100 nm diameter and an aspect ratio of at least 100.

3. *Nanoparticles (3D)*: nanofillers with 3D dimensions <100 nm.

A schematic representation of these three categories is reported in **Figure 5**. A further classification of nanofillers is given by their origin, namely natural, synthetic or semi-synthetic. One of the key features of nanofillers is given by their extremely large surface area per unit volume. This means that the polymer/nanofiller interface represents a significant volume fraction, even if the concentration of nanofiller is low.[43] For this reason, the use of nanoscale additives gives rise to unique properties that couldn't be achievable through bigger-sized fillers.

Different preparation procedures have been tested, and mainly rely on four strategies, namely solution mixing, melt mixing, *in situ* polymerization and template synthesis.[44] Regarding instead nanoadditive nature, a lot of different nanofillers have been tested for the preparation of PLA-based nanocomposites. Layered silicates, for example, play an important role when looking for mechanical strength and reduced permeability. Their platelet shape can indeed act as barrier against the permeation of gases. In addition, when highly exfoliated silicates structures are targeted, also crystallinity enhancement are obtained as a result. Cloisite[45] and montmorillonite[46] PLA-based nanocomposites were successfully obtained both through melt mixing and "grafting from" approach. This procedure allows to covalently graft polymeric chains onto the filler surface, resulting in optimal dispersion of the nanoplatelets within the matrix.

Carbonaceous nanofillers have also been extensively investigated. Both platelet-shaped graphene and nanofibrous carbon nanotubes containing nanocomposites have been described. In particular, carbon nanotubes (CNTs) not only possess exceptional physical properties,

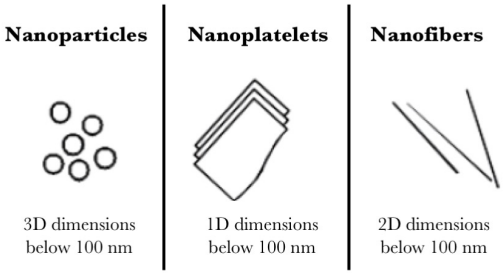

Figure 5: main nanoparticles geometries.

but they are also known to confer electric and thermal conductivity.[47] CNTs are an allotropic form of carbon and are composed of sp^2 bonds only. They show a diameter around 1-5 nm and several microns length. Depending on their production methodology, their properties and morphology can vary. CNT/PLA nanocomposites have been prepared through different techniques, among which melt-blending appears as the most straightforward.[48] The main hurdle in CNT/PLA nanocomposites preparation is given by the scarce compatibility between carbon nanotubes and polylactide. For this reason, surface modification reactions of CNTs are often carried out, in order to improve compatibility between the two phases and therefore dispersion. Similar procedures can be also exploited for the preparation of PLA/graphene nanocomposites.[49]

Another important class of PLA-based nanocomposites involves the use of metal based nanofillers. The use of metal nanoparticles can indeed confer outstanding optical, electrical, magnetic, antibacterial properties to the final material. Silver[50] and zinc oxide[51] nanoparticles are amongst the most remarkable examples in this field.

Besides these examples of PLA-based nanocomposites and other more niche ones, cellulose nanocrystals (CNC) and cellulose nanofibers (CNF) containing materials gained more and more value in recent years, since they allow the preparation of fully biodegradable materials with outstanding properties. Aiming at fully biodegradable and biocompatible PLA-based materials we focused our attention on these two cellulose-based nanofillers.

1.3.1.1 Cellulose nanocrystals.

Cellulose is one of the most abundant polymers on earth. It is a linear, stereoregular polysaccharide, formed by a repetition of D-glucopyranose units. Cellulose can be found within fiber walls of plants and cellulose fibers are characterized by an alternation of amorphous and crystalline regions (**Figure 6**).[52] These crystalline regions are constituted by densely packed cellulose chains, that give rise to crystalline domains, isolable by means of different techniques (either mechanical or chemical) to obtain CNC.[53] Cellulose nanocrystals have attracted the attention of researchers due to their unique combination of outstanding physicochemical properties with renewability. CNC can be indeed potentially extracted from every cellulose biomass and display large aspect ratio and surface area, together with great Young's modulus and surface functional groups. As previously said, CNC can be extracted either through mechanical or chemical treatment of cellulose fibers.

Figure 6: from trees to cellulose.

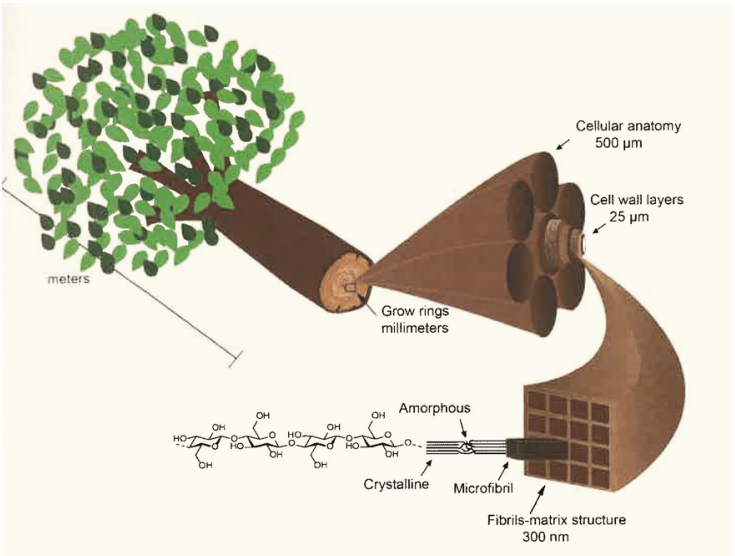

Mechanical treatment, however, ends up in highly irregular CNC in low yields. On the other hand, chemical extraction methodologies are far more reliable when aiming at high quality crystals. The principle behind these extraction reactions is that the close packing of cellulose chains in crystalline regions prevents them to be disrupted by chemicals. At the same time, in the looser amorphous regions reactants can attack carbohydrate rings with ease, resulting in their complete degradation. TEM micrograph of CNC is reported in **Figure 7**. Cellulose nanocrystals extraction can be performed with many different reagents; however, the most exploited methodologies make use of either sulfuric acid or ammonium persulfate. Acidic extraction with H_2SO_4 is the most classical procedure and the first described.[54] It is very efficient, but only when highly pure cellulose raw materials are used. Reaction conditions also have to be finely tuned in order to avoid over-hydrolysis. Ammonium persulfate oxidative extraction procedure has more recently been described.[55] This procedure allows to obtain partially oxidized CNC, which show better overall crystallinity and can be better dispersed in polar media. Extraction procedure also offers easier purification and can be applied even to lignin-containing cellulose raw materials.[56]

Figure 7: TEM micrograph of cellulose nanocrystals.

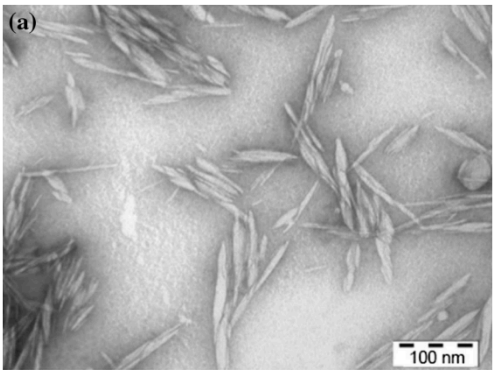

Given the great combination of CNC physicochemical properties with their biobased nature, their use as reinforcing agents in PLA-based nanocomposites has been extensively described throughout recent years. First preparation attempts relied on simpler techniques such as melt mixing or solvent casting, but with poor results. The main drawback of these approaches regards the great polarity differences between CNC (highly hydrophilic) and PLA (quite hydrophobic).[57, 58] However, thanks to free surface hydroxy groups cellulose nanocrystals offer a great number of functionalization possibilities. Aiming at PLA-CNC nanocomposites, one of the most investigated surface modifications involves the covalent bonding of polylactide oligomers onto crystals surface. This results in optimal compatibilization between filler and matrix and, thus, better dispersion with respect to more easy-access methodologies.[59] By looking at all PLA-CNC nanocomposites described in literature, it appears that cellulose nanocrystals give great improvements in PLA properties, especially regarding mechanical and barrier properties.[60, 61] However, problems like reduced thermal stability of the nanocomposites and the lack of fully uniform dispersion of the filler within the polymeric matrix still remain and have been addressed during this PhD.

1.3.1.2 Cellulose nanofibers.

CNF can be considered as close relatives of CNC and often treated as being the same nanospecies. However, cellulose nanofibers and cellulose nanocrystals present significant differences, mainly regarding the extraction methodologies and the morphology.

Figure 8: survey of CNF extraction methodologies.

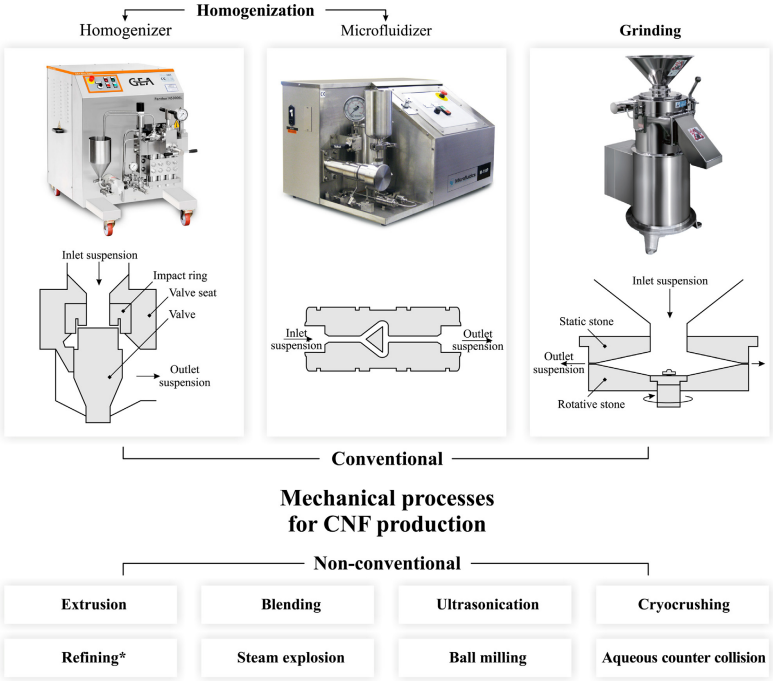

Morphologically-wise CNF can be considered as a less refined version of CNC, meaning that they are characterized by the presence of both crystalline and amorphous regions. This results in fibrils having a diameter of 5 to 50 nm and several micrometers length. CNF can be potentially extracted from every cellulose source as it's true for CNC. Furthermore, both the cellulose source and the extraction method significantly influence the morphology of the resulting nanomaterial, ending up in more than 50 different types of CNF.[62] Modern nanofibril extraction methodologies usually rely on three steps, mainly pretreatments, extraction and post-treatments. Pretreatments are either biological (enzymatic hydrolysis)[63] or chemical (for example TEMPO-mediated oxidation,[64] sulfonation[65] or carboxymethylation[66]) and are useful to reduce the energy demands for the following extraction step. Extraction methodologies mainly rely on mechanical treatments, since the final goal is a less refined product with respect to CNC. Reaction procedures can be indeed less harsh than chemical treatments, since some amorphous regions still have to be preserved.

Figure 9: SEM micrograph of cellulose nanofibers.

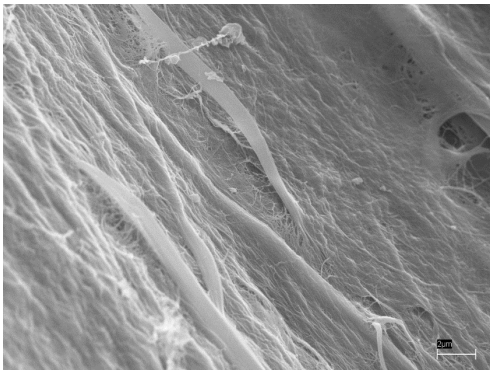

A schematic summary of the reported strategies for CNF extraction is shown in **Figure 8**, while a SEM micrograph of cellulose nanofibrils is reported in **Figure 9**. Finally, post-treatments can be used for the modification of nanofibril properties. As already discussed for CNC, the polysaccharide nature of these nanometric species opens many different functionalization possibilities, given by the active surface free -OH groups.

Cellulose nanofibrils, as well as CNC, have their strength in a winning combination of renewability together with remarkable chemical and physical properties (up to 150 GPa Young's modulus) that makes them another promising candidate for the preparation of high-performing PLA-based nanocomposites. With respect to CNC, the possibility of finely tune the morphology of the fibrils appears as an important added value, since it can strongly influence the crystallization behavior of the polymer matrix. In addition, CNF are known to form highly entangled structures that could in principle have beneficial effects on final properties of the nanocomposite. CNF/PLA nanocomposites have already been described in literature.[67] However, dispersion-related problems are even more pronounced for CNF than for CNC, even if functionalization reactions are performed in order to increase the hydrophobicity of the particles.[68]

For this reason, once a successful strategy for CNC-PLA nanocomposites preparation has been developed within this PhD, it was then applied to cellulose nanofibrils, in order to compare the final properties imparted by the two different fillers.

1.3.2 Approaches to highly functionalized PLA-based materials

Other opportunities for the improvement of PLA properties would come from the introduction of side groups along the polymer chain. This strategy could allow not only to improve the properties in which polylactide lacks, but also could eventually be useful for the implementation of new features in the final material. Unfortunately, the scarce monomer scope makes the synthesis of highly functionalized aliphatic polyesters extremely tricky. In addition, the lack of active functional groups on PLA chains implies that post-polymerization modifications are difficult. To this regard, radical functionalization and chain-end functionalization protocols have been developed, but still they are limited in scope. For this reason, increasing efforts have been spent in recent years towards the synthesis of novel monomers bearing active side groups, for the synthesis of PLA-like materials.

As it was already discussed in previous sections, the most efficient way to obtain PLA relies on the ROP of lactide. As direct polycondensation of free lactic acid is highly inefficient, it is reasonable to expect similar results when attempting polycondensation of modified α-hydroxy acids. As a natural consequence, the most intuitive approach would be the synthesis of functionalized lactides, starting from tailor-made α-hydroxy acids which are relatively easily accessible. However, even if methodologies for the synthesis of modified lactides are reported,[69, 70] their synthesis remains challenging under many aspects. The use of thermal cracking techniques requires highly stable monomers, while the use of condensation reactions gives the product in modest yields. In most cases, the steric hindrance of bulky substituents prevents cyclic dimers to form, yielding mostly oligomeric products even at very low concentrations and long reaction times.

Alternative synthetic routes making use of α-bromo acyl halides for the ring closure step were also described (**Scheme 1**).[71, 72] Also in this case, however, the competition between ring closure and oligomerization results in low yields. In addition, the use of racemic α-bromo acyl halides ends up in undesired racemic products.

Scheme 1: synthesis of lactides through the use of α-bromo acyl halides

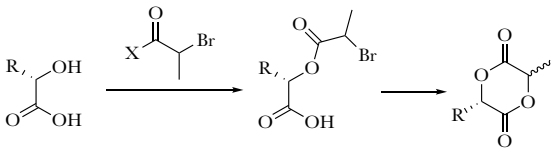

1.3.2.1 From lactides to lactide equivalents: OCAs and DOX polymerization

Given the inherent difficulties in modified lactide synthesis, the research around alternative and equivalent monomeric systems became more and more important. Among them, O-carboxyanhydrides (OCAs) have emerged as promising molecules for this task.[73] First studies on this kind of molecules started from the OCA of lactic acid (lacOCA). Following studies brought to the development of OCAs deriving from a great number of different α-hydroxy acids. O-carboxyanhydrides derived from mandelic acid,[74] malic acid[75] and amino-acids[76] are just some examples. Synthesis of OCAs relies on the carbonylation of the parent α-hydroxy acids using phosgene, diphosgene or triphosgene, as indicated in **Scheme 2**. When diphosgene or triphosgene are used, usually activated charcoal is added in order to promote the reaction.

The great OCAs breakthrough with respect to lactides comes from the activation energy for the polymerization reaction. ROP of lactide can be described to be an enthalpically favored but entropically disfavored reaction. The resulting ΔG for this process is fairly small (~-6.1 kcal mol^{-1} in gas phase, ~+1.2 kcal mol^{-1} in dichloromethane). The driving force for this reaction comes from the release of the ring strain in the skew boat conformation of lactide. Even if this driving force is high enough for the reaction to proceed, it is still modest. For this reason, back reactions at the equilibrium are not negligible. Shifting to OCAs, in this case the reaction is driven by the release of a small molecule (i.e. CO_2). This allows the reaction to have a much lower activation energy (~-18.1 kcal mol^{-1} in gas phase, ~-14.0 kcal mol^{-1} in dichloromethane) with respect to lactide in the same conditions (i.e. basic catalyst at room temperature). ROP of OCAs is an organocatalyzed process in most cases, even if metal-catalyzed reactions are also reported. While acidic catalysts proved to be non-effective, basic/nucleophilic species, such as pyridines, promote the polymerization of these monomers with good levels of control and selectivity. Alcohols and amines can be used as initiators and the high reactivity of these species allows the reaction to go to completion in

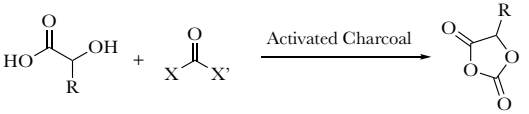

X, X' = Cl, Phosgene
X = Cl, X' = $OCCl_3$, Diphosgene
X = X' = $OCCl_3$ Triphosgene

Scheme 2: synthesis of OCAs.

short times. High molecular weights can be obtained in few hours with low polydispersity at room temperature. Given the great importance of the catalyst for the activation of the monomer, the right choice of the base is important. Depending on the parent α-hydroxy acid, different catalysts have to be used, in order to promote the reaction in the best way possible. The mild polymerization conditions, as well as the wide monomer scope make OCAs one of the best choices available for the preparation of highly functionalized aliphatic polyesters. During this PhD the potentialities of OCAs homo- and copolymerization have been investigated, with the aim of obtaining an intrinsically active PLA-based material that could in principle be applied in active packaging systems.

One of the main drawbacks of OCAs monomers comes from their instability. Even if this high activity has beneficial effects when polymerization reactions are carried out, it can also be a drawback. In particular, these molecules can be stored only for limited amounts of time and reactions have to be conducted in very controlled conditions. Taking a cue from the exploitation of a small molecule-release as driving force for ROP, Cairns et al.[76] developed the first polymerization of 1,3-dioxolan-4-ones (DOX). Similarly to OCAs, DOX polymerization takes advantage of the release of a small molecule during polymerization reaction, namely formaldehyde or acetone. The great advantage of this class of monomers comes from their increased stability with respect to OCAs, while preserving the possibility of a wide and variegated monomer scope. Given the high novelty of this polymerization approach, we decided to investigate the opportunities it can give as well as its limitations.

References

1 W.H. Carothers, G.L. Borough, F.J. Natta, Studies of polymerization and ring formation. X. The reversible polymerization of six-membered cyclic esters, *J. Am. Chem. Soc.* 54 (**1932**) 761–772. doi:10.1021/ja01341a046.

2 R. K. Kulkarni, K. C. Pani, C. Neuman, and F. Leonard Polylactic Acid for Surgical Implants (**1966**).

3 T. Ouchi, Y. Ohya, Design of Lactide Copolymers as Biomaterials, J. *Polym. Sci. Part A Polym. Chem.* 42 (**2004**) 453–462. doi:10.1002/pola.10848.

4 Y. Liu, X. Liang, S. Wang, W. Qin, Q. Zhang, Electrospun antimicrobial polylactic acid/tea polyphenol nanofibers for food-packaging applications, *Polymers* 10 (**2018**). doi:10.3390/polym10050561.

5 M.P. Arrieta, M.D. Samper, M. Aldas, J. López, On the use of PLA-PHB blends for sustainable food packaging applications, *Materials* 10 (**2017**) 1–26. doi:10.3390/ma10091008.

6 A.K. Urbanek, W. Rymowicz, A.M. Mirończuk, Degradation of plastics and plastic-degrading bacteria in cold marine habitats, *Appl. Microbiol. Biotechnol.* (**2018**) 1–10. doi:10.1007/s00253-018-9195-y.

7 Ellen MacArthur Foundation, The New Plastics Economy: Rethinking the future of plastics, *Ellen MacArthur Found.* (**2016**) 120. doi:10.1103/Physrevb.74.035409.

8 R. Geyer, J.R. Jambeck, K.L. Law, Production, uses, and fate of all plastics ever made, *Sci. Adv.* 3 (**2017**) 5. doi:10.1126/sciadv.1700782.

9 M.M. Hossain, J.L. Maisuria, Effects of organic phase, fermentation media, and operating conditions on lactic Acid extraction, *Biotechnol Prog.* 24 (**2008**) 757–765. doi:10.1021/bp0702267 ET - 2008/04/02.

10 M. Siebold, F. P.v, J. R, R. D, S. K, R. H, Comparison of the Production of Lactic Acid by Three Different Lactobacilli and its Recovery by Extraction and Electrodialysis, *Process Biochem.* 30 (**1995**) 81–95. doi:10.1016/0032-9592(95)87011-3.

11 D.S. Marques, M.H. Gil, C.M.S.G. Baptista, Improving lactic acid melt polycondensation: The role of co-catalyst, *J. Appl. Polym. Sci.* 128 (**2013**) 2145–2151. doi:10.1002/app.38413.

12 G.X. Chen, H.S. Kim, E.S. Kim, J.S. Yoon, Synthesis of high-molecular-weight poly(l-lactic acid) through the direct condensation polymerization of l-lactic acid in bulk state, *Eur. Polym. J.* 42 (**2006**) 468–472. doi:10.1016/j.eurpolymj.2005.07.022.

13 R. Miyoshi, N. Hashimoto, K. Koyanagi, Y. Sumihiro, T. Sakai, Biodegradable Poly (Lactic Acid) with High Molecular Weight, (**1996**).

14 M. Dusselier, P. Van Wouwe, A. Dewaele, P.A. Jacobs, B.F. Sels, Shape-selective zeolite catalysis for bioplastics production, *Science* 349 (**2015**) 78–80. doi:10.1126/science.aaa7169.

15 A. Duda, S. Penezek, Thermodynamics of L-Lactide Polymerization. Equilibrium Monomer Concentration, *Macromolecules.* 23 (**1990**) 1636–1639. doi:10.1021/ma00208a012.

16 O. Dechy-Cabaret, B. Martin-Vaca, D. Bourissou, Controlled ring-opening polymerization of lactide and glycolide, *Chem. Rev.* 104 (**2004**) 6147–6176. doi:10.1021/cr040002s.

17 D. da Silva, M. Kaduri, M. Poley, O. Adir, N. Krinsky, J. Shainsky-Roitman, A. Schroeder, Biocompatibility, biodegradation and excretion of polylactic acid (PLA) in medical implants and theranostic systems, *Chem. Eng. J.* 340 (**2018**) 9–14. doi:10.1016/j.cej.2018.01.010.

18 I. Grizzi, H. Garreau, S. Li, M. Vert, Hydrolytic degradation of devices based on poly(dl-lactic acid) size-dependence, *Biomaterials.* 16 (**1995**) 305–311. doi:10.1016/0142-9612(95)93258-F.

19 A. Göpferich, Mechanisms of polymer degradation and erosion, *Biomaterials.* 17 (**1996**) 103–114. doi:10.1016/0142-9612(96)85755-3.

20 L. Xu, K. Crawford, C.B. Gorman, Effects of temperature and pH on the degradation of poly(lactic acid) brushes, *Macromolecules.* 44 (**2011**) 4777–4782. doi:10.1021/ma2000948.

21 D.F. Williams Enzymic hydrolysis of polylactic acid *Engineering in Medicine* 10 (**1981**) 5 DOI: 10.1243/EMED_JOUR_1981_010_004_02

22 S. Farah, D. G. Anderson, R. Langer Physical and mechanical properties of PLA, and their functions in widespread applications — A comprehensive review *Advanced Drug Delivery Reviews* 107 (**2016**) 367–392.

23 E.T.H. Vink, K.R. Rábago, D.A. Glassner, P.R. Gruber, Applications of life cycle assessment to NatureWorks™ polylactide (PLA) production, *Polym. Degrad. Stab.* 80 (**2003**) 403–419. doi:10.1016/S0141-3910(02)00372-5.

24 R. Auras, B. Harte, S. Selke, An overview of polylactides as packaging materials, *Macromol. Biosci.* 4 (**2004**) 835–864. doi:10.1002/mabi.200400043.

25 M.L. Di Lorenzo, Crystallization behavior of poly(l-lactic acid), *Eur. Polym. J.* 41 (**2005**) 569–575. doi:10.1016/j.eurpolymj.2004.10.020.

26 A. Södergård, M. Stolt, Properties of lactic acid based polymers and their correlation with composition, *Prog. Polym. Sci.* 27 (**2002**) 1123–1163. doi:10.1016/S0079-6700(02)00012-6.

27 Y. Ikada, K. Jamshidi, H. Tsuji, S.H. Hyon, Stereocomplex Formation between Enantiomeric Poly(lactides), *Macromolecules.* 20 (**1987**) 904–906. doi:10.1021/ma00170a034.

28 G. Perego, G. Cella, C. Bastioli, Effect of molecular weight and crystallinity on poly (lactic acid) mechanical properties, *J. Appl. Polym.* 59 (**1996**) 37–43.

29 R.A. Auras, S.P. Singh, J.J. Singh, Evaluation of oriented poly(lactide) polymers vs. existing PET and oriented PS for fresh food service containers, *Packag. Technol. Sci.* 18 (**2005**) 207–216. doi:10.1002/pts.692.

30 S. Jacobsen, H.G. Fritz, Plasticizing polylactide?the effect of different plasticizers on the mechanical properties, *Polym. Eng. Sci.* 39 (**1999**) 1303–1310. doi:10.1002/pen.11517.

31 Y. Fan, H. Nishida, Y. Shirai, T. Endo, Thermal stability of poly (L-lactide): Influence of end protection by acetyl group, *Polym. Degrad. Stab.* 84 (**2004**) 143–149. doi:10.1016/j.polymdegradstab.2003.10.004.

32 S.-H. Hyon, K. Jamshidi, Y. Ikada, Effects of residual monomer on the degradation ofDL-lactide polymer, *Polym. Int.* 46 (**1998**) 196–202. doi:10.1002/(SICI)1097-0126(199807)46:3<196:AID-PI914>3.0.CO;2-Y.

33 X. Zhang, M. Espiritu, A. Bilyk, L. Kurniawan, Morphological behaviour of poly(lactic acid) during hydrolytic degradation, *Polym. Degrad. Stab.* 93 (**2008**) 1964–1970. doi:10.1016/j.polymdegradstab.2008.06.007.

34 H. Tsuji, Y. Echizen, Y. Nishimura, Photodegradation of biodegradable polyesters: A comprehensive study on poly(l-lactide) and poly(ε-caprolactone), *Polym. Degrad. Stab.* 91 (**2006**) 1128–1137. doi:10.1016/j.polymdegradstab.2005.07.007.

35 L. Zaidi, M. Kaci, S. Bruzaud, A. Bourmaud, Y. Grohens, Effect of natural weather on the structure and properties of polylactide/Cloisite 30B nanocomposites, *Polym. Degrad. Stab.* 95 (2010) 1751–1758. doi:10.1016/j.polymdegradstab.2010.05.014.

36 J.D. Badía, E. Strömberg, A. Ribes-Greus, S. Karlsson, Assessing the MALDI-TOF MS sample preparation procedure to analyze the influence of thermo-oxidative ageing and thermo-mechanical degradation on poly (Lactide), *Eur. Polym. J.* 47 (2011) 1416–1428. doi:10.1016/j.eurpolymj.2011.05.001.

37 R.M. Rasal, A. V. Janorkar, D.E. Hirt, Poly(lactic acid) modifications, *Prog. Polym. Sci.* 35 (2010) 338–356. doi:10.1016/j.progpolymsci.2009.12.003.

38 K. Hamad, M. Kaseem, M. Ayyoob, J. Joo, F. Deri, Polylactic acid blends: The future of green, light and tough, *Prog. Polym. Sci.* 85 (2018) 83–127. doi:10.1016/j.progpolymsci.2018.07.001.

39 J.M. Raquez, Y. Habibi, M. Murariu, P. Dubois, Polylactide (PLA)-based nanocomposites, *Prog. Polym. Sci.* 38 (2013) 1504–1542. doi:10.1016/j.progpolymsci.2013.05.014.

40 B. Chen, J.R.G. Evans, H.C. Greenwell, P. Boulet, P. V. Coveney, A.A. Bowden, A. Whiting, A critical appraisal of polymer–clay nanocomposites, *Chem. Soc. Rev.* 37 (2008) 568–594. doi:10.1039/B702653F.

41 A.P. Kumar, D. Depan, N. Singh Tomer, R.P. Singh, Nanoscale particles for polymer degradation and stabilization-Trends and future perspectives, *Prog. Polym. Sci.* 34 (2009) 479–515. doi:10.1016/j.progpolymsci.2009.01.002.

42 V. Krikorian, D.J. Pochan, Poly (L -Lactic Acid)/ Layered Silicate Nanocomposite : Fabrication , Characterization and Properties, (2003) 4317–4324.

43 S.S. Ray, K. Yamada, M. Okamoto, K. Ueda, Polylactide-Layered Silicate Nanocomposite: A Novel Biodegradable Material, *Nano Lett.* 2 (2002) 1093–1096. doi:10.1021/nl0202152.

44 Z. Spitalsky, D. Tasis, K. Papagelis, C. Galiotis, Carbon nanotube-polymer composites: Chemistry, processing, mechanical and electrical properties, *Prog. Polym. Sci.* 35 (2010) 357–401. doi:10.1016/j.progpolymsci.2009.09.003.

45 J. Ramontja, S.S. Ray, S.K. Pillai, A.S. Luyt, High-performance carbon nanotube-reinforced bioplastic, *Macromol. Mater. Eng.* 294 (2009) 839–846. doi:10.1002/mame.200900197.

46 X. Xu, Q. Yang, Y. Wang, H. Yu, X. Chen, X. Jing, Biodegradable electrospun poly(l-lactide) fibers containing antibacterial silver nanoparticles, *Eur. Polym. J.* 42 (**2006**) 2081–2087. doi:10.1016/j.eurpolymj.2006.03.032.

47 J. Ramontja, S.S. Ray, S.K. Pillai, A.S. Luyt, High-performance carbon nanotube-reinforced bioplastic, *Macromol. Mater. Eng.* 294 (**2009**) 839–846. doi:10.1002/mame.200900197.

48 M. Ioelovich, Cellulose as a nanostructured polymer: A short review, *BioResources*. 3 (**2008**) 1403–1418. doi:10.15376/biores.3.4.1403-1418.

49 D. Trache, M.H. Hussin, M.K.M. Haafiz, V.K. Thakur, Recent progress in cellulose nanocrystals: sources and production, *Nanoscale*. 9 (**2017**) 1763–1786. doi:10.1039/C6NR09494E.

50 R.F. Nickerson, J.A. Habrle, Cellulose Intercrystalline Structure, *Ind. Eng. Chem.* 39 (**1947**) 1507–1512. doi:10.1021/ie50455a024.

51 E. Mascheroni, R. Rampazzo, M.A. Ortenzi, G. Piva, S. Bonetti, L. Piergiovanni, Comparison of cellulose nanocrystals obtained by sulfuric acid hydrolysis and ammonium persulfate, to be used as coating on flexible food-packaging materials, *Cellulose*. 23 (**2016**) 779–793. doi:10.1007/s10570-015-0853-2.

52 R. Rampazzo, D. Alkan, S. Gazzotti, M.A. Ortenzi, G. Piva, L. Piergiovanni, Cellulose Nanocrystals from Lignocellulosic Raw Materials, for Oxygen Barrier Coatings on Food Packaging Films, *Packag. Technol. Sci.* 30 (**2017**). doi:10.1002/pts.2308.

53 M.A.S. Azizi Samir, F. Alloin, A. Dufresne, Review of recent research into cellulosic whiskers, their properties and their application in nanocomposite field, Biomacromolecules. 6 (2005) 612–626. doi:10.1021/bm0493685.

54 K.M.Z. Hossain, I. Ahmed, A.J. Parsons, C.A. Scotchford, G.S. Walker, W. Thielemans, C.D. Rudd, Physico-chemical and mechanical properties of nanocomposites prepared using cellulose nanowhiskers and poly(lactic acid), *J. Mater. Sci.* 47 (**2012**) 2675–2686. doi:10.1007/s10853-011-6093-4.

55 S. Gårdebjer, A. Bergstrand, A. Idström, C. Börstell, S. Naana, L. Nordstierna, A. Larsson, Solid-state NMR to quantify surface coverage and chain length of lactic acid modified cellulose nanocrystals, used as fillers in biodegradable composites, *Compos. Sci. Technol.* 107 (**2015**) 1–9. doi:10.1016/j.compscitech.2014.11.014.

56 J. Ambrosio-Martín, M.J. Fabra, A. Lopez-Rubio, J.M. Lagaron, Melt polycondensation to improve the dispersion of bacterial cellulose into polylactide via melt compounding: enhanced barrier and mechanical properties, *Cellulose*. 22 (**2015**) 1201–1226. doi:10.1007/s10570-014-0523-9.

57 P. Dhar, D. Tarafder, A. Kumar, V. Katiyar, Effect of cellulose nanocrystal polymorphs on mechanical, barrier and thermal properties of poly(lactic acid) based bionanocomposites, *RSC Adv.* 5 (**2015**) 60426–60440. doi:10.1039/c5ra06840a.

58 O. Nechyporchuk, M.N. Belgacem, J. Bras, Production of cellulose nanofibrils: A review of recent advances, *Ind. Crops Prod.* 93 (**2016**) 2–25. doi:10.1016/j.indcrop.2016.02.016.

59 M. Henriksson, G. Henriksson, L.A. Berglund, T. Lindström, An environmentally friendly method for enzyme-assisted preparation of microfibrillated cellulose (MFC) nanofibers, *Eur. Polym. J.* 43 (**2007**) 3434–3441. doi:10.1016/j.eurpolymj.2007.05.038.

60 T. Saito, Y. Nishiyama, J.L. Putaux, M. Vignon, A. Isogai, Homogeneous suspensions of individualized microfibrils from TEMPO-catalyzed oxidation of native cellulose, *Biomacromolecules*. 7 (**2006**) 1687–1691. doi:10.1021/bm060154s.

61 H. Liimatainen, M. Visanko, J. Sirviö, O. Hormi, J. Niinimäki, Sulfonated cellulose nanofibrils obtained from wood pulp through regioselective oxidative bisulfite pre-treatment, *Cellulose*. 20 (**2013**) 741–749. doi:10.1007/s10570-013-9865-y.

62 L. Wågberg, G. Decher, M. Norgren, T. Lindström, M. Ankerfors, K. Axnäs, The build-up of polyelectrolyte multilayers of microfibrillated cellulose and cationic polyelectrolytes, *Langmuir*. 24 (**2008**) 784–795. doi:10.1021/la702481v.

63 P. Qu, Y. Gao, G.F. Wu, L.P. Zhang, Nanocomposites of Poly(lactic acid) reinforced with cellulose nanofibrils, *BioResources*. 5 (**2010**) 1811–1823.

64 P. Qu, Y. Gao, G.F. Wu, L.P. Zhang Surface Modification of Cellulose Nanofibrils for Poly(lactic acid) Composite Application *Journal of Applied Polymer Science*, 125, (**2012**) 3084–3091. DOI 10.1002/app.36360

65 X. Lou, C. Detrembleur, R. Jérôme, Novel aliphatic polyesters based on functional cyclic (Di)esters, *Macromol. Rapid Commun.* 24 (**2003**) 161–172. doi:10.1002/marc.200390029.

66 R.J. Pounder, A.P. Dove, Towards poly(ester) nanoparticles: Recent advances in the synthesis of functional poly(ester)s by ring-opening polymerization, *Polym. Chem.* 1 (**2010**) 260–271. doi:10.1039/b9py00327d.

67 M. Leemhuis, C.F. Van Nostrum, J.A.W. Kruijtzer, Z.Y. Zhong, M.R. Ten Breteler, P.J. Dijkstra, J. Feijen, W.E. Hennink, Functionalized poly(α-hydroxy acid)s via ring-opening polymerization: Toward hydrophilic polyesters with pendant hydroxyl groups, *Macromolecules.* 39 (**2006**) 3500–3508. doi:10.1021/ma052128c.

68 W.W. Gerhardt, D.E. Noga, K.I. Hardcastle, A.J. García, D.M. Collard, M. Weck, Functional lactide monomers: Methodology and polymerization, *Biomacromolecules.* 7 (**2006**) 1735–1742. doi:10.1021/bm060024j.

69 B. Martin Vaca, D. Bourissou, O -Carboxyanhydrides: Useful Tools for the Preparation of Well-Defined Functionalized Polyesters, *ACS Macro Lett.* 4 (**2015**) 792–798. doi:10.1021/acsmacrolett.5b00376.

70 A. Buchard, D.R. Carbery, M.G. Davidson, P.K. Ivanova, B.J. Jeffery, G.I. Kociok-Köhn, J.P. Lowe, Preparation of stereoregular isotactic poly(mandelic acid) through organocatalytic ring-opening polymerization of a cyclic O-carboxyanhydride, *Angew. Chemie - Int. Ed.* 53 (**2014**) 13858–13861. doi:10.1002/anie.201407525.

71 R.J. Pounder, D.J. Fox, I.A. Barker, M.J. Bennison, A.P. Dove, Ring-opening polymerization of an O-carboxyanhydride monomer derived from l-malic acid, *Polym. Chem.* 2 (**2011**) 2204–2212. doi:10.1039/c1py00254f.

72 O. Thillaye Du Boullay, C. Bonduelle, B. Martin-Vaca, D. Bourissou, Functionalized polyesters from organocatalyzed ROP of gluOCA, the O-carboxyanhydride derived from glutamic acid, *Chem. Commun.* (**2008**) 1786–1788. doi:10.1039/b800852c.

73 C. Bonduelle, B. Martín-Vaca, F.P. Cossío, D. Bourissou, Monomer versus alcohol activation in the 4-dimethylaminopyridine-catalyzed ring-opening polymerization of lactide and lactic O-carboxylic anhydride, *Chem. - A Eur. J.* 14 (**2008**) 5304–5312. doi:10.1002/chem.200800346.

74 O. Dechy-Cabaret, B. Martin-Vaca, D. Bourissou, Controlled ring-opening polymerization of lactide and glycolide, *Chem. Rev.* 104 (**2004**) 6147–6176. doi:10.1021/cr040002s.

75 X.L. Zhuang, H.Y. Yu, Z.H. Tang, K. Oyaizu, H. Nishide, X.S. Chen, Polymerization of lactic O-carboxylic anhydride using organometallic catalysts, *Chinese J. Polym. Sci.* (English Ed. 29 (**2011**) 197–202. doi:10.1007/s10118-010-1013-7.

76 S.A. Cairns, A. Schultheiss, M.P. Shaver, A broad scope of aliphatic polyesters prepared by elimination of small molecules from sustainable 1,3-dioxolan-4-ones, *Polym. Chem.* 8 (**2017**) 2990–2996. doi:10.1039/c7py00254h.

Polylactide/cellulose nanocrystals: the *in situ* polymerization approach to improved nanocomposites

The *in situ* polymerization of L-lactide in the presence of various amounts of cellulose nanocrystals (CNC) is described. CNC was prepared efficiently by acidic hydrolysis of cotton linters. Molecular weight, morphology, thermal, mechanical and crystallization properties of the PLA-CNC nanocomposites were evaluated. From size-exclusion chromatography (SEC) analysis, the actual occurrence of chemical bond between CNC and PLA can be assessed. The effect of CNC has been evaluated through differential scanning calorimetry (DSC) analysis, which highlights the probable formation of α' crystals in the obtained materials. More importantly, from thermogravimetric analysis (TGA) a marked improvement in thermal stability of nanocomposites has been demonstrated, with respect to standard PLA and to previously described PLA-CNC blends. Nanocomposites show also an improvement in rheological properties with respect to standard PLA. In particular, storage modulus greatly increases, indicating a reinforcing effect of CNC. The described in situ synthetic methodology allows an optimal compatibilization between the two entities (PLA and CNC), facing one of the major problems inherent to the preparation of nanocomposites. It leads furthermore to remarkably improved thermal and rheological properties of the obtained materials.

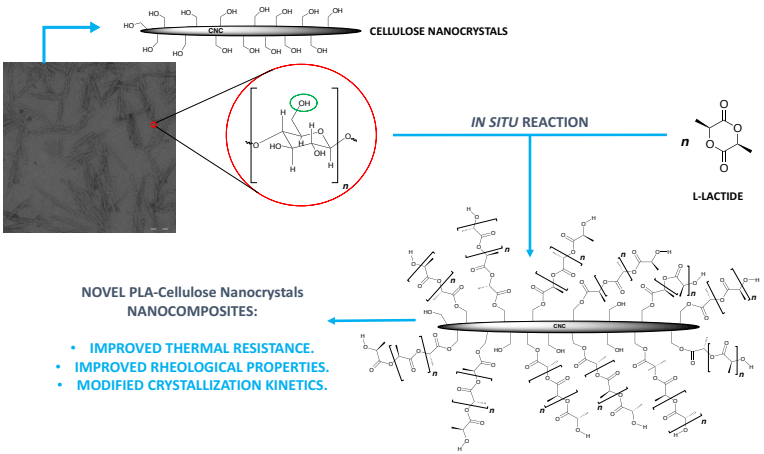

European Polymer Journal 94 (2017) 173–184.

1. Introduction

In recent years environmental awareness has been focused onto the replacing of traditional plastics based on petrochemical resources with alternative, more eco-friendly materials. Among them, poly(lactic acid), shortly PLA, is one of the most attractive to researchers and industry,[1] because of its good biodegradability and availability from renewable sources, such as starch and sugar beet.[2] The growing attention towards this thermoplastic polymer comes from both its outstanding properties, such as the good optical and elastic behavior and the excellent melt-processability, and, at the same time, from its cost competitiveness, also with respect to more traditional, not biodegradable polyesters such as PET.[3,4] For all these reasons, nowadays PLA has gained commercial significance and greatly increased its market, especially for what regards packaging and disposables applications.
However, PLA suffers from a lot of drawbacks that strongly limit possibilities for its wide application in many sectors. Indeed, it is endowed with low thermal and mechanical stability upon processing conditions, scarce flexibility and poor barrier properties. All these characteristics place it behind commonly used plastics, for instance for food packaging applications.[5]

Among possible alternatives to overcome some of these limitations, the preparation of nanocomposites has emerged as the most promising suitable solution.[6] In nanocomposites, the surface area/volume ratio of employed reinforcement additives is crucial to the enhancement of material properties. Indeed, as dimensions reach the nanometer level, interactions at phase interfaces become largely improved, bringing nanocomposites to exhibit properties not expected with larger scale particulate reinforcements. A lot of different additives can in principle be used as nanofillers. Among others, carbon nanotubes,[7,8] montmorillonite[9,10] and nanosilica[11,12] have been studied, with satisfactory achievements, in the design of PLA nanocomposites.

Aiming to produce fully organic bionanocomposites, cellulose nanocrystals (CNC) have recently emerged as a kind of biocompatible, biodegradable and renewable additive that could be dispersed into the PLA polymer matrix for the preparation of high performance blends. CNC are acquiring more and more interest in several fields of application thanks to unique chemical and mechanical properties. They are rod-like particles with extremely high aspect ratio, high Young modulus, low density and high surface area. CNC can be extracted from

almost every cellulose source, with different extraction methods properly described in literature.[13, 14, 15] Basically, they all rely onto the disruption of amorphous regions in cellulose fibers that are more susceptible of reaction (acid hydrolysis or oxidation reactions mainly), while preserving crystalline regions that can be isolated. Alongside the cited outstanding physical properties, the carbohydrate nature of these crystals ensures interesting chemical properties. The presence of a great quantity of free hydroxyl groups, primary and secondary, on CNC surface can be both a drawback and an advantage when blends with PLA are prepared. In fact, at a first glance, the high polarity of CNC clashes with the relatively apolar nature of PLA, resulting in dispersion problems that can seriously impact the properties of the obtained composite material. On the other side, however, the high quantity of reactive moieties on CNC opens to a lot of possible chemical derivatizations, that can be exploited in order to confer better compatibility with the polymer matrix.

Various preparation methods have been developed to obtain biocomposites by blending PLA with different amounts of CNC.[16, 17] In some of these biocomposites, CNC have been preventively chemically modified in order to improve the interfacial adhesion with the polymer matrix.[18, 19] One effective method for chemical modification of CNC is to grow polymers directly off their surface, using the "grafting-from" approach.[20] By this way, short PLA oligomers have been successfully grafted from CNC using a ring-opening polymerization (ROP) protocol, affording PLA-bearing CNC, which were then blended with PLA.[21, 22, 23] Quite recently, a further enhancement of compatibilization of CNC with the PLA matrix was described by Dhar and co-workers, who employed a reactive extrusion process in order to graft PLA chains onto CNC through a radical reaction.[24] In PLA-CNC nanocomposites obtained via compounding, thermal degradation of both PLA and CNC during extrusion is an unsolved issue. Only small improvements in thermal stability of the obtained materials are reported in few cases, especially when reactive extrusion is carried out in the presence of chain extenders and radical initiators.[25]

On the basis of our related experience on preparation of PLA nanocomposites containing nanosilica (NS)[11] or modified montmorillonite (MMT),[9] we looked at PLA-CNC nanocomposites via the *in situ* polymerization of L-lactide in the presence of various amounts of CNC.

It is well established that in situ polymerization in the presence of fillers provides distinct advantages when compared to other nanocomposite synthesis techniques, appearing more

appropriate in providing excellent dispersion of the nanoparticles, which should have a greater impact on achievable properties. The *in situ* polymerization technique has been recently applied for the preparation of various PLA nanocomposites, incorporating for instance TiO_2[26] or MMT fillers.[27] Marked improvements in thermal properties and crystallinity of the resultant composites were obtained, compared to those of the standard polymers.

To the best of our knowledge, no in situ polymerization strategies employing CNC have been described for the preparation of PLA nanocomposites. In this study, the *in situ* polymerization of L-lactide was performed with different loading ratios of CNC, prepared by acidic hydrolysis of cotton linters. The protocol exploits the alcoholic moieties of CNC as initiators in ring opening polymerization reaction of L-lactide. Molecular weight, morphology, thermal, mechanical and crystallization properties of the obtained nanocomposites were evaluated.

2. Experimental

2.1 Synthesis of Cellulose Nanocrystals

Cellulose nanocrystals were obtained by acidic hydrolysis, as described in literature.[15] Triturated cotton linters were slowly added to a preheated solution of 64 % w/w sulfuric acid. The ratio fiber : sulfuric acid was 1 : 17.5 g/mL. The cotton hydrolysis was performed under vigorous stirring at 45 °C for 45 min. After this period, the solution was diluted with 10 times-volume deionized water in order to stop the acidic hydrolysis. The suspension was then centrifuged at least 5 times at 10000 rpm for 20 minutes each round. The precipitated solid was repeatedly rinsed and centrifuged with deionized water. In order to remove the acid excess, the centrifuged solution was put into a dialysis tubes immersed in deionized water for 3 days. The suspension was then sonicated repeatedly (0.7 cycles of 15 min at 70 % output) to create cellulose crystals of colloidal dimensions. In order to complex any stray ions, an ion-exchange resin was put into the dispersion for 24 hours at room temperature. After resin removal, the suspension was filtered under vacuum with a Whatman glass microfiber filter to remove the largest cellulose-fiber agglomerates. Finally, the dispersion was lyophilized using a lab lyophilizator, obtaining a white-dried powder.

2.2 Synthesis of PLA

PLA was synthesized from L-lactide in bulk according to the following procedure. L-lactide (25 g) and tin octanoate (0.3 % w/w on lactide), added as catalyst, were introduced in a 250 mL three necked round bottomed flask. Slow nitrogen flow was used to ensure the presence of inert atmosphere during polymerization reaction. Mechanical stirring was provided (40 rpm). Reaction was conducted in a closed oven at 180 °C for 2 hours. At the end of the reaction, the polymer was left cooling overnight under nitrogen atmosphere.

2.3 Synthesis of PLA-CNC nanocomposites

Nanocomposites were synthesized by *in situ* polymerization, from L-lactide in bulk according to the following procedure. CNC in different quantities, from 0.125 grams – used to synthesize PLA0.5 – to 1.250 grams – used to synthesize PLA5 (see **Table 1**), were put in

Table 1: Samples synthesized and CNC relative and absolute quantities.

Sample	Cellulose Nanocrystals	
	(%wt)	(g)
PLA	0	0
PLA0.5	0.5	0.125
PLA2	2	0.500
PLA2.5	2.5	0.625
PLA3	3	0.750
PLA5	5	1.250

a three-necked round bottomed flask and dispersed in 50 mL of acetone under vigorous stirring and ultrasound treatment. This procedure ensures the disaggregation of the lyophi lized CNC fluffy mass into single crystals.

25 g of L-lactide were then added and left under stirring until complete dissolution. Acetone was then evaporated using nitrogen flux. The reaction mixture was then heated to 70 °C under vacuum in a closed oven for 2 hours in order to remove any residual moisture. After this drying step, reaction was performed following the procedure described for the synthesis of PLA. Five nanocomposites samples (PLA0.5, PLA2, PLA2.5, PLA3, PLA5) were prepared varying the percentage of employed CNC (see **Table 1**).

2.4 Characterization

2.4.1 Size Exclusion Chromatography (SEC)

The effect of CNC on the molecular weight of obtained nanocomposites was evaluated using a SEC system having Waters 1515 Isocratic HPLC pump and a four Waters Styragel columns' set (HR3-HR4-HR5-HR2) with an UV detector Waters 2487 Dual λ Absorbance Detector set at 230 nm using a flow rate of 1 mL/min and 60μL as injection volume. Samples were prepared dissolving 50 mg of polymer in 1 mL of anhydrous CH_2Cl_2 and filtering the solution on 0.45 μm filters. Given the relatively high loading, a check was performed using lower concentration of polymer (5mg/mL), in order to verify that no column overloading could be observed. Anyway higher loadings were preferred as UV signal of PLA is relatively weak.

Molecular weight data are expressed in polystyrene (PS) equivalents. The calibration was built using monodispersed PS standards having the following nominal peak molecular weight: (Mp) and molecular weight distribution (D): Mp=1,600,000 Da (D≤1.13), Mp=1,150,000 Da (D≤1.09), Mp=900,000 Da (D≤1.06), Mp=400,000 Da (D≤1.06), Mp=200,000 Da (D≤1.05), Mp= 90,000 Da (D≤1.04), Mp=50,400 Da (D=1.03), Mp=30,000 Da (D=1.06), Mp=17,800 Da (D=1.03), Mp=9,730 Da (D=1.03), Mp=5,460 Da (D=1.03), Mp=2,032 Da (D=1.06), Mp=1,241 Da (D=1.07), Mp=906 Da (D=1.12), Mp=478 Da (D=1.22); Ethyl benzene (molecular weight=106 g/mol). For all analyses, 1,2-dichlorobenzene was used as internal reference.

2.4.2 Differential Scanning Calorimetry (DSC)

DSC analyses were conducted using a Mettler Toledo DSC1, on samples weighting from 5 to 10 mg each. Melting and crystallization temperatures were measured using the following temperature cycles:

1. Heating from 25 °C to 200 °C at 10 °C/min;
2. 5 min isotherm at 200 °C;
3. Cooling from 200 °C to 25 °C at 10 °C/min;
4. 2 min isotherm at 25 °C;
5. Heating from 25 °C to 70 °C at 10 °C/min;
6. Heating from 70 °C to 200 °C at 5 °C/min.

The first two cycles were run to eliminate residual internal stresses deriving from the synthesis. Glass transition temperature (T_g), cold crystallization temperature (T_{cc}) and melting temperature (T_m) were determined. The lower heating rate in the last cycle (i.e. cycle number 6) was used in order to better separate the cold crystallization and melting peaks.

2.4.3 Thermogravimetric Analysis (TGA)

TGA were performed using a TGA 4000 Perkin Elmer instrument; tests were conducted in air on samples weighting from 5 to 10 mg each, with a program that provides a single heating cycle from 30 °C to 800 °C at 10 °C/min.

2.4.4 Rheological Curves

Rheological analyses, conducted using frequency sweep experiments, were performed with a Physica MCR 300 rotational rheometer with a parallel plate geometry (diameter = 25 mm, distance between plates = 1 mm). Linear viscoelastic regimes of neat PLA and PLA nanocomposites were studied; strain was set equal to 5% and curves of complex viscosity as function of frequency were recorded, taking 30 points ranging from 100 Hz to 0.1 Hz with a logarithmic progression, at 190 °C.

2.4.5 Wide Angle X-Ray Scattering (WAXS)

Wide Angle X-Ray Scattering (WAXS) experiments were performed using a Rigaku DMAX-II diffractometer. Diffraction patterns were obtained in the range $5° < 2\theta < 60°$ with Cu-Kα radiation (λ = 1.5405 Å) under the following conditions: 40 kV, 40 mA, step width 0.02°, time per step 2 sec, divergence slit 0.25°, Soller slit 0.04 rad and antiscatter slit 0.5°. X-Ray patterns are normalized on the main peak.

2.4.6 Films Casting

Films for WAXS analyses were obtained from a chloroform solution; 10 grams of polymer were dissolved into 50 grams of $CHCl_3$. The solution was cast on a glass surface and the solvent was evaporated at room temperature and pressure overnight. Film thickness was determined by Nikon eclipse ME600 optical microscope with Nikon digital camera light DS-Fil, software NIS-Element BR, and magnification 50x, and it was in the range 60-90 μm.

2.4.7 Transmission Electron Microscopy (TEM) analysis

For the analysis of CNC, drops of aqueous dispersions of CNC (1 wt%) were deposited on carbon-coated electron microscope grids, negatively stained with uranyl acetate and allowed to dry. For the analysis of nanocomposites, a representative sample was chosen: PLA5 was cut with a microtome and the slices obtained were negatively stained with uranyl acetate. Samples were analyzed with a Hitachi Jeol-10084 TEM operated at an accelerating voltage of 80 kV.

2.4.8 Fourier Transform Infrared Spectroscopy (FT-IR)

FT-IR Spectrometer (Spectrum 100, PerkinElmer) with an attenuated total reflection (ATR) was used to register spectra for PLA sample, all nanocomposites and CNC alone.

FT-IR spectra of PLA, CNC and of PLA5 are shown in Supporting Information file. For what regards PLA spectrum, peak relative to ester carbonyl groups can be described at 1747 cm^{-1}, as well as signals between 1000 and 1200 cm^{-1} which are typical bands relative to C-O bonds in aliphatic esters. CNC spectrum is characterized by the presence of a strong signal at 3335 cm^{-1} which can be attributed to the free -OH groups on crystals surface. Also, a strong band at 1032 cm^{-1} is visible, which is related to C-O ether bonds in cellulose.

Nanocomposites spectra closely resemble the standard PLA spectrum even if some CNC peaks are anyway visible. This result was indeed what expected since the hypothesis is that PLA chains fully cover CNC surface, preventing most of typical cellulose signals to be detected.

2.4.9 ^1H NMR analyses

^1H NMR spectra for PLA sample and nanocomposites were registered with a Bruker 400 Mhz working at 399.921 MHz. The chemical shifs are reported in ppm and referred to TMS as internal standard. All samples were prepared by dissolving 6-8 mg of polymer into 1 mL of $CDCl_3$.

Spectra of PLA and PLA5 are shown in Supporting Information file. No significant differences are detected between the spectra, with the presence of a quartet signal centered at

5.18 ppm, relative to hydrogen in α position with respect to carbonyl and a doublet signal centered at 1.60 ppm relative to methyl group.

3. Results and discussion

3.1 Synthesis of PLA-CNC nanocomposites

A schematic representation of the *in situ* synthesis of PLA-CNC nanocomposites is reported in **Scheme 1**. The product of the reaction is likely to be a complex mixture of species, with both free PLA chains and PLA-grafted CNC. Free PLA shows a molecular weight distribution from SEC analyses. CNC can be characterized by different degrees of functionalization. Synthesis provided materials characterized by an increasing brownish shade as the concentration of nanocrystals increased. This variation in color with respect to standard white PLA can be attributed to a slight thermal degradation of CNC which, however, has no influences on the synthesis.

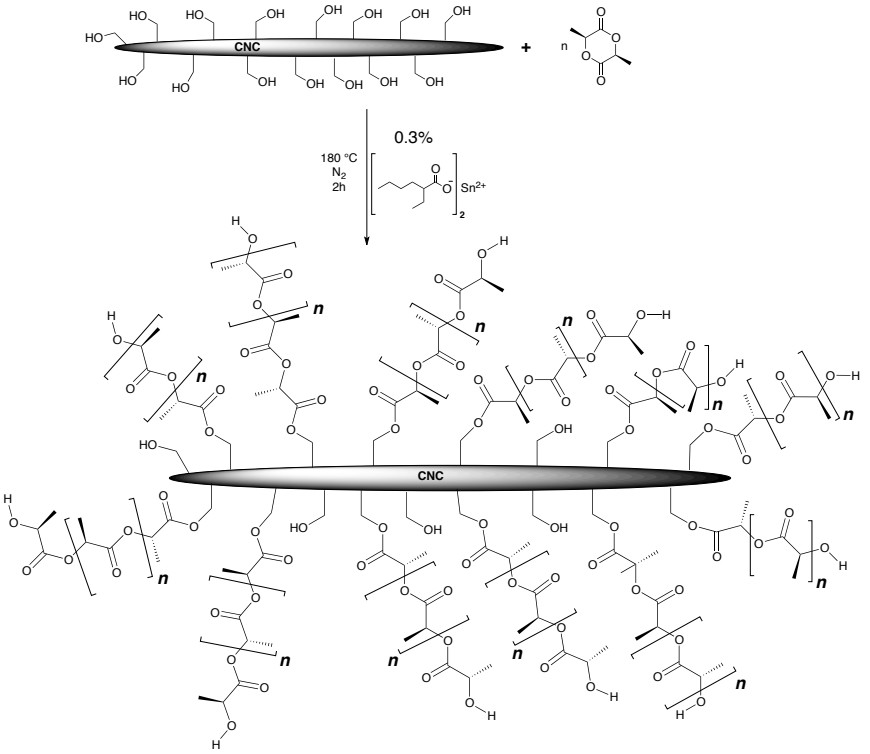

Scheme 1: schematic representation of the *in situ* synthesis of PLA-CNC.

3.2 Size exclusion chromatography (SEC)

SEC curves were obtained for all samples. As described in experimental section, samples were filtered on 0.45 μm filters before the analysis, therefore SEC data refer only to the polymer present in solution.

In **Figure 1** selected SEC graphs (PLA, PLA0.5 and PLA3) are reported. Curves have been normalized with respect to the peak relative to the most abundant polymeric species for all samples. As expected, PLA SEC curve shows only a peak at low retention time, related to the polymer. The peaks between 2400 secs and 2700 secs are attributable to low molecular weight species and residual monomer. PLA0.5 and PLA3 samples, containing 0.5 wt.% and 3 wt.% of CNC respectively, show two additional peaks at very low retention times (around 1100 secs and 1200 secs). It should be noted that such peaks get more intense as the wt.% of CNC increases. Given the presence of additional peaks, $\overline{M_n}$ and $\overline{M_w}$ values for CNC-containing nanocomposites cannot be considered reliable. For this reason, only M_p values are presented in **Table 2**, where M_p refers to the peak around 1400-1700 secs. M_p can be defined as the mass value for the most abundant species in chromatogram. Observing the trend moving from PLA to PLA0.5 and PLA3 graphs, it can be stated that the peak around 1400-1700 secs is attributable to "standard" PLA chains, straightly obtained through ROP of lactide. Hydroxyl groups present as moisture in the polymerization apparatus and the small quantity of lactic acid present together with lactide likely promote such conventional process.

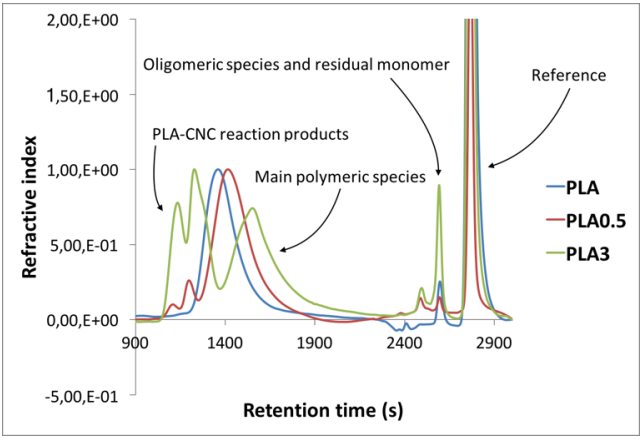

Figure 1: SEC graphs for PLA, PLA0.5 and PLA3 samples.

Table 2: Peak molecular weight for synthesized nanocomposites relative to peaks between 1400 and 1700 sec.

SAMPLE	CNC CONTENT (%W/W)	M_p (Da)
PLA	0	283600
PLA0.5	0.5	182400
PLA2	2	110600
PLA2.5	2.5	81900
PLA3	3	55000
PLA5	5	53500

However, employing CNC in the *in situ* polymerization process, covalently bound CNC are also obtained, as CNC can act as initiators through their hydroxyl groups, affording various possible CNC containing polymeric species.

From **Figure 1**, it could be noted that higher wt.% of CNC present in the feed leads to a decrease of molecular weight of standard PLA chains. This datum strongly supports the hypothesis that free OH groups on CNC's surface participate in the ROP of lactide. In fact, as the CNC's concentration increases in the feed, more initiators will be actually present, leading to shorter chains. The additional peaks which are present in the SEC-graphs of PLA0.5 and PLA3 at very high hydrodynamic volumes are likely attributable to polymeric species containing covalently bound CNC. In order to exclude the possibility that such peaks are due to CNC themselves, SEC analysis of CNC alone was also performed in the same experimental conditions. No signals were registered, confirming that such peaks in the chromatograms of PLA-CNC can only be related to nanocomposites produced by chemical reaction of CNC with lactide. In principle, further macromolecular entities could be also formed from CNC and lactide, whose dimensions are larger than those of filter pores used for SEC.

3.4 Thermal analyses (DSC)

Figure 2 reports the second heating scan for DSC thermograms of all samples, compared to the thermogram of standard PLA. All samples show similar behavior. Indeed, after the first heating cycle necessary to eliminate residual internal stresses deriving from the synthesis, they do not crystallize during cooling. Crystallization occurs during the second heating (cold crystallization), affording a crystalline phase which is characterized by two melting

peaks. It can be noted that the peak at lower temperature becomes more intense as the wt.% of CNC increases. It is well known[28, 29] that PLA can crystallize in three different forms, depending on the crystallization conditions, namely α, β and Ɣ forms. Crystallization from the melt above 120 °C results in the formation of stable crystals labeled as α-crystals. They are characterized by the packing of two chain segments with a 10_3 helical conformation to form an orthorhombic unit cell. The α-form is the most common PLA crystalline phase, while β and Ɣ ones form through different thermal/mechanical treatments.

It has been demonstrated[30, 31] that, when crystallization from the melt occurs with isothermal analyses at temperatures lower than 120 °C, the formation of more disordered and metastable α'-crystals is promoted. Such crystals show slightly larger unit-cell dimensions as well as lower packing density in comparison to α-crystals. Their existence can explain the splitting of melting peaks in PLA, observed also in previous literature.[32]

Coming to our DSC experiment, the high regularity of the chains in the standard PLA sample leads to the formation of α-crystals during cold crystallization, resulting in a single melting peak, bearing a slight shoulder at lower temperature, probably due to a small presence of α'-crystals. When CNC are added in the polymerization feed, giving rise to *in situ* polymerization with lactide, they probably lead to more disordered crystals, with the melting

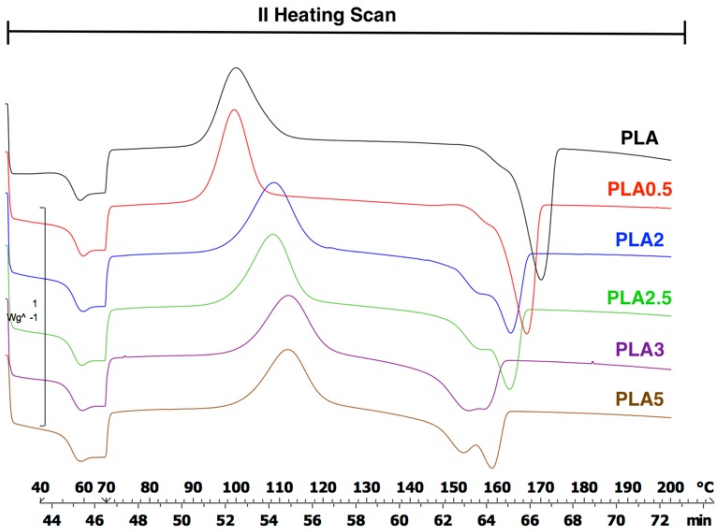

Figure 2: DSC thermograms for all samples.

Table 3: thermal DSC data for all samples.

Sample	Tg (°C)	TCC (°C)	Tm (°C)
PLA	54	100	170
PLA0.5	53	99	166
PLA2	54	109	163
PLA2.5	54	108	163
PLA3	54	112	157
PLA5	53	112	159

peak at lower temperature becoming more and more evident as CNC wt.% increases. This seems to indicate that the higher is the wt.% of CNC, the more favored will be the formation of α'-phase. From **Figure 2** it can also be noticed that cold crystallization temperature increases as the wt.% of CNC increases.

Analyzing DSC data, reported in **Table 3**, it appears that CNC make crystallization of PLA more difficult. Interestingly, in literature data relative to PLA-CNC blends, an opposite trend is reported, i.e. an improvement in crystallization kinetics with respect to standard PLA.[33] In those cases, nanocrystals seem to have a nucleating effect, favoring the formation of crystals. It appears, however, that an increase in affinity between PLA and CNC (i.e. by modification through grafting approaches) leads to lower crystallization kinetics.[20, 24] In particular, it was hypothesized that the greater is the adhesion of polymer chains onto nanocrystals surface, the lower is the mobility for chains themselves, with consequent slowing in crystals' formation.

In our nanocomposites, CNCs act presumably as disturbing agents for crystallization since the chemical anchoring onto nanocrystals surface brings to a decrease of the degrees of freedom for polymeric chains. This eventually leads to a more difficult organization of macromolecules and, therefore, to a more difficult formation of crystals.

3.5 Thermal analyses (TGA)

Figure 3 shows TGA curves of all PLA-CNC nanocomposites. All samples show a single step degradation pathway. Thermal stabilities of PLA nanocomposites were evaluated from TGA thermograms checking temperatures corresponding to 5%, 30%, 50% and 95% of

weight loss ($T_{5\%}$, $T_{30\%}$, $T_{50\%}$ and $T_{95\%}$ respectively). It has to be pointed out that all nanocomposites show higher thermal stability in comparison to standard PLA. This result marks an important difference from what reported for PLA-CNC nanocomposites obtained via compounding, for which a decrease, or in the best cases no variations in thermal stability in comparison to PLA are detected.[18, 19] It must be considered that CNC are routinely obtained through H_2SO_4-based hydrolysis of cellulose fibers and they are therefore recovered bearing sulfate groups. It is reported that thermal stability of CNC is strongly related to the acidity of the sulfate groups on the crystals surface,[17, 34, 35] i.e. the higher is the quantity of sulfate groups, the easier is expected to be the thermal degradation. Most likely, this is the reason also for the observed enhanced thermal degradation in the case of physical mixtures between PLA and CNC.

Functionalization of CNC with different moieties has been explored, in order to obtain a higher thermal stability of crystals themselves and, in turn, of resulting nanocomposites.[20] In almost all reported cases, however, no improvements were registered for what regards the thermal stability of the materials obtained. An increase of thermal degradation temperature (around 12 °C in the best case) was reported by Dhar and co-workers, when the reactive extrusion process was adopted (see Introduction).[25] In this latter case T_{onset} increased of about 12 °C and $T_{50\%}$ of around 5 °C.

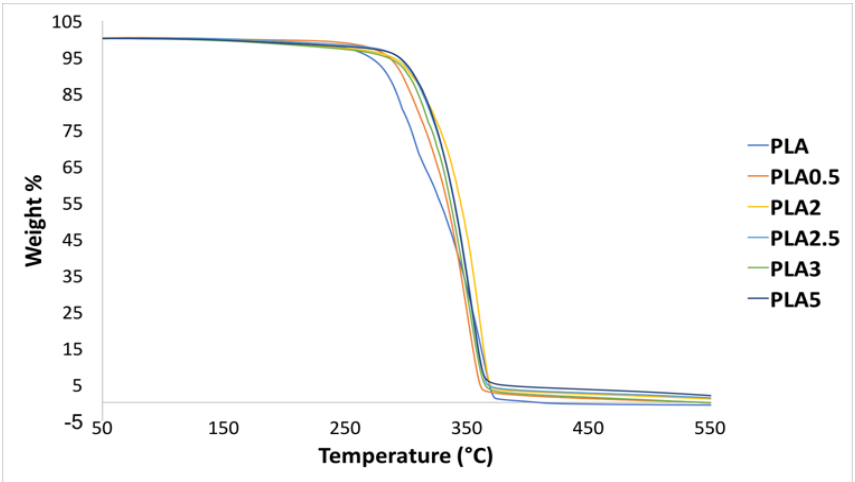

Figure 3: TGA curves for all samples.

Table 4: Thermal degradation temperatures corresponding to defined weight losses for all samples.

SAMPLE	$T_{5\%}$ (°C)	$T_{30\%}$ (°C)	$T_{50\%}$ (°C)	$T_{95\%}$ (°C)
PLA	262	301	325	360
PLA0.5	279	314	330	353
PLA2	281	325	340	361
PLA2.5	286	322	335	359
PLA3	282	320	332	358
PLA5	286	322	335	366

As shown by the data reported in **Table 4**, all PLA-CNC samples show higher degradation temperatures with respect to standard PLA. Among data reported, $T_{5\%}$, corresponding to 5% weight loss, can be considered as the starting point for thermal degradation. It appears that all nanocomposites show improved thermal resistance, with $T_{5\%}$ that increases up to 25 °C in the best case in comparison to standard PLA. The difference in weight loss between standard PLA and nanocomposites becomes less pronounced with the increase of temperature. It has to be said, however, that all CNC containing samples appear to possess higher $T_{30\%}$ (up to ~25 °C) and higher $T_{50\%}$ (up to ~14 °C), indicating a marked improvement over best previous literature results.

The improvement of thermal stability for nanocomposites can be hypothetically ascribed to two factors. From one side it is reasonable to think that reaction between CNC and L-lactide allows to "mask" the deleterious sulfate groups that otherwise would increase thermal degradation.

Secondly, it is possible that, the reduced mobility of chains due to their linkage to nanocrystals allows a better thermal stability, making chains stiffer and less prone to oxidation and degradation reactions.

3.6 Rheological analyses

Since the reinforcing effect of CNC in PLA matrices is well known,[36, 37] we performed rheological analyses, in order to evaluate the effect of the *in situ* polymerization protocol on the complex viscosity and storage modulus. As the wt.% of CNC increases, two effects can be

Figure 4: complex viscosity curves for all samples.

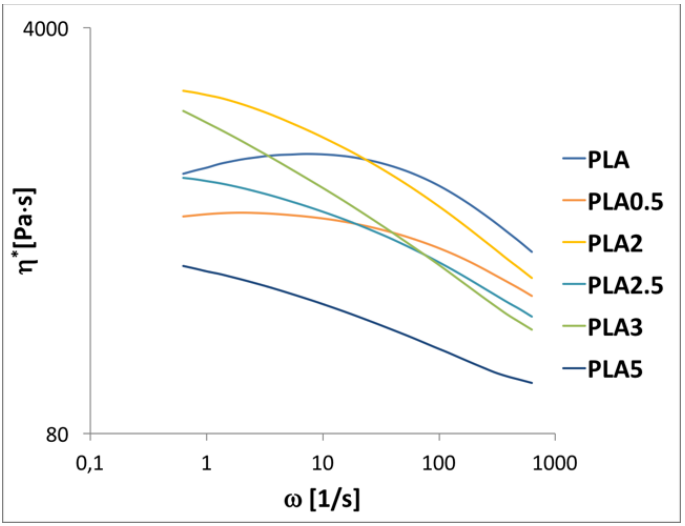

observed. From one side, the high rigidity of CNC contributes to increase the melt viscosity. This trend is in contrast with the related decrease in molecular weight of the PLA polymer, observed by SEC, that acts in the opposite direction, lowering the melt viscosity.

Rheological curves obtained via frequency sweep experiments are reported in **Figure 4** for all samples. Sample PLA0.5 shows viscoelastic behavior with a Newtonian plateau at low shear rates and a shear thinning behavior. PLA sample shows a decrease in viscosity at low shear rates, caused by partial degradation of the sample during the analysis: in PLA0.5 such effect is not visible, probably thanks to the thermal stabilizing effect of CNC, as explained in TGA paragraph. Although all materials behave as thermoplastics, with the increase of wt.% CNC samples tends to have an increased shear sensitivity in all range of frequencies. This behavior is marked for PLA 2 and PLA3 samples.

Storage (G') modulus curves (**Figure 5**) show that PLA sample has the typical behavior of a thermoplastic polymer, with the low shear zone slope of G' curve being around 2. With the increase of CNC wt.%, the slope of the curve becomes significantly lower and the whole G' plot tends to a straight line. A trend of this type can be attributed to the progressive transition

Figure 5: storage modulus curves for all samples.

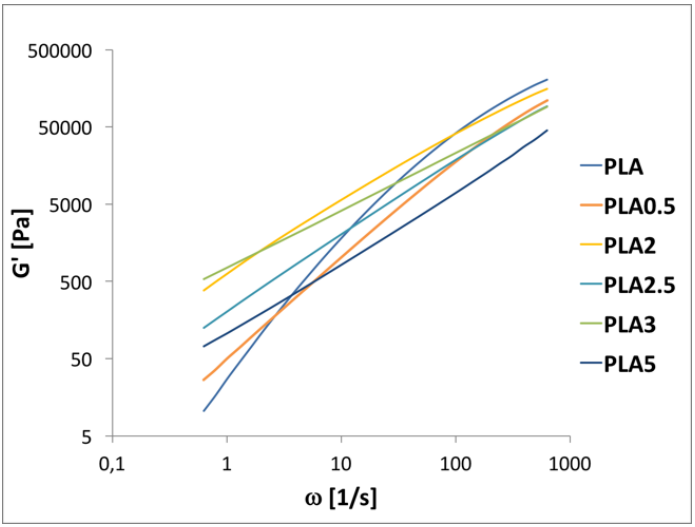

from liquid- to solid-like behavior, which therefore indicates a good dispersion of nanoparticles into the polymeric matrix. As expected, PLA0.5 shows the smallest difference with standard PLA. In **Table 5** storage modulus values at ω = 628.3 s^{-1} and at ω = 0.6823 s^{-1}, which are the extremes of the curves, are reported. The trend just described is here well highlighted, with PLA sample that shows the highest G' at high frequency and the lowest at low frequency, while all nanocomposites show a less pronounced decrease of storage modulus values.

Sample	G' [Pa]	
	at ω = 628.3 s^{-1}	at ω = 0.6823 s^{-1}
PLA	205800	10
PLA0.5	110300	26
PLA2	154600	381
PLA2.5	92950	126
PLA3	90490	537
PLA5	45380	72

Table 5: storage modulus values at the two extremes of the curves.

3.7 WAXS Analyses

Crystalline structure of PLA and PLA-CNC nanocomposites was studied through WAXS analyses on films obtained by casting from a PLA solution in $CHCl_3$ as previously described. As **Figure 6** shows, PLA sample appears to have four characteristic peaks at 2θ = 14.60°, 16.68°, 19.14° and 22.27°, as already reported in literature.[38] Crystallinity of PLA0.5 sample seems to be not significantly affected by the presence of cellulose nanocrystals. As concentration of CNC increases, however, the crystallinity of nanocomposites decreases. In the case of PLA2 signals relative to PLA are still present. However they are less sharp and the peak at 22.27° is barely appreciable. An additional increase of concentration (namely PLA2.5, PLA3 and PLA5 samples) brings to a further decreased of crystallinity. These three nanocomposites show a broad peak centered around 2θ = 16° and characteristic PLA peaks are not detectable anymore. Interestingly, however, it should be noted that with the increase in w/w% of CNC, the crystalline peak of PLA shifts towards lower values of 2θ. To this regard, it is well known in literature that the peak at 2θ = 16.7° is relative to α crystalline phase of PLA.[16] This signal shifts as the contribution of α' form becomes higher, reaching values equal to 2θ = 16.4°.[39, 40] As **Figure 6** shows, all nanocomposites with except of PLA0.5, show lower values of 2θ in this spectral region, therefore confirming DSC data regarding the presence of differently ordered crystalline phases.

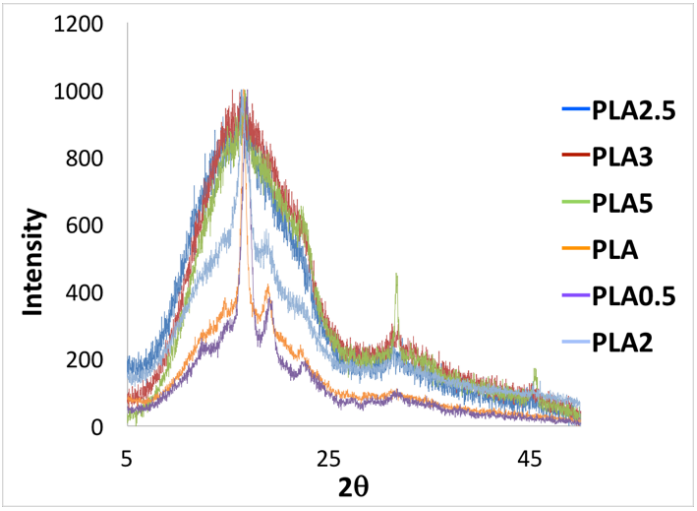

Figure 6: WAXS diffractograms for all nanocomposites and PLA sample.

Figure 7: WAXS diffractograms for all nanocomposites and CNC sample.

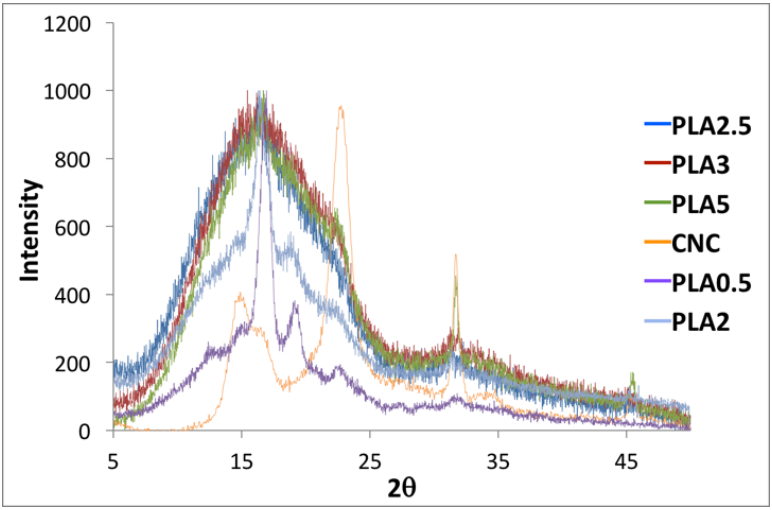

In addition, it appears that for samples with the highest concentrations of CNC, the signals pattern of nanocrystals becomes more and more evident. As shown in **Figure 7**, CNC show four main peaks at 2θ = 14.79°, 16.58°, 22.83° and 45.23°. The peak at 2θ = 32° is spurious and presumably related to K_2SO_4 generated during the extraction of nanocrystals. Meanwhile the two peaks at 14.79° and 16.58° respectively cannot be detected under the broad signal in PLA2.5, PLA3 and PLA5 samples. It appears that the other two peaks appear with increasing intensity as the concentration of CNC increases in the material. In particular, for what regards PLA5, both a shoulder around 22.5° and a peak around 54.5° are present, closely resembling signals relative to pure CNC. It is therefore reasonable to think that at high concentration of CNC the dispersion of nanocrystals in the matrix becomes less efficient, leading to the presence of some CNC crystalline domains.

3.8 TEM analyses

The dimensions of cellulose nanocrystals used for the preparation of nanocomposites were determined via TEM. In **Figure 8** a TEM image of CNC is reported. Cellulose nanocrystals have an average length of 195 ± 28 nm and an average diameter of 16 ± 4 nm, resulting in an aspect ratio of 13 ± 4.

Figure 8: TEM micrograph of CNC.

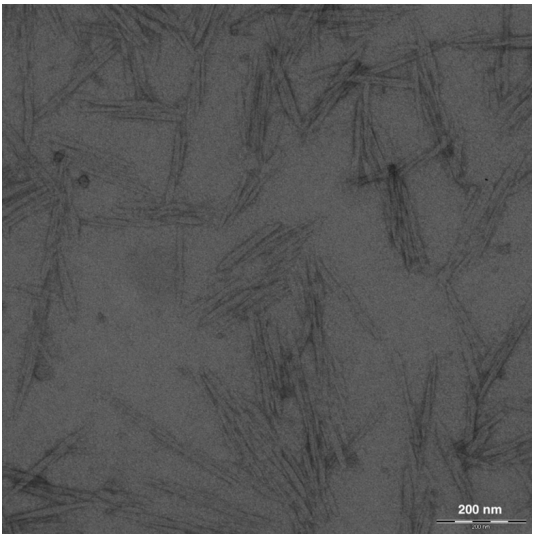

In **Figure 9** a TEM micrograph of PLA5 is reported. PLA5 was chosen because it is the sample having the higher content of CNC among all nanocomposites samples. In **Figure 9**, a TEM micrograph of PLA5 is reported. PLA5 was chosen because it is the sample having the higher content of CNC among all nanocomposites samples. In **Figure 9**, CNC can be distinguished over the polymeric matrix as randomly distributed dark halos.

CNC are not clearly different from the polymeric matrix, differently from what reported for CNC-PLA blends.[41] Such difference can be ascribed to the scarce affinity between CNC and PLA in classical blends, which results in a distinct separation of the two phases. In our case, the *in situ* growth of PLA chains onto CNC surface allows the crystals to be fully embedded in the polymer, with an intimate interfacial contact.

It is also important to note that crystals' dimensions in PLA5 appear to be of the same order of magnitude as in CNC alone, even if dimensions cannot be accurately determined because of the indefinite profile of dispersed crystals. Again, this result underlines a clear morphological difference between nanocomposites here described and PLA-CNC blends, in which the formation of CNC agglomerates is reported.[42] The uniform dispersion within the

Figure 9: TEM micrograph of PLA5 sample.

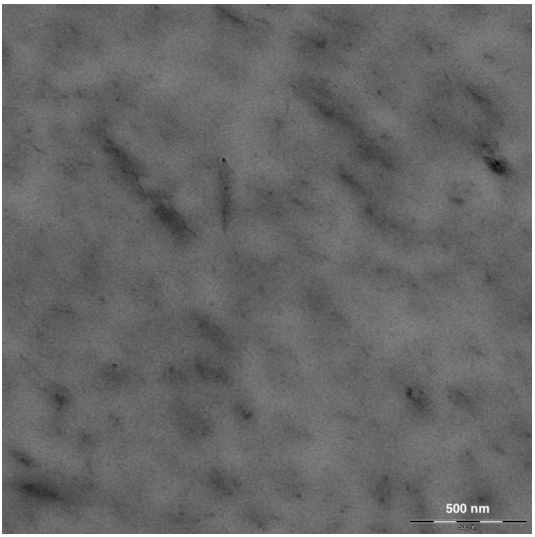

polymeric matrix is another proof of the efficacy of the *in situ* approach for the preparation of PLA-CNC nanocomposites even at relatively high loadings of CNC.

3.9 FT-IR and ^{1}H NMR analyses

In PLA FT-IR spectrum the peak relative to ester carbonyl groups can be recognized at 1747 cm^{-1}, as well as signals between 1000 and 1200 cm^{-1} can be ascribed to CeO bonds in aliphatic esters. CNC spectrum is characterized by the presence of a strong signal at 3335 cm^{-1} that can be attributed to the free OH groups on crystals surface. The intense band at 1032 cm^{-1} can be attributed to CeO ether bonds in cellulose. Nanocomposites spectra closely resemble the standard PLA spectrum although some typical CNC peaks are however visible. The hypothesis is that PLA chains fully cover the CNC surface, preventing most of typical cellulose signals to be detected. ^{1}H NMR analyses show no significant differences between the spectra of PLA and nanocomposites, with the presence of a quartet signal centered at 5.18 ppm, relative to hydrogen in α position with respect to the carbonyl group and a doublet signal centered at 1.60 ppm relative to the methyl group.

4. Conclusions

In this work, cellulose nanocrystals were successfully synthesized, starting from cotton linters through acidic hydrolysis, and they were subsequently used for *in situ* melt polymerization of PLA.

Full characterization of nanocomposites has been performed, aimed to investigate the effect of CNC on the morphological and thermo-mechanical properties of materials.

Through SEC analysis it has been possible to assess the actual occurrence of chemical bonds between CNC and PLA chains. Indeed, as the quantity of added CNC increases, the molecular weight of the polymer decreases, possibly indicating a role of free OH groups on cellulose surface, as initiators during the *in situ* polymerization process.

DSC analyses were performed to evaluate the thermal behavior of the materials. The presence of CNC in the reaction system seems to favor the formation of α' crystals, which are less ordered with respect to the more common α crystal form in PLA. Again, it can be argued that free OH groups act as initiators, perhaps forming complex star-like macromolecular architectures which are more prone to form less ordered crystals.

From TGA analyses it has been clearly demonstrated that synthesized bionanocomposites show a marked improvement in thermal stability with respect to standard PLA. Results indicate an improvement also with respect to literature data regarding the thermal stability of various types of PLA-CNC nanocomposites.

Finally, nanocomposites show an improvement in rheological properties with respect to standard PLA. In particular it has been shown that storage modulus markedly increases in the presence of CNC, indicating a reinforcing effect given by these species.

In conclusion, the described *in situ* synthetic methodology allows not only an optimal compatibilization between the two entities, facing one of the major problems inherent to the preparation of nanocomposites, but also leads to remarkably improved thermal and rheological properties of the obtained materials, with respect to standard PLA and conventional PLA-CNC nanocomposites. Among tested CNC concentrations, the 2 %w/w appeared to be the most promising. In fact, while TGA data remain very similar for all nanocomposites, PLA2 sample proved to possess the best rheological properties, probably thanks to a combination of high molecular weight and reinforcing effect given by CNC.

References

1 Inkinen, S.; Hakkarainen, M.; Albertsson, A.; Sodegard, A.; *Biomacromolecules*; **2011**; 12; 523-532.

2 Datta, R.; Henry, M.; *J. Chem. Technol.* Biotechnol; **2006**; 81; 1119-1129.

3 Armentano, I.; Bitinis, N.; Fortunati, E.; Mattioli, S.; Rescignano, N.; Verdejo, R.; Lopez-Manchado, M.A.; Kenny, J.M.; *Progress in Polymer Science*; **2013**; 38; 1720-1747.

4 Lunt, J.; *Polymer Degradation and Stability*; **1998**; 59; 145-152.

5 Auras, R.; Harte, B.; Selke, S.; *Macromol. Biosci.*; **2004**; 835-864.

6 Raquez, J.M.; Habibi, Y.; Murariu, M.; Dubois, P.; *Progress in Polymer Science*; **2013**; 38; 1504-1542.

7 Ramontja, J.; Sinha Ray, S.; Pillai, S.K.; Luyt, A.S.; *Macromol. Mater. Eng.*; **2009**; 294; 839-846.

8 Kaseem, M; Hamad, K; Deri, F; Gun Ko, Y; *Polym. Bull.*; **2016**.

9 Sabatini, V.; Farina, H.; Basilissi, L.; Di Silvestro, G.; Ortenzi, M.A.; *Journal of Nanomaterials*; **2015**; 1-16.

10 Castiello,S.; Coltelli, M.B.; Conzatti, L.; Bronco, S.; *Journal of Applied Polymer Science;* **2012**; 125; E413-E428.

11 Basilissi, L.; Di Silvestro, G.; Farina, H; Ortenzi, M.A.; *J. App. Polym. Sci.*; **2013**; 1575-1582.

12 Ortenzi, M.A.; Basilissi, L.; Farina, H.; Di Silvestro, G.; Piergiovanni, L.; Mascheroni, E.; *European Polymer Journal*; **2015**; 66; 478-491.

13 Ioelovich, M.; *BioResources*; **2008**; 3; 1403-1418.

14 Trache, D; Hazwan Hussin, M.; Mohamad Haafiz, M. K.; Kumar Thakur, V.; *Nanoscale*; **2017**.

15 Mascheroni, E.; Rampazzo, R.; Ortenzi, M. A.; Piva, G.; Bonetti, S.; Piergiovanni, L.; *Cellulose*; **2016**; 23; 779-793.

16 Dhar, P.; Tarafder, D.; Kumar, A.; Katiyar, V.; *RSC Adv.*; **2015**; 5; 60426-60440.

17 Ambrosio-Martin, J.; Fabra, M. J.; Lopez-Rubio, A.; Lagaron, J. M.; *Cellulose*; **2015**; 22; 1201-1226.

18 Pracella, M.; Minhaz-Ul Haque, Md.; Puglia, D.; *Polymer*; **2014**; 55; 3720-3728.

19 Spinella, S.; Lo Re, G.; Liu, B.; Dorgan, J.; Habibi, Y.; Leclere, P.; Raquez, J. M.; Dubois, P.; Gross, R. A.; *Polymer*; **2015**; 65; 9

20 Bledzki, A. K.; Gassan, J.; *Prog. Polym. Sci.*; **1999**; 24; 221-274.

21 Lizundia, E.; Fortunati, E; Dominici, F; Vilas, J. L.; Leon, L. M.; Armentano, I.; Torre, L.; Kenny, J. M.; *Carbohydrate Polymers*; **2016**; 142; 105-113.

22 Mujica-Garcia, A.; Hooshmand, S.; Skrifvars, M.; Kenny, J. M.; Oksman, K.; Peponi, L.; *RCS Adv.*; **2016**; 6; 9221-9231.

23 Goffin, A. L.; Raquez, J. M.; Duquesne, E.; Siqueira, G.; Habibi, Y.; Dufresne, A.; Dubois, P.; *Biomacromolecules*; **2011**; 12; 2456-2465.

24 Dhar, P.; Tarafder, D.; Kumar, A.; Katiyar, V.; *Polymer*; **2016**; 87; 268-282.

25 Yang, W.; Dominici, F.; Fortunati, E.; Kenny, J.M.; Puglia, D.; *RSC Adv.*; **2015**; *5*; 32350-32357.

26 Nakayama, N; Hayashi, T.; *Polymer degradation and stability*; **2007**; 92; 1255-1264.

27 Kaewprapan, K.; Phattanarudee, S.; *J. Nanosci. Nanotechnol.*; **2012**; 12; 781-786.

28 Kawai, T.; Rahman, N.; Matsuba, G.; Nishida, K.; Kanaya, T.; Nakano, M.; Okamoto, H.; Kawada, J.; Usuki, A.; Honma, N.; Nakajima, K.; Matsuda, M.; *Macromolecules*; **2007**; 40; 9463-9469.

29 Cocca, M.; Di Lorenzo, M. L.; Malinconico, M.; Frezza, V.; *European Polymer Journal*; **2011**; 47; 1073-1080.

30 Righetti, M. C.; Gazzano, M.; Di Lorenzo, M. L.; Androsch, R.; *European Polymer Journal*; **2015**; 70; 215-220.

31 Zhang, J.; Tashiro, K.; Tsuji, H.; Domb, A. J.; *Macromolecules*; **2008**; 41; 1352-1357.

32 Di Lorenzo, M. L.; Androsch, R.; *Macromol. Chem. Phys.*; **2016**.

33 Gardebjer, S.; Bergstrand, A.; Idstrom, A.; Borstell, C.; Naana, S.; Nordstierna, L.; Larsson, A.; *Composites Science and Technology*; **2015**; 107; 1-9.

34 Lu, P.; Hsieh, Y. L.; *Carbohydrate Polymers*; **2010**; 82; 329-336.

35 Roman, M.; Winter, W. T.; *Biomacromolecules*; **2004**; *5*; 1671-1677.

36 Bagheriasl, D.; Carreau, P. J.; Riedl, B.; Dubois, C.; Hamad, W. Y.; *Cellulose*; **2016**; 23; 1885-1897.

37 Kamal, M. R.; Khoshkava, V.; *Carbohydrate Polymers*; **2015**; 123; 105-114.

38 Ki, W. K.; Seong, I. W.; *Macromol. Chem. Phys.*; **2002**; 203; 2245.

39 Marubayashi, H.; Akaishi, S.; Akasaka, S.; Asai, S.; Sumita, M.; *Macromolecules*; **2008**; 41; 9192-9203.

40 Zhang, J.; Duan, Y.; Sato, H.; Tsuji, H.; Noda, I.; Yan, S.; Ozaki, Y.; *Macromolecules*; **2005**; 38; 8012-8021.

41 Sanchez-Garcia, M.D.; Lagaron, J.M.; *Cellulose*; **2010**; 17; 987-1004.

42 Gupta, A.; Simmons, W.; Schueneman, G.T.; Hylton, D.; Mintz, E.A.; ACS Sustainable Chem. Eng.; **2017**; *5*; 1711-1720.

Supporting information

Polylactide/cellulose nanocrystals: the *in situ* polymerization approach to improved nanocomposites

SEC Analysis

Are here after reported SEC graphs for all synthesized samples (**Figure S1**). Only the region between 900 and 2000 s is considered for what regards the retention times, in order to highlight the increasing differences with increasing concentration of CNC.

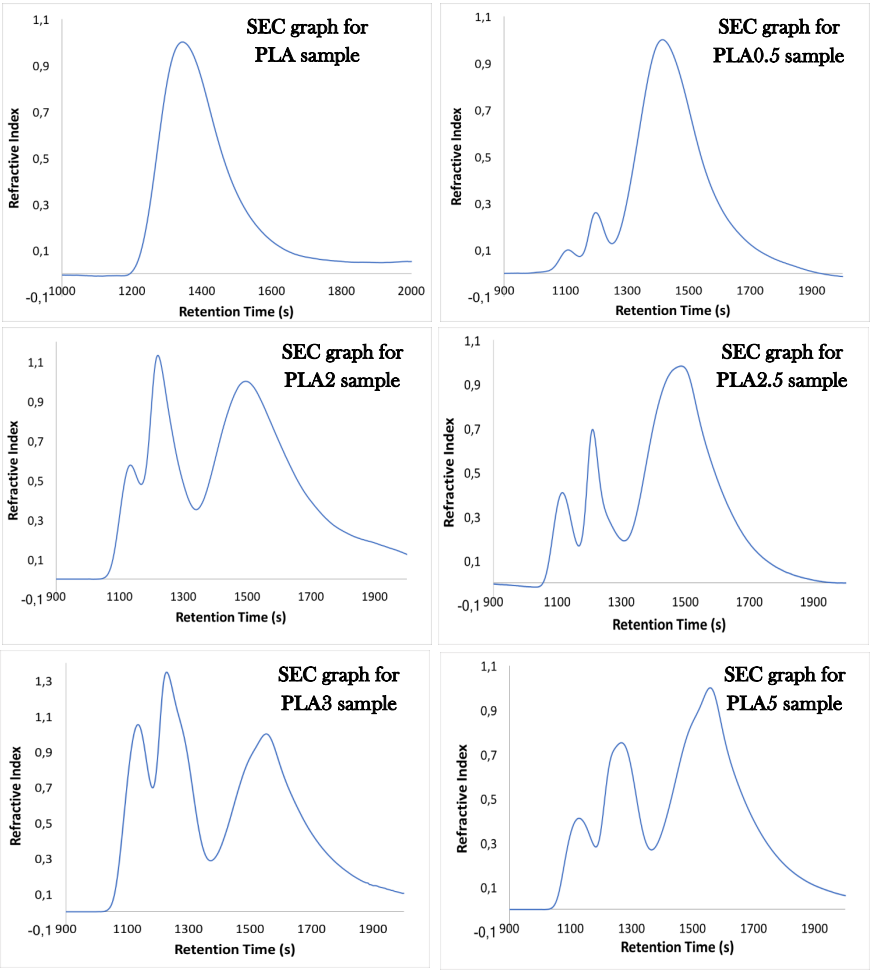

Figure S1: SEC graphs for all synthesized samples.

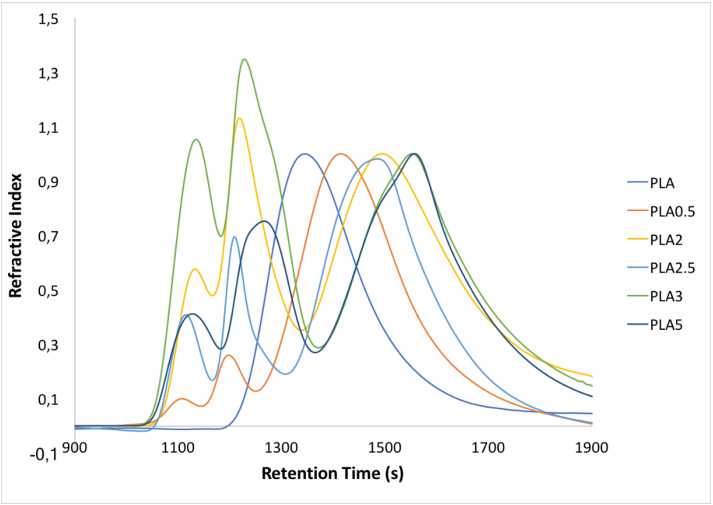

Figure S2: Comparison of SEC graphs for all samples.

A comparison of all graphs is reported in **Figure S2**.

FT-IR Analysis

In **Figure S3** and **Figure S4** FT-IR spectra of CNC and PLA sample are reported. What is important is that for FT-IR spectra of nanocomposites no differences can be detected with respect to standard PLA's one, as shown in **Figure S5**, where FT-IR spectrum of PLA5 sample is reported.

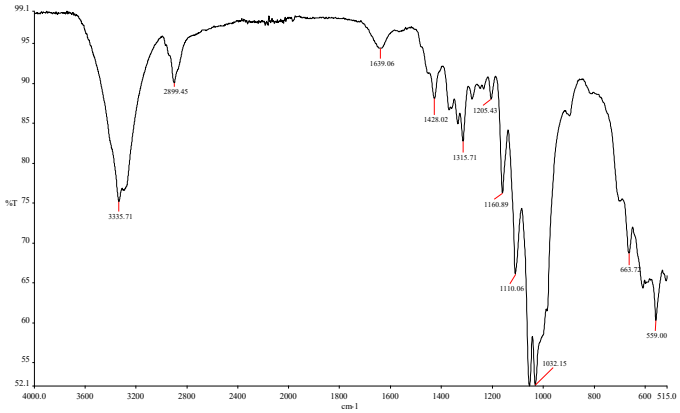

Figure S3: FT-IR spectrum for CNC sample.

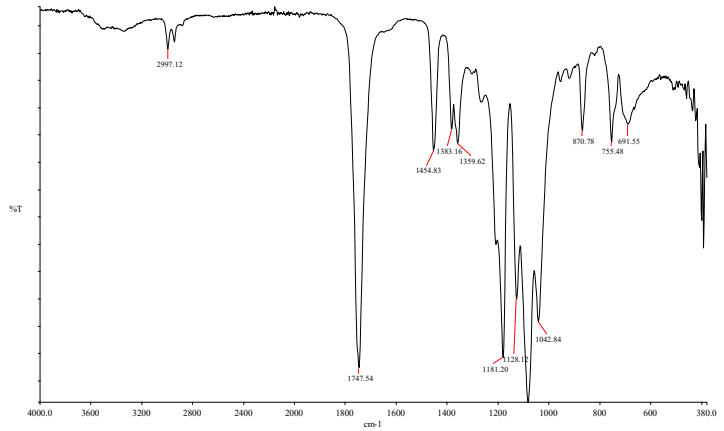

Figure S4: FT-IR spectrum for PLA sample.

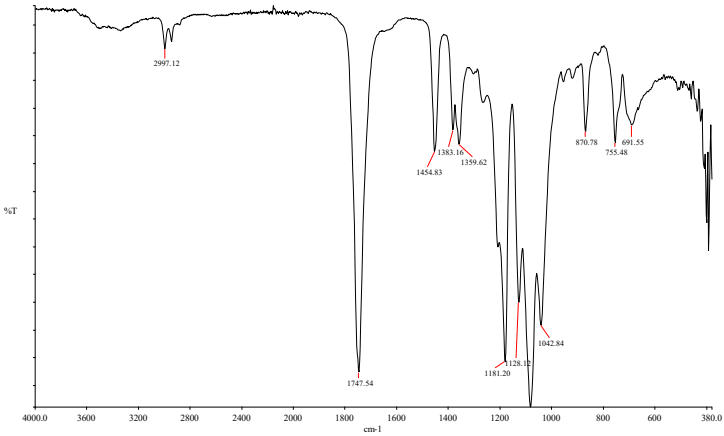

Figure S5: FT-IR spectrum of PLA5 sample.

^{1}H NMR analysis

In **Figure S6** is reported the ^{1}H NMR spectrum of PLA sample. As already seen for FT-IR spectra, no differences can be detected between standard PLA and nanocomposites spectra.

PLA5 spectrum is reported in **Figure S7.** ^{1}H NMR (400 MHz, $CDCl_3$) H-1 δ=5.18 ppm (q, J = 4 Hz), H-2 δ=1.60 ppm (d, J = 4 Hz).

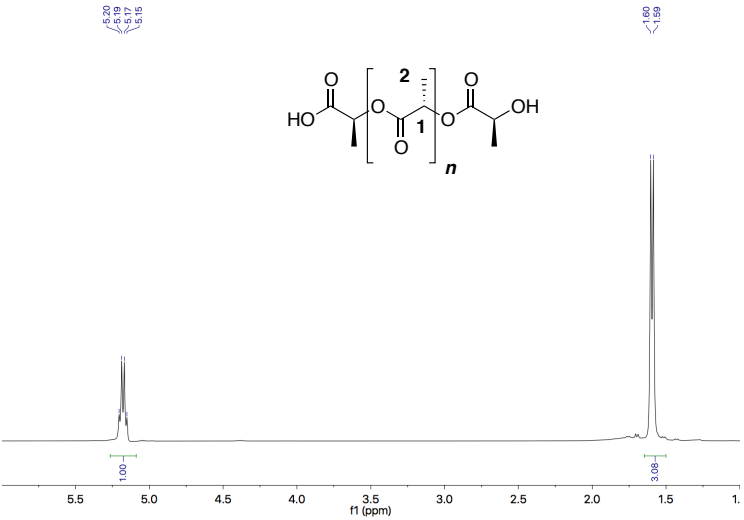

Figure S6: ^{1}H NMR spectrum for PLA sample.

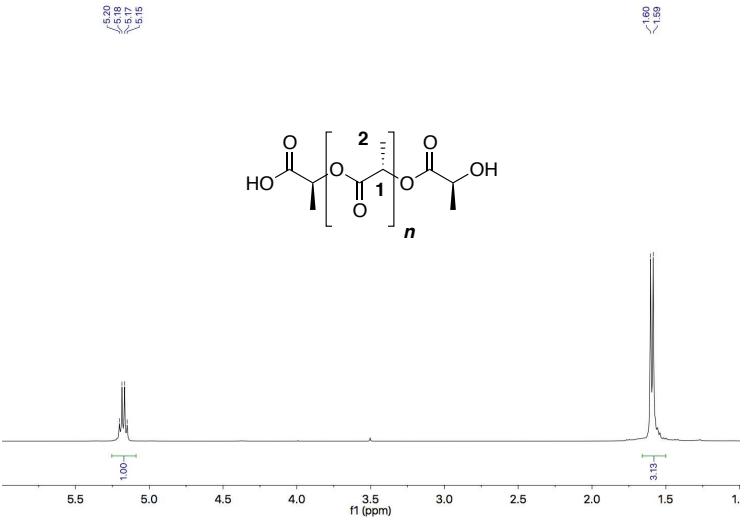

Figure S7: ^{1}H NMR spectrum for PLA5 sample.

DSC Analysis

In **Figure S8** DSC thermograms for PLA, PLA0.5 and PLA2 samples are reported, while in **Figure S9** DSC thermograms for PLA2.5, PLA3 and PLA5 are reported.

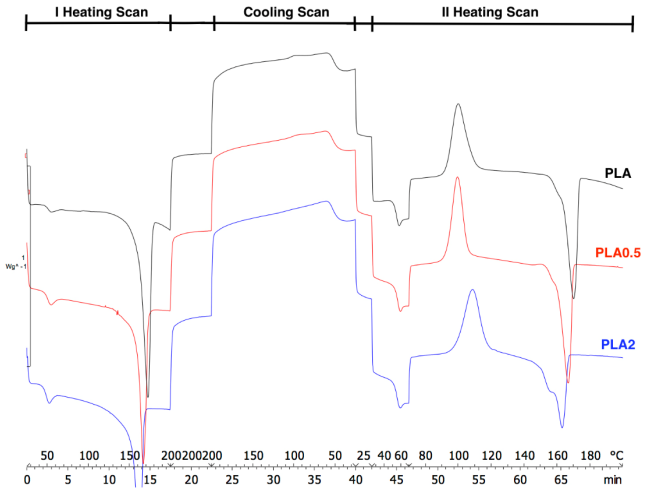

Figure S8: DSC thermograms for PLA, PLA0.5 and PLA2 samples.

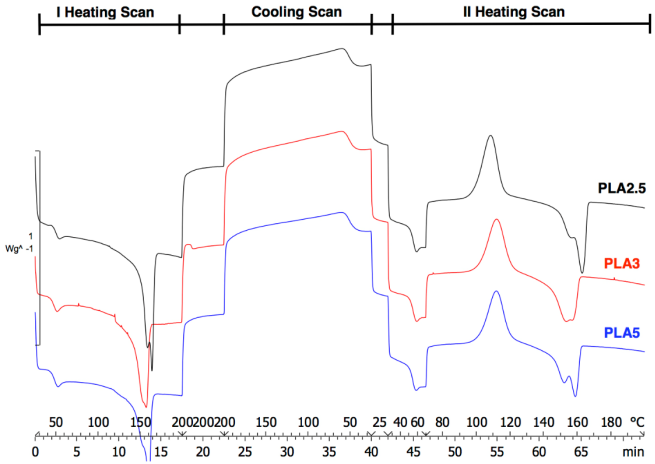

Figure S9: DSC thermograms for PLA, PLA0.5 and PLA2 samples.

Filtration and analysis

Solutions of nanocomposites in dichloromethane were filtered and the residue weighted, in order to make an estimation of the quantity of PLA grafted onto CNC surface. PLA3 and PLA0.5 samples were chosen for an initial comparison with the aim to determine if this methodology could give accurate results. In **Table S1** weight data relative to PLA0.5 and PLA3 are reported.

	Sample	
	PLA0.5	**PLA3**
Weighted Sample (mg)	172.47	142.86
Theoretical CNC weight (mg)	0.86	4.16
Measured CNC weight (mg)	0.90	4.35
Excess percentage	4.65	4.56

Table S6: data relative to residual weight after filtration of PLA0.5 and PLA3 dichloromethane solutions.

It appears that a residue remains in the filter in both samples. What is important is that in both cases filter has been washed extensively with dichloromethane, in order to avoid possible PLA residues on the filter. That said, all weighted residues has to be attributed to insoluble species with dimensions greater than the filter pores (i.e. 0.45 μm). Given the small dimensions of nanocrystals they are expected to surpass the membrane without being retained. It is reasonable to assume, however, that CNC aggregates can form during the synthesis, generating species with greater dimensions than filter pores. As **Table S1** indicates, both samples show an excess of around 4% greater in residual weight over the theoretical CNC weight. This datum cannot be considered reliable, since a part of cellulose nanocrystals passes through filter pores (i.e. the peaks at low retention times in SEC analyses are relative to these species) but cannot be quantified. Since a part of the crystals passes through the pores and a part remains on the filter, it is impossible to correctly quantify the quantity of PLA grafted onto CNC surface through this experimental approach.

The residue on the filter has been analyzed through FT-IR analysis, in order to determine its nature. In **Figure S10** is reported the FT-IR spectrum of the filter residue alone. In **Figure S11** and **Figure S12** are reported comparisons between filter residue spectrum and PLA and CNC spectra. It appears that the spectrum of the residue closely resembles the spectrum of the CNC alone. However, it can be noticed that signals relative to PLA are present

in the residue, particularly for what regards the peak at 1756 cm^{-1} which belongs to PLA carbonyl. This comparison is useful to demonstrate that filter residue is a CNC based material with PLA on it. It can be assumed that these PLA signals are not relative to PLA residues after filtration since the filter had been extensively washed with DCM.

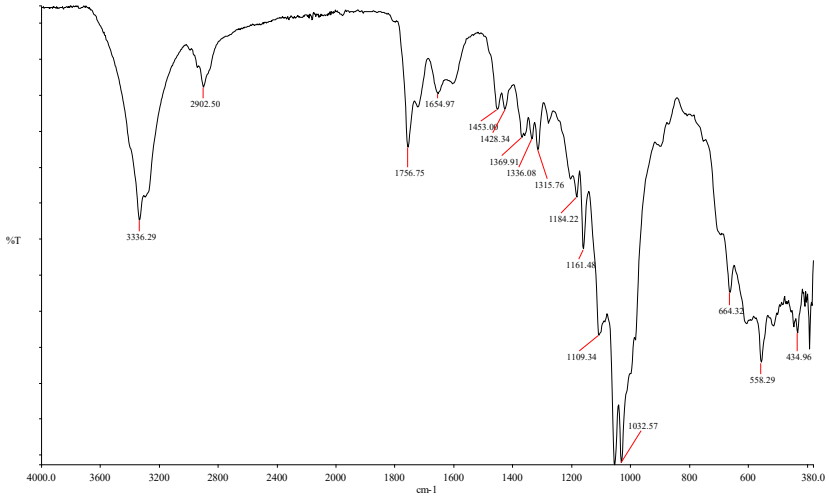

Figure S10: FT-IR spectrum of filter residue.

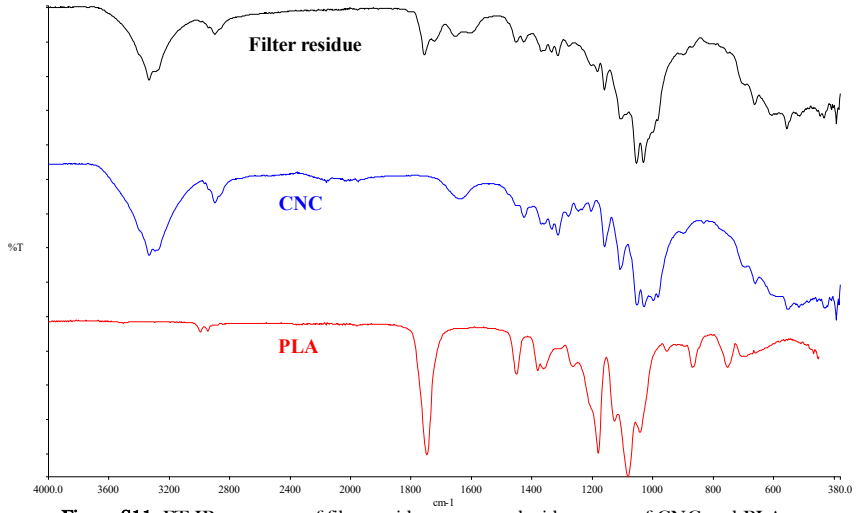

Figure S11: FT-IR spectrum of filter residue compared with spectra of CNC and PLA.

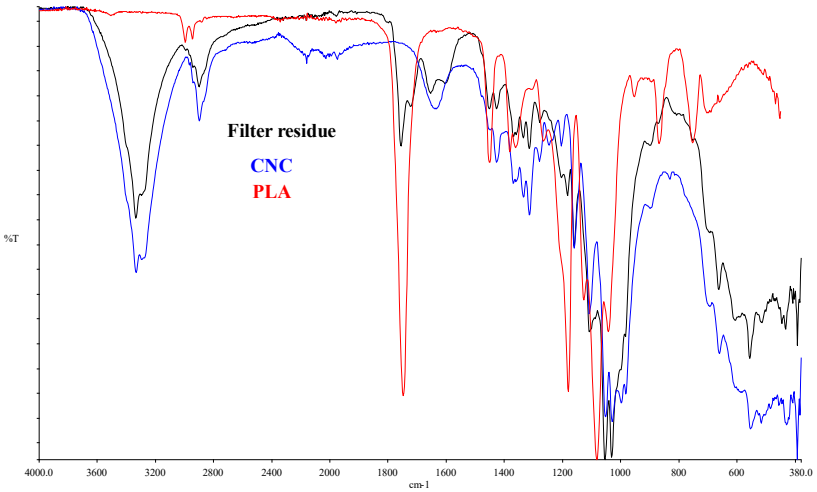

Figure S12: FT-IR spectrum of filter residue compared with spectra of CNC and PLA.

Cellulose Nanofibrils as reinforcing agents for PLA-based nanocomposites: an *in situ* approach

One-pot *in situ* polymerization approach was explored for the preparation of polylactide (PLA)-cellulose nanofibril (CNF) bio-nanocomposites. CNF were first prepared through enzymatic and mechanical treatment of softwood pulp. The bio-nanocomposites- were then fabricated through ring opening polymerization (ROP) of L-lactide, in the presence of various amounts of fibrils. Molecular weight, thermal properties, surface morphology, mechanical and wettability properties of the PLA-CNF nanocomposites were evaluated. DSC analysis demonstrated the effect of CNF on crystallization and crystalline morphology of PLA. Improved modulus for the nanocomposites with respect to standard PLA was demonstrated, however, the differences in tensile stress were small propably do to the counteracting effects of reinforcement from CNF and the decreasing molecular weight as a function of CNF concentration. The absence of pulled-out fibers was assessed, highlighting the strong interface and covalent attachment of PLA chains on CNF surface. Finally, the covalent bonding of PLA chains on CNF surface was demonstrated by isolating the non-soluble part, consisting of PLA-grafted CNF, and characterization of this residue.

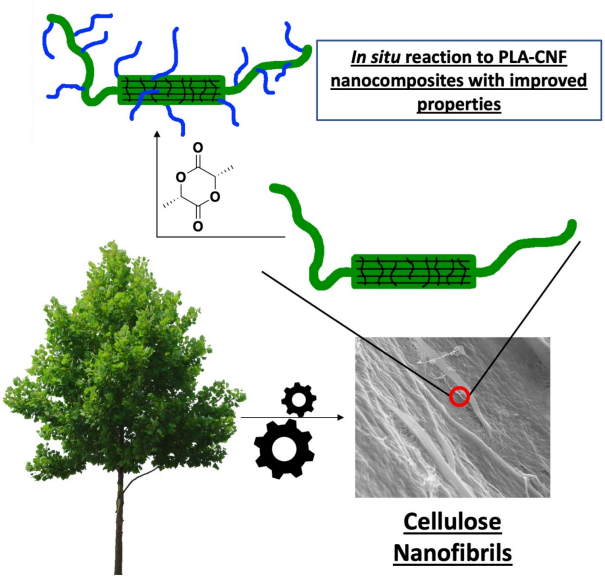

Submitted to Composites Science and Technology

1. Introduction

Industrial interest around Polylactide (PLA) as a promising environmentally friendly alternative to oil- derived plastics continuously increases year by year. In 2012 the world production of PLA was quantified in c.a. 180,000 tons, but according to estimates, it could rise to 800,000 tons by 2020.[1] Today one large research goal is to improve the chemical, physical and mechanical properties of PLA, in order to fully exploit its potential. To fill the performance gaps one of the most investigated approaches is the preparation of *nanocomposites*, i.e. composite materials consisting of nanometric size additives dispersed within a polymeric matrix leading potentially to improvement of e.g. thermal and mechanical properties of the final material.[2, 3] The nanometric size coupled with the high area to volume ratio, provides huge interface between the particle itself and the polymeric matrix. When good interfacial interaction and proper dispersion of the filler into the polymer is reached, the newly formed material can exhibit significantly improved properties, that couldn't be achieved with larger scale particulate reinforcements, at least not on the same low level of filler material.

Many PLA-based nanocomposites have been prepared and described. Among them, the best results have been obtained with carbon nanotubes,[4] montmorillonite,[5-8] nanosilica[9] and carbon dots.[10] Aiming to produce fully organic *bio*-nanocomposites, we recently considered cellulose nanocrystals (CNC) as biocompatible, biodegradable and renewable additives with strong properties useful for increasing the performance of the final PLA-nanocomposite.[11,12] An *in situ* melt polymerization approach was described for the preparation of PLA-CNC nanocomposites. The exploitation of free -OH groups on CNC surface as initiators for the ring opening polymerization (ROP) of lactide resulted in an optimal compatibilization between the two phases. Final materials showed a considerable improvement in thermal and rheological properties with respect to standard PLA and conventional PLA-CNC nanocomposites.[13]

Aiming at further exploring the potentialities of an *in situ* approach for the preparation of new generation nanocomposites, the use of cellulose nanofibrils (CNF) as fillers was here investigated.

CNF are described as an aggregation of 10-50 cellulose elementary fibrils, showing extremely high Young modulus (≈140 GPa), high aspect ratio and large surface area.[14-16]

These properties make them ideal candidates as strengthening agents for polymeric materials. They can be extracted from almost all cellulose sources, e.g. wood,[17] hardwood and softwood pulps,[18] cotton fibers,[19] banana peel,[20] *cassava root bagasse and peelings*,[21] waste papers[22] and many others sources, through mechanical defibrillation, making them valuable also from an environmental point of view.

Given their green nature coupled with outstanding mechanical properties, CNF can be considered as one of the most promising reinforcing agents for the preparation of PLA-based bionanocomposites.[23] Common PLA-CNF nanocomposite preparation methodologies rely on either melt blending[24] or solution casting.[25] These preparation strategies suffer from the strong difference in polarity between CNF and PLA, that makes the dispersion of the filler inefficient.[26, 27] For this reason, many different cellulose functionalization approaches were developed, in order to improve the compatibility between the two phases. Surface silylation,[28, 29] esterification[30, 31] and amination[32] are some of the most investigated reactions. Surface modification reaction prior to dispersion usually offers good results in terms of compatibilization but requires additional synthetic steps that could in principle damage the crystalline integrity of the fibers. In addition, the use of additional chemicals required for functionalization reactions could be negative from the environmental point of view. The application of an "one pot" approach, such as *in situ* synthesis, would therefore be highly advantageous from an environmental point of view and could, in principle, end up in an optimal interface between CNF and PLA. In particular, the free surface hydroxyl groups on CNF could be exploited as initiators in the ring opening polymerization (ROP) of lactide. This would result in a direct functionalization of CNF with PLA chains, anticipated to result in strong interface and good dispersion of the filler within PLA matrix.

2. Experimental section

2.1 Chemicals and Materials

The bleached softwood pulps used as raw materials for CNF production were kindly supplied by Innovhub (Milan; Italy). Endo-1,4-β-D-glucanase (FiberCare R) was purchased from Novozymes Italia S.r.l. (Monza; Italy) and L-lactide was purchased from Corbion (Gorinchem; Netherlands). All other chemicals including Tin(II) 2-ethylhexanoate, 92.5-100 %; Chloroform ($CHCl_3$), ≥ 99.5 %; Dichloromethane (CH_2Cl_2, DCM), ≥ 99.8 % were purchased by Sigma-Aldrich and used as received.

2.2 CNF extraction

In accordance with UNI EN ISO 5264-2:2011, bleached softwood pulps were initially mildly treated until achieving 25-30 °SR level of freeness with a lab PFI mill. The obtained cellulose pulp was then subjected to an enzymatic treatment by using FiberCare R type enzyme, an endoglucanase able to hydrolyze the 1,4 -D-glycosidic bonds of cellulose. The enzymatic reaction was conducted in a reactor equipped with elix shaft at 50°C for 1h. The enzyme dosage was 0.1 kg/ton. Final part of the enzymatic treatment was a further refining of the cellulose pulp in order to achieve level of freeness around 75-80 °SR, which represents the maximum limit of refining obtainable with lab equipment.

Cellulose pulp water dispersed with 2 % w/w fiber concentration was subjected to 7 homogenization cycles. The first 3 cycles were subjected to a different pression each one (500; 1000; 1300 bar) follow by the last 4 cycles with 1500 bar as a level of pressure. CNF dispersion obtained at the end of the treatment had a solid concentration of approximately 2 % w/w.

2.3 Synthesis of PLA

PLA was synthesized from L-lactide in bulk according to the following procedure. L-lactide (25 g) and tin octanoate (0.3 % w/w on lactide), added as a catalyst, were introduced in a 250 mL three necked round bottomed flask. Slow nitrogen flow was used to ensure the presence of inert atmosphere during the polymerization reaction. Mechanical stirring was

provided (40 rpm). Reaction was conducted in a closed oven at 180 °C for 1 hour. At the end of the reaction, the polymer was left to cool overnight under nitrogen atmosphere.

2.4 Synthesis of PLA-CNF nanocomposites

Nanocomposites were synthesized by in situ polymerization, from L-lactide in bulk according to the following procedure. CNF were put in a three-necked round bottomed flask and dispersed in 50 mL of acetone under vigorous stirring and ultrasound treatment. This procedure ensured the disaggregation of the lyophilized fluffy CNF mass into single fibrils.

25 g of L-lactide was then added and left under stirring until complete dissolution. Acetone was evaporated using nitrogen flux and the reaction mixture was heated to 70 °C under vacuum in a closed oven for 2 hours in order to remove any residual moisture. After this drying step, reaction was performed following the procedure described for the synthesis of PLA. Plain PLA and four nanocomposite samples with percentage of CNF 0, 0.1, 0.25, 0.5 and 1.0 % w/w were prepared and named as PLA, NC1, NC2, NC3 and NC4, respectively.

2.5 Differential scanning calorimetry (DSC)

Mettler-Toledo 820 was utilized to conduct the measurements. 5 mg of each sample was placed in a 100 µl aluminium cup with a pinhole on the lid. The applied heating rate was 10 °C min-1 in a nitrogen atmosphere (rate 50 ml min-1). Thermal behaviour of the samples was investigated using the following temperature cycles: First heating from 25 °C to 200 °C, then kept 5 min isothermally at 200 °C, cooling from 200 °C to 25 °C and kept 2 min isothermally at 25 °C. This was followed by second heating from 25 °C to 200 °C. The first heating and cooling, were run to eliminate residual internal stresses deriving from the synthesis. Glass transition temperature (T_g), cold crystallization temperature (T_{cc}) and melting temperature (T_m) were determined from the second heating curve.

2.6 Thermogravimetric analysis (TGA)

Mettler-Toledo TGA/SDTA 851e was utilized for thermal analysis. 5 mg of each sample was placed into a 70 µl alumina cup and heated at a rate of 10 °C min^{-1}. The measurements were performed under 80 ml min^{-1} nitrogen flow.

2.7 Size exclusion chromatography (SEC)

Verotech PL-GPC 50 Plus system equipped with a PL-RI Detector and two PLgel 5 µm MIXED-D (300 x 7.5 mm) columns from Varian were employed for the measurements. Chloroform was used as the mobile phase (1 ml/min, 30 °C) and toluene as an internal standard to correct for flow rate fluctuations. The calibration was based on polystyrene standards with a narrow molecular weight ranging from 160 to 371 000 g/mol. Samples solutions were filtered on 0.45 µm filters before the analysis. Molecular weight data therefore refers only to the soluble part that went through the filter pores.

2.8 Tensile testing

The testing was conducted on an INSTRON 5944 module equipped with pneumatic grips. A 500 N load cell was used for the measurements with a gauge length of 10 mm, and a crosshead speed of 5 mm/min was applied. The samples were cut into strips of width 0.5 cm with a thickness of an average of 0.1 mm. Before analysis, the test strips were preconditioned according to ASTM D618−96 (40 h at 50 % ± 5 % relative humidity and 23°C ± 1 °C).

2.9 Fourier transform infrared spectroscopy (FT-IR)

FT-IR Spectrometer (Spectrum 100, PerkinElmer) with an attenuated total reflection (ATR) was used to register spectra for PLA, all nanocomposites and CNF alone.

2.10 Water contact angle

Wettability of the PLA/CNF films with different % of CNF (0; 0.1; 0.25; 0.5) were determined by measuring static contact angles (θ) of polar Milli-Q water (18.3 MΩ cm) using a KSV Instruments LTD CAM 200 contact angle meter. All the static contact angles were determined by using sessile drop method at room temperature (23 °C; ≈ 40% RH) on four different positions for each sample by dropping 3 ± 0.5 µL of liquid onto the substrate. The contact angle values (θ) were detected 5 s after the deposition of water droplet onto the

sample. Statistical analysis experimental data were analyzed using a one-way analysis of variance (ANOVA) conducted using Statgraphics® S-plus 5.1 as statistical software, assuming p-value ≤ 0,05.

2.11 Scanning electron microscopy (SEM)

SE- 4800 SEM (Hitachi, Japan), operating at a low accelerated voltage of 0.5 keV to avoid damaging the matrix, was utilized to characterize the films. Prior to SEM observation, all samples were sputter-coated with a 3.5 nm-thick gold layer. For additional SEM observations of the sample morphology, the PLA and NC4 films were etched in a water−methanol (1:2, v:v) solution containing 0.025 mol/L of sodium hydroxide and 1 mol/L of sodium chloride for 16 h at 10 °C.

2.12 Films Casting

Films for SEM analyses and tensile testing were obtained by casting from a chloroform solution; 2 grams of polymer was dissolved into 30 mL of $CHCl_3$ at 30 °C. The solution was cast on a glass surface and the solvent was evaporated at room temperature and pressure overnight. Films were then kept in vacuum at 25 °C for three days. Complete evaporation of the solvent was checked through TGA analysis.

2.13 Isolation of CNF

CNF in nanocomposites was isolated through centrifugation process as indicated: ≈ 1 g of sample (PLA, NC1, NC2, NC3 and NC4) was dissolved in 50 ml of DCM and centrifuged at 4000 rpm for 10 minutes. This operation was repeated three times for each sample, removing each time the liquid part, in order to completely remove the soluble species. Residue was dried in vacuum oven at room temperature until constant weight was reached. Quantity of PLA bounded to CNF surface was determined as ratio between the weight of the isolated species and theoretical weight of CNF introduced in the feed.

3. Results and discussion

The efficacy of an in situ polymerization approach for the synthesis of cellulose nanofibril-containing PLA-based nanocomposites was demonstrated. Different nanocomposites were synthesized, with increasing concentration of CNF in the feed. Properties of the resulting materials were studied and the effect of different CNF concentrations investigated. Cellulose nanofibrils were also isolated after the reaction and characterized, demonstrating the presence of PLA bounded to the surface.

3.1 Synthesis of nanocomposites

Nanocomposites were synthesized through an *in situ* polymerization reaction with different concentrations of CNF in the feed. The aim was to exploit the free OH groups on CNF surface as initiators for the ROP of L-lactide to directly functionalize the surface of the fibrils by "grafting-from" approach. The covalent bond between the nanofibrils and PLA-grafts is expected to lead to effective compatibilization between the nanofiller and the polymer matrix. A schematic representation of the reaction is shown in **Figure 1**.

The product of the reaction was expected to be a complex mixture of species including both PLA chains bounded to CNF surface, as represented in **Figure 1**, as well as free PLA chains. These free chains can be analyzed through SEC analysis and they also give an indication of the length of the PLA chains grafted on the surface of CNF.

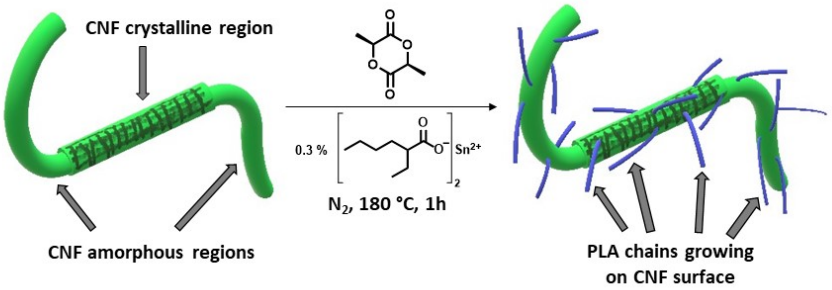

Figure 1: Schematic representation of the "grafting-from" reaction resulting in PLA chain growing from the CNF surface.

3.2 Molecular weight determination

SEC analyses were performed in order to determine the effect of CNF on the reaction outcome in terms of molecular weights of the synthesized PLA chains. The results are reported in **Table 1**.

Table 1. The molecular weight of the PLA chains with increasing concentration of CNF.

Sample	Cellulose Nanofibrils (wt%)	$\overline{M_n}$ (g mol^{-1})[a]	$\overline{M_w}$ (g mol^{-1})[a]	Đ
PLA	0	284 000	384000	1.4
NC1	0.1	247 000	351000	1.4
NC2	0.25	212 000	294000	1.4
NC3	0.5	106 000	153000	1.4
NC4	1	54000	74000	1.4

[a] The molecular weight was determined against PS calibration.

Molecular weight data show a steady decrease of the molecular weight as a function of increasing CNF concentration in the feed (see **Figure 2**). This is in good agreement with the hypothesis and expectation that the free -OH groups on CNF surface act as initiators for the ROP of lactide. The increase in CNF concentration, thus, resulted in an increase of initiator concentration, which further resulted in larger number of PLA chains initiated leading to decreased average molecular weight. Differences were already detectable between NC1 and NC2 samples and it appears that going from NC2 to NC3 as the concentration of CNF doubles, the molecular weight of the product decreases by half. Similar behavior and further halving is observed going from NC3 to NC4.

Figure 2: Graphical representation of the decrease of the molecular weight as a function of increasing CNF concentration.

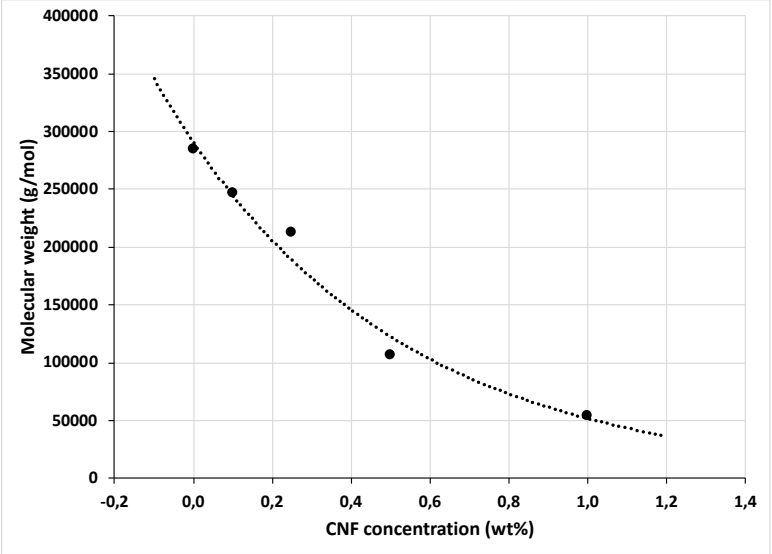

3.3 Thermal properties and cristallinity

The thermal stability of the composites and PLA were investigated by TGA and the degradation data for all the materials are reported in **Table 2** with temperatures relative to 5 % ($T_{5\%}$), 50 % ($T_{50\%}$) and 95 % ($T_{95\%}$) weight loss. No significant differences were detectable among all the nanocomposites nor in comparison with the plain PLA sample.

The influence of CNF on the thermal properties and crystallinity was evaluated by DSC. The DSC thermograms related to second heating scan for all the samples are reported in

Sample	$T_{5\%}$	$T_{50\%}$	$T_{95\%}$
PLA	242.4	285.0	309.1
NC1	242.0	279.2	306.3
NC2	236.7	283.4	309.3
NC3	237.9	283.2	309.1
NC4	234.8	284.1	309.7

Table 2. $T_{5\%}$, $T_{50\%}$ and $T_{95\%}$ from TGA for all the samples.

Figure 3. DSC thermograms illustrating the second heating scan as well as an expansion of the first heating scan in the melting peak region.

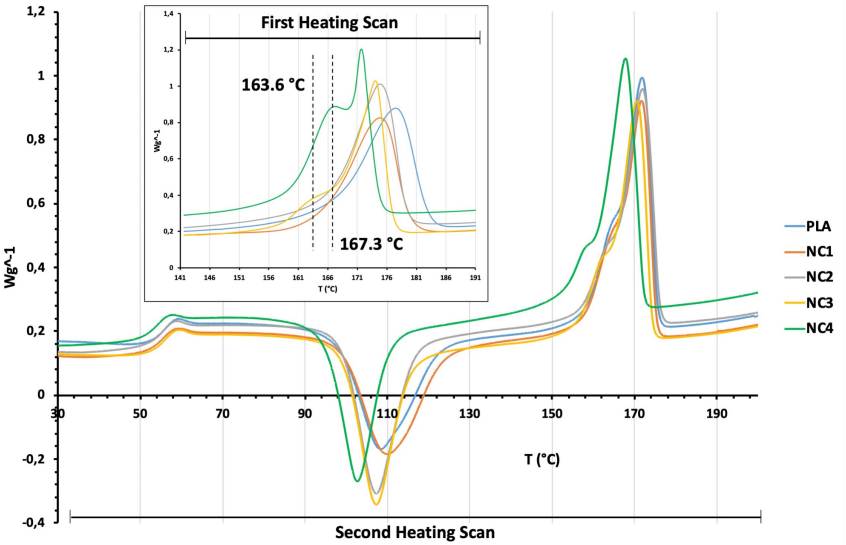

Figure 3, together with an expansion of the first heating scan in the melting peak region. Complete thermograms for all samples are reported in the SI file.

Sample	*First Heating Scan*			*Second Heating Scan*		
	T_g	T_m	χ_c	T_{cc}	T_m	χ_c
PLA	54.5	177.8	57.5	108.4	171.8	6.2
NC1	53.7	174.2	52.7	110.0	171.7	4.2
NC2	53.6	175.2	50.8	107.2	171.9	2.9
NC3	54.3	174.2	53.6	107.2	170.7	5.1
NC4	52.6	171.8	65.3	102.7	167.8	10.0

Table 3. Thermal properties and crystallinity data for all samples.

Thermal characteristics from the DSC thermograms from both first and second heating scans are reported in **Table 3**. The thermal behavior of the samples, aside the glass transition temperature (T_g), is affected by the concentration of CNF, which particularly influenced

the crystallinity of the samples. It has been reported that for classical PLA-CNF nanocomposites, prepared through post-polymerization solution mixing, there are two observed influences. In particular, at low concentrations (≤ 1 wt %) the addition of CNF promoted the crystallization.[33] On the other hand, at higher concentrations (10 wt %) the nanofibrils had detrimental effect on crystallization behavior of PLA.[34] These results were attributed to the large CNF aspect ratio as well as to the entanglements that restricted the conformational freedom of PLA chains which is necessary for efficient organization in ordered crystals. As the DSC data in **Table 3** shows, the synthesized samples were characterized by a peculiar trend that can be related to the previous observations. In particular, there is a decrease in degree of crystallinity going from PLA to NC1 and NC2 samples. Then, the crystallinity again increases for NC3 and reaches the highest value among the studied materials for NC4. In order to explain this trend, the covalent bond between CNF and PLA, could reduce the mobility of the chains, hindering the crystallization. Since several PLA chains can be attached to one CNF, the total molecular weight of these grafted products can be multiple to the values reported in **Table 3**, which will also increase the number of entanglements and could further decrease the chain mobility. However, as the concentration of fibrils increased, the molecular weight of the PLA-grafts decreased, which probably promoted the crystallization process. This hypothesis fits well with thermal data relative to NC4 sample, which also clearly exhibited the lowest cold crystallization temperature among all samples, indicating a higher tendency to crystallize. Although the actual degrees of crystallinity are very different from the first and second heating scan, due to the low crystallization rate of PLA, the same degree of crystallinity trend can be observed during the first and second heating scans. In addition, during the first heating scan, NC4 sample and to some degree NC3 show a bimodal melting peak, as highlighted by the expansion in **Figure 3**. In particular, the melting transition of NC3 is characterized by a small shoulder at 163.6 °C, in addition to the main melting peak at 174.2 °C, while NC4 appears to have two clear melting peaks at 167.3 °C and 171.8 °C. The other materials, PLA, NC1 and NC2, have single melting peaks at temperature range 174.2-177.8 °C. This behavior can be explained by the formation of two different crystalline phases. PLA can either crystallize in a well-ordered α crystalline phase as well as in a less ordered α' structure. α' crystals form as disordered counterparts of α crystals with lower melting temperature as compared to α crystals.[35] Their presence in these samples could be explained by the high concentration of CNF possibly both acting as nucleation agents and causing some prevention of chain movement due to the covalent attachment, which could lead to less ordered crystal structure.

3.3 Morphological characterization by SEM

The film surfaces were also characterized through SEM analyses to evaluate how CNF affects the surface morphology of the films. The difference in polarity between CNF and PLA has been described as the biggest hurdle for an efficient dispersion of the filler. For this reason, different compatibilization reactions have been described with the aim of improving dispersibility.[28-32] Here the covalent attachment between PLA chains and CNF should effectively improve the dispersion of CNF. SEM micrographs of films' surface are reported in **Figure 4**.

Samples showed significantly different surfaces, depending on the CNF concentration. In particular, the observed surface morphologies correlated with the degree of crystallinity of the films determined through DSC analyses from the first heating scan. Round spherulite crystal structures became less and less visible going from PLA to NC2.

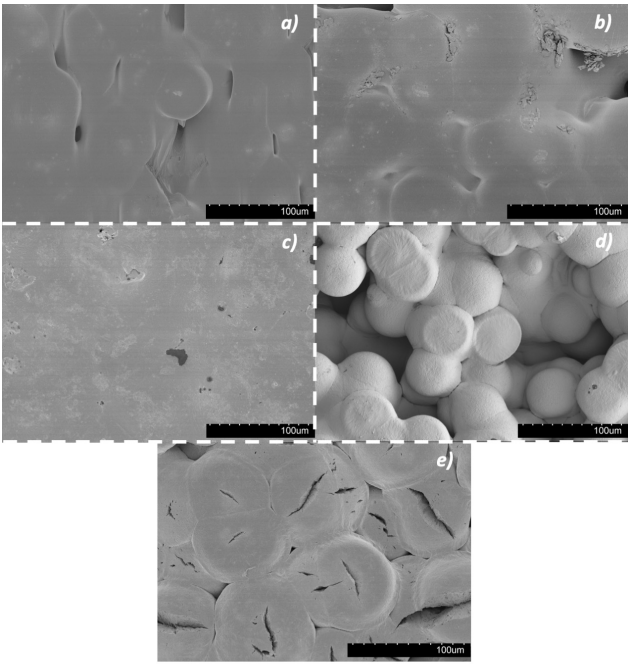

Figure 4. SEM micrographs for ***a)*** PLA, ***b)*** NC1, ***c)*** NC2, ***d)*** NC3, and ***e)*** NC4.

Figure 5. SEM micrographs of **a)** etched PLA sample and **b)** etched NC4 sample.

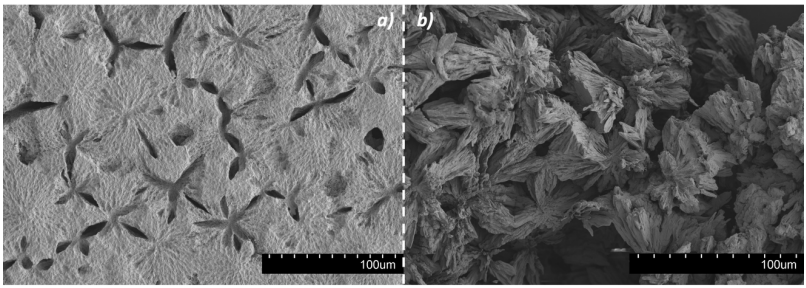

Figure 4*c* shows an almost completely flat surface of NC2, which had the lowest crystallinity degree among all synthesized polymers. NC3 product was characterized by a highly irregular surface, with well defined, round spherulite type structures. Finally, NC4 illustrated again spherulite type structures on the surface of the films. Etching process was conducted on PLA and NC4 samples, in order to remove the amorphous parts and better expose the crystalline structure of the materials. Micrographs of the etched samples are reported in **Figure 5**.

The etched samples showed clear differences in crystalline patterns between the two samples. Standard PLA appears to have a much more regular disposition of crystal lamellae in more planar spherulite structures. In NC4 nanocomposite crystallites were significantly more exposed after the etching, probably due to the lower molecular weight of the polymer. Their spatial arrangement seems less ordered and they are growing in more tridimensional manner. Even if it was not possible to fully observe CNF embedded in the matrix, it can be assumed that they had a strong effect in defining these clearly different morphologies of the final material, as already reported in literature.[34]

3.4 Tensile testing

Tensile testing was performed to evaluate the effect of CNF on the mechanical properties of the synthesized nanocomposites.

Tensile testing was performed on the prepared films. However, the testing of NC4 film was not possible due to the brittleness of the material.

Table 4. Mechanical properties of the synthesized samples.

Sample	Young's Modulus [GPa]	Tensile strain at break [%]	Tensile stress at break [MPa]
PLA	1.9 ± 0.1	40.6 ± 0.7	23.7 ± 0.6
NC1	2.2 ± 0.1	11.8 ± 0.6	24.8 ± 0.8
NC2	2.2 ± 0.2	5.5 ± 0.3	23.0 ± 0.9
NC3	2.6 ± 0.2	2.2 ± 0.2	21.0 ± 0.6

The results for PLA, NC1, NC2 and NC3 are reported in **Table 4.** An increased brittleness and decreased tensile strain were detected with increasing concentration of CNF, while Young's modulus shows a significant increase as a function of CNF concentration (maximum increase ≈ 37%). Literature data report a strengthening effect of CNF in PLA/CNF nanocomposites, given the outstanding mechanical strength of nanofibrils.[36] In particular, previous reports of such nanocomposites prepared through solvent casting demonstrate an increase of both modulus and tensile strength. As data reported in **Table 4** show, tensile stress at break of NC1 and NC2 is quite similar to that of PLA, while slight decreases are noticed for NC3. In order to explain this behavior, the molecular weight of the matrix has to be considered. To this regard, it was reported that the decrease of molecular weight of pure PLA has detrimental effect on material's mechanical properties.[37] In addition, lower molecular weight matrices in nanocomposites lead to a significant decrease in tensile strength of the final material.[38, 39] That said, considering the great difference in molecular weight between PLA and NC3 samples (> 50%), the small decrease registered still appears as a promising result.

With increasing concentration of CNF in the feed, the material becomes stiffer, resulting in a consistent decrease in strain at break. The stiffening effect of CNF in many different polymeric matrices has been widely discussed.[40-43]

The fractured surfaces were examined by SEM, in order to determine the possible presence of pulled-out fibers, see **Figure 6.**

Figure 6. SEM images of the fractured surfaces of **a)** PLA, **b)** NC1, **c)** NC2, **d)** NC3.

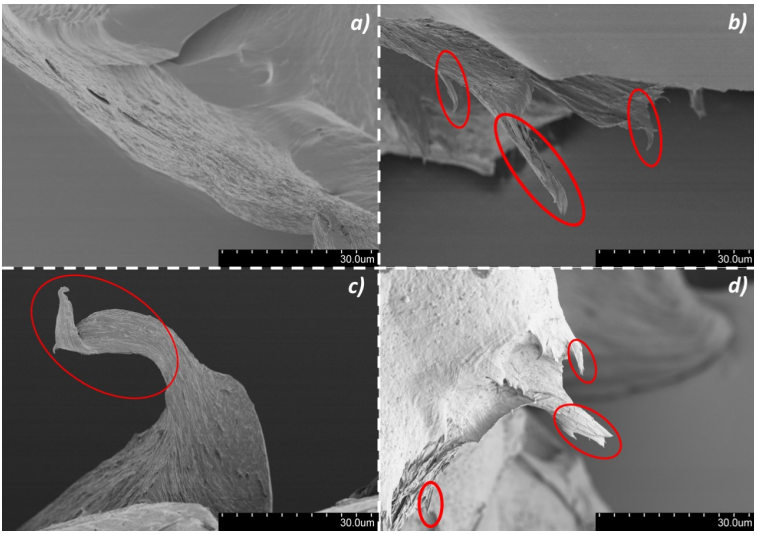

Samples showed clearly different morphologies depending whether cellulose nanofibers were present or not. In particular, the fracture surface for PLA sample appears to be smooth and regular. On the other hand, NC1, NC2 and NC3 samples are characterized by the presence of protruding regions that are likely attributable to PLA-covered fibers.

During the mechanical stress, CNF can act as bridging species between the two halves of the breaking specimen and remain exposed after breakage. This bridging action of CNF is highlighted in **Figure 7** on a non-completely broken surface of NC2 sample.

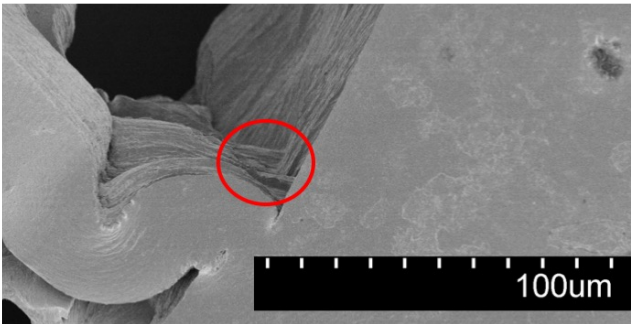

Figure 7. An example of the bridging effect CNF in NC2 sample.

None of the analyzed samples show signs of pulled-out fibers. This is a good indicator of the efficiency of the applied synthetic methodology, which results in strong interface between the filler and the matrix coupled together by covalent bonds.

3.5 Water contact angle measurements

The water contact angle measurements were performed on PLA, NC1, NC2 and NC3 films, since NC4 was too brittle to obtain a good film. Static water contact angle values are reported in **Table 5**.

Table 5. Water contact angle values for the analyzed samples.

Sample	Static contact angle (θ)
PLA	69.4 ± 4.0^{a}
NC1	69.2 ± 3.6^{a}
NC2	74.3 ± 2.3^{a}
NC3	53.1 ± 0.4^{b}

PLA, NC1 and NC2 samples didn't show significant differences ($p \leq 0.05$) in terms of wettability. The surface of NC3, however, had clearly lower contact angle value, indicating more wettable surface as compared to the other materials tested.

FT-IR of the film surfaces (reported in the SI file) showed an -OH absorption band with higher intensity for nanocomposites in comparison to PLA. However, this difference could not be explanatory for the trend observed for water contact angle values. For this reason, it is reasonable to assume that these differences arise mainly from the significantly different surface topography, especially for NC3 described through SEM micrographs. In addition, NC2 had the most planar or smooth surface, which might explain the slightly higher contact angle value as compared to PLA and NC1.

3.6 Isolation of CNF with grafted PLA

CNF with grafted PLA chains were isolated from the free PLA chains through centrifugation protocol described in the experimental section. In **Table 6** the weight of the residue isolated through centrifugation is reported (residue weight) and compared to the theoretical CNF content in the sample, considering the initial loading of nanofibrils before the reaction. Weight of PLA grafted per milligram CNF was then been calculated as the ratio between the grafted PLA and the theoretical weight of CNF added.

Table 6. The weight of CNF, CNF-grafted and free PLA as well as the amount of PLA grafted per milligram CNF.

Sample	Theoretical CNF weight[a] (mg)	Residue weight (CNF+CNF grafted PLA)[a] (mg)	Soluble part (free PLA)[a] (mg)	PLA grafted to CNF (mg PLA/mg CNF)
PLA	0	0	1	0
NC1	1.0	79	921	78
NC2	2.5	82	918	32
NC3	5.0	222	778	43
NC4	10.0	219	781	21

[a]Normalized to 1 g of weighted sample.

It appears as a general trend that the more CNF in the feed, the less PLA is bounded to their surface. This observation is consistent with the observed values for molecular weight detected via SEC. As the concentration of CNF increases the length of the grafted chains decreases, due to the higher quantity of initiating species in the feed.

Isolated products were also characterized through FTIR spectra, which are reported in **Figure 8**.

Figure 8. FT-IR spectra of PLA; CNF and the products isolated after centrifugation.

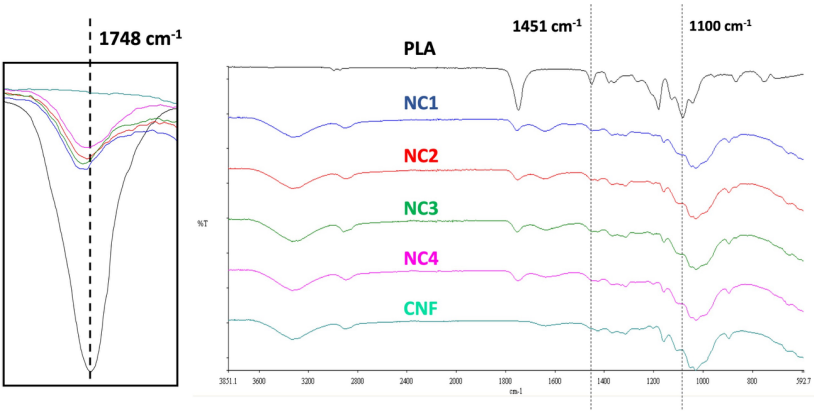

The spectra of the products isolated by centrifugation closely resembled the spectrum of CNF, therefore indicating the clear presence of CNF in these residues. As expected PLA-related signals were also be clearly detected. In particular, signals at 1451 and 1100 cm^{-1} are detected only for PLA and its nanocomposites. Even more evident is the band around 1750 cm^{-1} related to the carbonyl groups in PLA. As magnification in **Figure 8** shows, intensity of this carbonyl group signal in the nanocomposites follows the same trend observed for weight residues, confirming the different quantities of surface-bound PLA.

SEM images showing a comparison between starting CNF and isolated residue after centrifugation of sample NC4 are reported in **Figure 9**.

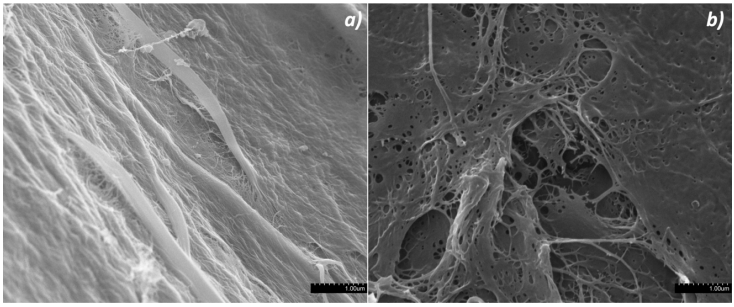

Figure 9. SEM comparison between ***a)*** neat CNF and ***b)*** isolated residue after centrifugation of sample NC4.

Figure 9a shows the presence of fibrous aggregates as well as free fibers. These aggregates are not more visible after the reaction (Figure 9b), further indicating good dispersion of CNF within the matrix. In addition, isolated fibers after centrifugation appear embedded in the polymer, demonstrating the covalent connection between the two phases.

4. Conclusions

On-pot *in situ* approach was successfully exploited for the synthesis of PLA-CNF nanocomposites. Different samples containing different quantities of fibrils were synthesized and the effects on the properties of the resulting materials studied accordingly. Exploiting free -OH groups as initiators in lactide ROP, the increase of CNF in the feed resulted in a decrease of the molecular weight of the product. While the presence of the fillers didn't have noticeable effects on the thermal stability of the products, their crystallization behavior and crystalline morphology was affected. It appeared that the dimensions and shape of crystallites could be correlated with the differences in crystallinity degree and melting temperatures observed through DSC analysis. Tensile tests proved an increased Young's modulus even with the decrease of the molecular weight. On the other hand, higher concentrations of CNF resulted in more brittle materials. Finally, the covalent bond between CNF and PLA chains was demonstrated, through isolation and analysis of the reacted fibrils.

References

1 M. Karamanlioglu, R. Preziosi, G. D. Robson, Abiotic and biotic environmental degradation of the bioplastic polymer poly(lactic acid): A review. *Polymer Degradation and Stability* **2017**, 137, 122-130.

2 A. J. Crosby and J. Y. Lee, Polymer Nanocomposites: The "Nano" Effect on Mechanical Properties. *Polymer Reviews* **2007**, 47, 217–229.

3 G. Armstrong, An introduction to polymer nanocomposites. *Eur. J. Phys.* **2015**, 36.

4 A. Akbari, M. Majumder and A. Tehrani, Polylactid acid (PLA) Carbon nanotubes composites. Handbook of Polymer Nanocomposites. Processing, Performance and application. **2015** DOI: 10.1007/978-3-642-45229-1_45.

5 M. Pluta, A. Galeski, M. Alexandre, M. A. Paul, P. Dubois, Polylactide/Montmorillonite nanocomposites and microcomposites prepared by melt blending: structure and some physical properties. *Journal of applied polymer science* **2002**, 86, 1497-1506.

6 P. Gelineau, S. Weigand, L. Cauvin, F. Bedoui, Compatibility effects of modified montmorillonite on elastic properties of nano-reinforced Poly(lactid acid): Experimental and modeling study. *Polymer testing* **2018**, 70, 441-448.

7 K. Fukushima, A. Fina, F. Geobaldo, A. Venturello, G. Camino, Properties of poly(lactid acid) nanocomposites based on montmorillonite, sepiolite and zirconium phosphonate. *eXPRESS Polymer letters* **2012**, 6, 914-926.

8 M. A. Ortenzi, L. Basilissi, H. Farina, G. Di Silvestro, L. Piergiovanni, E. Mascheroni, Evaluation of crystallinity and gas barrier properties of films obtained from PLA nanocomposites synthesized via "in situ" polymerization of L-lactide with silane-modified nanosilica and montmorillonite. *European polymer journal* **2015**, 66, 478-491.

9 L. Basillissi, G. Di Silvestro, H. Farina, M. A. Ortenzi, Synthesis and characterization of PLA nanocomposites containing nanosilica modified with different organosilanes II: effect of the organosilanes on the properties of nanocomposites: thermal characterization. *Journal of applied polymer science* **2012**.

10 H. Xu, L. Xie, J. Li, M. Hakkarainen, Coffee Grounds to Multifunctional Quantum Dots: Extreme Nanoenhancers of Polymer Biocomposites. *ACS Appl. Mater. Interfaces* **2017**, 9, 27972-27983.

11 F. V. Ferreira, A. Dufresne, I. F. Pinheiro, D. H. S. Souza, R. F. Gouveia, L. H. I. Mei, L. M. F. Lona, How do cellulose nanocrystals affect the overall properties of biodegradable polymer nanocomposites: a comprehensive review. *European polymer journal* **2018**, 108, 274-285.

12 E. Mascheroni, R. Rampazzo, M. A. Ortenzi, G. Piva, S. Bonetti, L. Piergiovanni, Comparison of cellulose nanocrystals obtained by sulfuric acid hydrolysis and ammonium persulfate, to be used as coating on flexible food-packaging materials. *Cellulose* **2016**, 23, 779-793.

13 S. Gazzotti, H. Farina, G. Lesma, R. Rampazzo, L. Piergiovanni, M. A. Ortenzi, A. Silvani, Polylactide/cellulose nanocrystals: The in situ polymerization approach to improved nanocomposites *European Polymer Journal* **2017**, 94, 173–184.

14 H. P. S. Abdul Khalil, A. H. Bhat, A. F. Ireana Yusra, Green composites from sustainable cellulose nanofibrils: A review. *Carbohydrate Polymers* **2012**, 87, 963–979.

15 K. Y. Lee, Y. Aitomäki, L. A. Berglund, K. Oksman, A. Bismarck, On the use of nanocellulose as reinforcement in polymer matrix composites. *Composites Science and Technology* **2014**, 105, 15–27.

16 K. Oksman, Y. Aitomäki, A. P. Mathew, G. Siqueira, Q. Zhou, S. Butylina, S. Tanpichai, X. Zhou, S. Hooshmand, Review of the recent developments in cellulose nanocomposite processing. *Composites: Part A* **2016**, 83, 2–18.

17 K. Abe, S. Iwamoto, H. Yano, Obtaining cellulose nanofibers with a uniform width of 15 nm from wood. *Biomacromolecules* **2007**, 8, 3276-3278.

18 W. Stelte, A. R. Sanadi, Preparation and characterization of cellulose nanofibers from two commercial hardwood and softwood pulps. *Industrial & engineering chemistry research* **2009**, 48, 11211-11219.

19 E. M. T. Teixeira, A. C. Correa, A. Manzoli, F. Leite, C. R. Oliveira, L. H. C. Mattoso, Cellulose nanofibers from white and naturally colored cotton fibers. *Cellulose* **2010**, 17, 595-606.

20 H. Tibolla, F. M. Pelissari, J. T. Martins, A. A. Vicente, F. C. Menegalli, Cellulose nanofibers produced from banana peel by chemical and mechanical treatments: characterization and cytotoxicity assessment. *Food Hydrocolloids* **2018**, 72, 192-201.

21 A. L. M. P. Leite, C. D. Zanon, F. C. Menegalli, Isolation and characterization of cellulose nanofibers from cassava root bagasse and peelings. *Carbohydrate polymers* **2017**, 157, 962-970.

22 H. Takagi, A. N. Nakagaito, M. Shahrill, Extraction of cellulose nanofiber from waste papers and application to reinforcement in biodegradable composites. *Journal of reinforced plastics and composites* **2013**, 32, 1542-1546.

23 Q. Ping, G. Yuan, W. Guo-feng, Z. Li-ping, Nanocomposites of poly(lactic acid) reinforced with cellulose nanofibrils. *BioResources* **2010**, 5, 1811-1823.

24 S. Yeng-Fong, C. Man-Yun, C. Wen-Chuan, L. Hong-Yuan, C. Chih-Ming, Completely biodegradable composites reinforced by the cellulose nanofibers of pineapple leaves modified by eco-friendly methods. *J. Polym. Res.* **2016**, 24, 209.

25 J. Trifol, D. Plackett, C. Sillard, P. Szabo, J. Bras, A. E. Daugaard, Hybrid poly(lactic acid)/nanocellulose/ nanoclay composites with synergistically enhanced barrier properties and improved thermomechanical resistance. *Polym. Int.* **2016**, 65, 988–995.

26 Y. Habibi, L. A. Lucia, O. J. Rojas, Cellulose Nanocrystals: Chemistry, Self-Assembly, and Applications. *Chem. Rev.* **2010**, 110, 3479–3500.

27 S. Fujisawa, T. Saito, S. Kimura, T. Iwata, A. Isogai, Surface Engineering of Ultrafine Cellulose Nanofibrils toward Polymer Nanocomposite Materials. *Biomacromolecules* **2013**, 14, 1541−1546.

28 C. Gousse, H. Chanzy, M.L. Cerrada, E. Fleury, Surface silylation of cellulose microfibrils: preparation and rheological properties. *Polymer* **2004**, 45, 1569–1575.

29 P. Qu, Y. Zhou, X. Zhang, S. Yao, L. Zhang, Surface Modification of Cellulose Nanofibrils for Poly(lactic acid) Composite Application. *Journal of Applied Polymer Science* **2012**, 125, 3084–3091.

30 S. Ifuku, M. Nogi, K. Abe, K. Handa, F. Nakatsubo, H. Yano, Surface Modification of Bacterial Cellulose Nanofibers for Property Enhancement of Optically Transparent Composites: Dependence on Acetyl-Group DS. *Biomacromolecules* **2007**, 8, 1973-1978.

31 S. Berlioz, S. Molina-Boisseau, Y. Nishiyama, L. Heux, Gas-Phase Surface Esterification of Cellulose Microfibrils and Whiskers. *Biomacromolecules* **2009**, 10, 2144–2151.

32 Y. Lua, M. C. Cueva, E. Lara-Curzio, S. Ozcan, Improved mechanical properties of polylactide nanocomposites-reinforced with cellulose nanofibrils through interfacial engineering via amine-functionalization. *Carbohydrate Polymers* **2015**, 131, 208–217.

33 W. Ding, R. K. M. Chu, L. H. Mark, C. B. Park, M. Sain, Non-isothermal crystallization behaviors of poly(lactic acid)/cellulose nanofiber composites in the presence of CO_2. *European Polymer Journal* **2015**, 71, 231–247.

34 H. Yu, H. Zhang, M. Song, Y. Zhou, J. Yao, Q. Ni, From Cellulose Nanospheres, Nanorods to Nanofibers: Various Aspect Ratio Induced Nucleation/Reinforcing Effects on Polylactic Acid for Robust-Barrier Food Packaging. *ACS Appl. Mater. Interfaces* **2017**, 9, 43920−43938.

35 M. Di Lorenzo, R. Androsch, Stability and Reorganization of α′-Crystals in Random L/D-Lactide Copolymers. *Macromol. Chem. Phys.* **2016**, 217, 1534−1538.

36 Z. Ying, D. Wu, Z. Wang, W. Xie, Y. Qiu, X. Wei, Rheological and mechanical properties of polylactide nanocomposites reinforced with the cellulose nanofibers with various surface treatments. *Cellulose* **2018**, 25, 3955–3971.

37 G. Perego, G. Cella, C. Bastioli, Effect of Molecular Weight and Crystallinity on Poly(lactic acid) Mechanical Properties. *Journal of Applied Polymer Science* **1996**, *59*, 37-43.

38 T.D. Fornes, P.J. Yoon, H. Keskkula, D.R. Paul, Nylon 6 nanocomposites: the effect of matrix molecular weight. *Polymer* **2001**, 42, 9929-9940.

39 D. Chu, Q. Nguyen, D. G. Baird, Effect of Matrix Molecular Weight on the Dispersion of Nanoclay in Unmodified High Density Polyethylene. *Polymer Composites* **2007**.

40 E. Abraham, B. Deepa, L. A. Pothan, M. John, S. S. Narine, S. Thomas, R. Anandjiwala, Physicomechanical properties of nanocomposites based on cellulose nanofibre and natural rubber latex. *Cellulose* **2013**, 20, 417–427.

41 M. J. Silva, A. O. Sanches, E. S. Medeiros, L. H. C. Mattoso, C. M. McMahan, J. A. Malmonge, Nanocomposites of natural rubber and polyaniline-modified cellulose nanofibrils. *J. Therm. Anal. Calorim.* **2014**, 117, 387–392.

42 T. H. S. Maia, N. M. Larocca, C. A. G. Beatrice, A. J. de Menezes, G. de Freitas Siqueira, L. A. Pessan, A. Dufresne, M. P. Franc, A. de Almeida Lucas, Polyethylene cellulose nanofibrils nanocomposites. *Carbohydrate Polymers* **2017**, 173, 50–56.

43 A. O. Sanches, L. H. S. Ricco, L. F. Malmonge, M. J. da Silva, W. K. Sakamoto, J. A. Malmonge, Influence of cellulose nanofibrils on soft and hard segments of polyurethane/cellulose nanocomposites and effect of humidity on their mechanical properties. *Polymer Testing* **2014**, 40, 99-105.

Supporting Information

Cellulose Nanofibrils as reinforcing agents for PLA-based nanocomposites: an *in situ* approach

TGA analyses

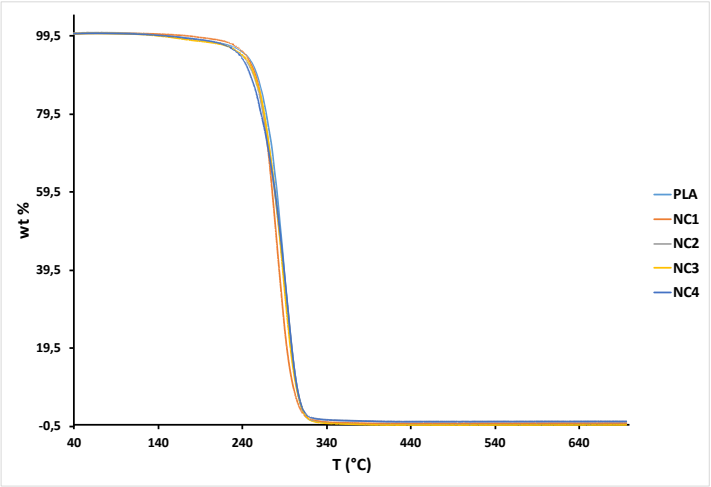

DSC analyses

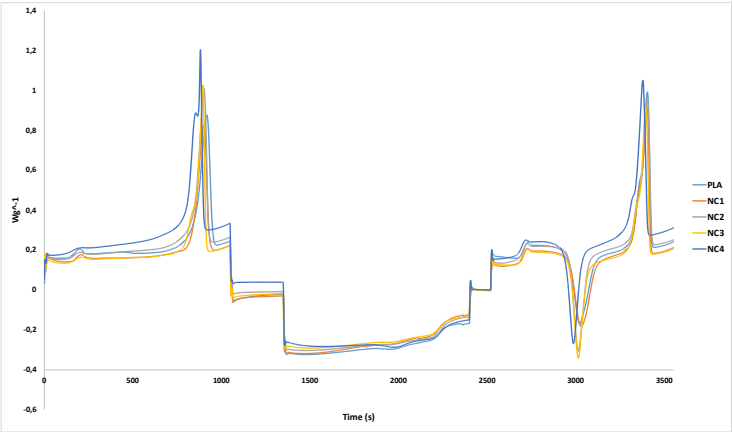

FT-IR analysis of the samples surface

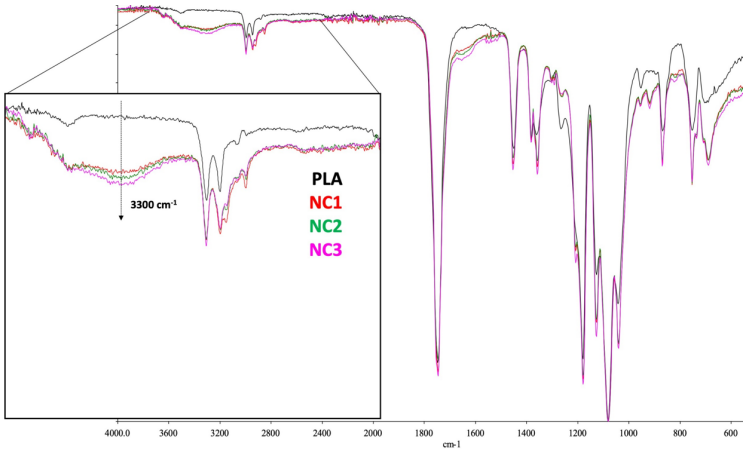

Eugenol-grafted aliphatic polyesters: towards inherently antimicrobial PLA-based materials through OCAs copolymerization

O-Carboxyanhydrides (OCAs) chemistry was exploited for the synthesis of highly functionalized PLA-based materials. Biobased enantiopure L-malic acid was chosen as core element and naturally occurring eugenol as active side group. Eugenol-bearing L-malic acid-derived OCA (L-MalOCA) was synthesized and used as monomer. The product was characterized, and its antimicrobial properties were demonstrated. Homopolymerization kinetics for L-MalOCA and L-Lactic acid-derived OCA (L-LacOCA) were performed and compared in the same conditions, proving the feasibility of copolymerization reactions. Copolymerization tests were conducted with different L-MalOCA to L-LacOCA relative ratios, showing the possibility of tuning the degree of functionalization in the final polymer. The synthetic strategy reported herein has proved promising for the development of novel biobased antimicrobial materials.

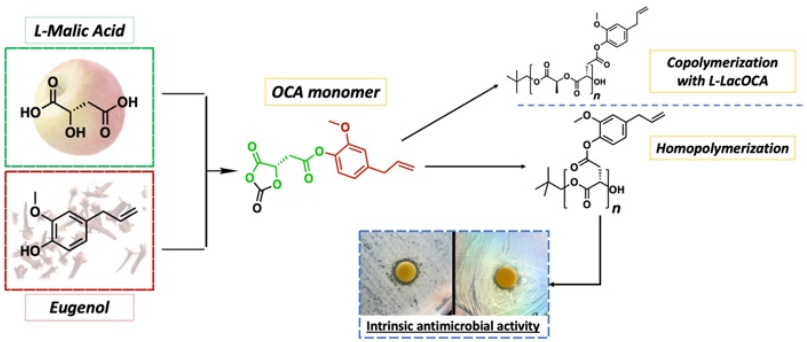

Submitted to ACS Biomacromolecules

1. Introduction

The development of antimicrobial polymeric systems is gaining more and more interest from year to year since the early '90s. The increasing attention towards this field is mainly aimed at fighting the spread of illnesses through the improvement of health conditions of medical and food-related environments.[1-3] For this reason, a lot of different antimicrobial materials were developed and described, for example bearing surface cationic moieties that target the microbial membrane avoiding the development of resistance.[4-6] The most significant applications of these materials are in the biomedical and active packaging fields. In particular, the development of antimicrobial packaging systems is a key strategy for improving the shelf-life of the food and therefore reducing its waste.[7]

Aiming at an antimicrobial polymeric material for packaging applications, it is important to consider its non-toxicity and biocompatibility. Furthermore, facing the necessity to replace oil-derived plastics, the use of renewable and biodegradable polymers appears valuable.[8] For these reasons, many different antimicrobial packaging systems either based on natural (i.e. chitosan[9]) or synthetic but biobased polymers[10] were recently described. Among the last ones, Polylactic acid (PLA) is one of the most attracting, due to its renewability,[11] biodegradability[12] and biocompatibility[13] coupled with good mechanical properties and processability.[14] Up to date, all strategies available for the preparation PLA-based antimicrobial materials rely on post polymerization incorporation of active principles (i.e. silver,[15] sorbic acid,[16] essential oils[17]). The development of an intrinsically active PLA-based material would be advantageous to avoid diffusion phenomena of the active principles,[18] but, at the best of our knowledge, it was never attempted before. One of the main challenges towards this approach comes from the scarce monomer scope for PLA. The recent discovery of O-Carboxyanhidrides (OCAs) monomers as lactide equivalents for the preparation of PLA-based materials gave new opportunities in this direction.[19] OCAs derived from lactic acid,[20] but also from mandelic[21] and malic acid,[22] have been successfully synthesized and used as monomers. However, the catalytic system for polymerization has to be finely tuned, depending on the OCA structure. For this reason, the copolymerization reaction between different α-hydroxy acid-derived OCAs is quite challenging and, until now, scarcely reported.[23, 24]

Following our interest in the synthesis of highly functionalized polyesters,[25] we looked at eugenol as a promising antimicrobial product, well suited to be incorporated in various polymeric materials.[26-28] Eugenol can be extracted from natural sources such as lignin and clove oil and it is active against a great number of bacteria, both Gram-negative and Gram-positive. In particular, it is also reported to be active against the proliferation of foodborne pathogens and fungi.[29, 30] Since a maintained, and in some cases increased, activity has been demonstrated for esterified eugenol,[31] the incorporation of eugenol in polymeric chains exploiting its phenolic group appears as a promising strategy towards intrinsically antimicrobial materials.

We describe herein the preparation of a eugenol-containing OCA monomer, its organocatalyzed homopolymerization and its copolymerization with the already known lactic acid derived OCA (L-LacOCA). Polymerization kinetics were investigated, and the obtained products fully characterized. At the best of our knowledge, they represent the first example of polyester-based polymers bearing eugenol as bioactive pendant group. Aiming at a novel biomaterial with intrinsic activity, their antimicrobial properties were also assessed and are described herein.

2. Experimental section

2.1 Chemicals and materials

All chemicals were purchased by Sigma Aldrich and used as received. L-malic acid, 97%, ee 99%; 2,2-dimethoxypropane, 98%; *p*-toluenesulfonic acid monohydrate (*p*-TSA), ≥ 98.5%; dichloromethane (DCM), N,N-Diisopropylethylamine (DIPEA), ≥ 99 %; N-(3-Dimethylaminopropyl)-N′-ethylcarbodiimide hydrochloride (EDC·HCl), crystalline; 1-Hydroxybenzotriazole hydrate (HOBt), ≥ 97 %; 4-(Dimethylamino)pyridine (DMAP), ≥ 99 %; Eugenol ≥ 98 %; HCl, ≥ 37 %; Tetrahydrofuran (THF); Ethyl Acetate (AcOEt); trichloromethyl chloroformate, ≥ 97 %; L-(+) Lithium lactate, 95 %; 2,2-dimethyl-1-propanol, 99 %; 4-methoxypyridine, 97 %; Dimethyl sulfoxide-d6 (DMSO-d6) minimum deuteration degree 99.8 %; Chloroform-d ($CDCl_3$), minimum deuteration degree 99.8 %.

2.2 Synthesis of (L)-2-(2,2-dimethyl-5-oxo-1,3-dioxolan-4-yl)acetic acid (1)

To a solution of L-malic acid (20 g, 149 mmol) in 2,2-dimethoxypropane (200 mL) under N_2 atmosphere, *p*-toluenesulfonic acid monohydrate (0,285 g; 1,5 mmol) was added. The reaction mixture was left reacting at room temperature overnight, then an aqueous solution of $NaHCO_3$ (126 mg, 1.5 mmol in 30 mL of H_2O) was added. 2,2-Dimethoxypropane was removed under reduced pressure, the aqueous phase was extracted with DCM (3 x 15 mL). The organic phases were dried over Na_2SO_4 and the solvent was evaporated to obtain **1** as a white solid (63% yield). ^{1}H and ^{13}C NMR spectra were in agreement with those reported in literature.[32]

2.3 Synthesis of 4-allyl-2-methoxyphenyl (L)-2-(2,2-dimethyl-5-oxo-1,3-dioxolan-4-yl)acetate (2).

To a solution of **1** (3 g, 17.2 mmol) in dry DCM (150 mL) at 0° C, DIPEA (12 mL), EDC·HCl (9.9 g, 51.7 mmol), HOBt (2.3 g, 17.2 mmol) and DMAP (catalytic amount) were added in sequence. After stirring the mixture for 15 min at room temperature, eugenol (3.1 g, 18.9 mmol) was added and the solution was left under stirring overnight under N_2 atmosphere.

The solution was then diluted with DCM (100 mL) and washed with distilled water (4 x 50 mL). The organic phase was dried over Na_2SO_4 and the solvent was evaporated to obtain the crude product as a dark red oil. It was purified by flash column chromatography on silica gel (eluent: DCM) to give **2** as a yellowish solid (67% yield). ^{1}H NMR ($CDCl_3$, 400 MHz) δ 6.99 (d, *J* = 8.0 Hz, 1H), 6.81 (s, 1H), 6.78 (d, *J* = 8.0 Hz, 1H), 5.97 (m, 1H), 5.12 (m, 2H), 4.84 (dd, *J* = 6.5, 3.8 Hz, 1H), 3.83 (s, 3H), 3.39 (d, *J* = 6.7 Hz, 2H), 3.24 (dd, *J* = 17.2, 3.8 Hz, 1H), 3.08 (dd, *J* = 17.2, 6.5 Hz, 1H), 1.67 (s, 3H), 1.61 (s, 3H). ^{13}C NMR (101 MHz, $CDCl_3$) δ 172.54, 168.15, 151.35, 139.96, 138.35, 137.63, 123.04, 121.31, 116.85, 113.46, 111.94, 71.34, 56.48, 40.73, 36.68, 27.42, 26.57.

2.4 Synthesis of (L)-4-(4-allyl-2-methoxyphenoxy)-2-hydroxy-4-oxobutanoic acid (3)

To a solution of **2** (0.5 g, 1.56 mmol) in THF (5 mL), 1M aq HCl (5 mL) was added dropwise, and the solution was left under stirring overnight under N_2 atmosphere.

The THF was then evaporated and aq $NaHCO_3$ was added until pH 9. After washing with AcOEt (3 x 10mL), the aqueous phase was treated with 3M aq HCl until reaching pH 1.

Solution was then saturated with NaCl and extracted with DCM (4 x 15 mL). Organic phases were collected and dried over Na_2SO_4. Solvent was evaporated to obtain **3** as a yellowish viscous oil (87% yield). ^{1}H NMR ($CDCl_3$, 400 MHz) δ 6.99 (d, *J* = 7.9 Hz, 1H), 6.80 (m, 2H), 5.97, (m, 1H), 5.12 (m, 2H), 4.70 (dd, *J* = 6.6, 4.3 Hz, 1H), 3.83 (s, 3H), 3.40 (d, *J* = 6.7 Hz, 2H), 3.23 (dd, *J* = 16.8, 4.3 Hz, 1H), 3.13 (dd, *J* = 16.8, 6.6 Hz, 1H). ^{13}C NMR (101 MHz, $CDCl_3$) δ 176.84, 169.83, 151.08, 140.15, 138.13, 137.55, 123.05, 121.48, 116.94, 113.43, 67.77, 56.55, 40.72, 38.96.

2.5 Synthesis of 4-allyl-2-methoxyphenyl (L)-2-(2,5-dioxo-1,3-dioxolan-4-yl)acetate (L-MalOCA, 4)

To a solution of **3** (240 mg, 0.85 mmol) in dry THF (1.5 mL) at 0°C, 5 mg of activated charcoal were added, then trichloromethyl chloroformate (0,12 mL; 1.02 mmol) was added dropwise under N_2 atmosphere.

After stirring overnight, the solution was diluted with dry DCM and filtrated over a celite pad to remove charcoal. Solvent was removed under reduced pressure and the crude product was triturated with a pentane/diisopropyl ether 1:1 solution, to obtain **4** as a yellowish solid (73% yield). ^{1}H NMR ($CDCl_3$, 400 MHz) δ 6.94 (d, J = 7.9 Hz, 1H), 6.76 (m, 2H), 5.93 (m, 1H), 5.24 (s, 1H), 5.09 (m, 2H), 3.79 (s, 3H), 3.42, (s, 2H), 3.36 (d, J = 6.7 Hz, 2H). 3.36 (d, J = 6.7 Hz, 2H). ^{13}C NMR (101 MHz, $CDCl_3$) δ 166.32, 166.14, 150.31, 147.97, 139.99, 137.13, 136.78, 121.92, 120.68, 116.38, 112.84, 74.99, 55.83, 40.07, 34.33.

2.6 Synthesis of (S)-5-methyl-1,3-dioxolane-2,4-dione (L-LacOCA, *5*)

According to literature procedure.[33]

2.7 Synthesis of (L)-4-(4-allyl-2-methoxyphenoxy)-2-hydroxy-4-oxobutanoic acid 4-methoxypyridinuim salt

To a solution of **3** (261 mg, 0.93 mmol) in dry Et_2O (1.5 mL) at 0°C, dry 4-methoxy pyridine (0.1 mL, 0.93 mmol) was added and left under stirring for 3 hours at room temperature. Reaction flask was then left at -10°C overnight. Solvent was then evaporated and the resulting white solid triturated with pentane, to obtain a white solid (31% yield).

2.8 General homopolymerization procedure

To a flask containing 2,2-dimethyl-1-propanol (7 mg, 0.082 mmol), a solution of monomer (**4** or ***5***, 1.64 mmol) in dry DCM (10 mL) was added. After cooling at 0° C, 4-methoxypyridine (27 μL, 0.082 mmol) was added dropwise. The solution was left under stirring at room temperature overnight, then the solvent was removed under reduced pressure to obtain a transparent crude oil. It was triturated with pentane to obtain the final product.

2.9 General copolymerization procedure

To a flask containing **4** (2% (11.6 mg, 0.038 mmol) or 10% (58.2 mg, 0.19 mmol) with respect to ***5*** and 2,2-dimethyl-1-propanol (8 mg, 0.095 mmol), a solution of ***5*** (220 mg, 1.9 mmol) in dry DCM (10 mL) was added. After cooling to 0 °C, 4-methoxypyridine (31 μL,

0.095 mmol) was slowly added. The solution was left under stirring at room temperature overnight, then the solvent was removed under reduced pressure to obtain a transparent crude oil. It was triturated with pentane to obtain the final product.

2.10 Antimicrobial tests

The antibacterial activity was evaluated by the disc diffusion method (Matuscheck et al., 2014) using Gram-negative (*Escherichia coli* ATCC25922 and *Pseudomonas aeruginosa* DSM22644) and Gram-positive (*Staphylococcus aureus* ATCC25923 and *Bacillus cereus* DSM31) bacteria. Several morphologically similar colonies for each microrganism, grown overnight at 37°C or 30°C (*P.* aeruginosa) on Tryptic Soy Agar (TSA, Scharlab, Barcelona, Spain), were selected and suspended in sterile saline solution (0.85% NaCl w/v) to a turbidity of 0.5 McFarland standard, approximately corresponding to 1–2 $x10^8$ CFU/mL. Each bacterial suspension was then spread over Mueller–Hinton Agar (MHA, Merck KGaA, Darmstadt, Germany) plates by swabbing in three directions. Solution of the test compound (1 M) was made in dimethyl sulfoxide (DMSO), and each solution (10 µL) was added to a sterile disc (6 mm) placed on the agar plates. After incubation at 37°C or 30°C for 18-24h, the antibacterial effect was verified by measuring the diameter of zones of inhibition around the discs.

2.11 Size exclusion chromatography (SEC)

Molecular weight of homo- and copolymers was evaluated using a SEC system having Waters 1515 Isocratic HPLC pump and a four Waters Styragel columns' set (HR3-HR4-HR5-HR2) with an UV detector Waters 2487 Dual λ Absorbance Detector set at 230 nm using a flow rate of 1 mL/min and 60µL as injection volume. Samples were prepared dissolving 50 mg of polymer in 1 mL of anhydrous CH_2Cl_2 and filtering the solution on 0.45 µm filters. Given the relatively high loading, a check was performed using lower concentration of polymer (5mg/mL), in order to verify that no column overloading could be observed. Anyway higher loadings were preferred as UV signal of PLA is relatively weak.

Molecular weight data are expressed in polystyrene (PS) equivalents. The calibration was built using monodispersed PS standards having the following nominal peak molecular weight.

(Mp) and molecular weight distribution (D): Mp = 1,600,000 Da (D ≤ 1.13), Mp = 1,150,000 Da (D ≤ 1.09), Mp = 900,000 Da (D≤1.06), Mp=400,000Da (D≤1.06), Mp=200,000Da (D≤1.05), Mp=90,000Da (D≤1.04), Mp=50,400Da (D=1.03), Mp=30,000Da (D=1.06), Mp=17,800Da (D=1.03), Mp=9730Da (D=1.03), Mp=5460Da (D=1.03), Mp=2032Da (D=1.06), Mp=1241Da (D=1.07), Mp=906Da (D=1.12), Mp=478Da (D=1.22); Ethyl benzene (mole- cular weight = 106 g/mol). For all analyses, 1,2-dichlorobenzene was used as internal reference.

2.12 Differential scanning calorimetry (DSC)

DSC analyses were conducted using a Mettler Toledo DSC1, on samples weighting from 5 to 10 mg each. Melting and crystallization temperatures were measured using the following temperature cycles:

1. Heating from 0 °C to 150 °C at 10 °C/min.
2. Cooling from 150 °C to 0 °C at 10 °C/min.
3. Heating from 0 °C to 300 °C at 10 °C/min.

The first two cycles were run to eliminate residual internal stresses deriving from the synthesis. Glass transition temperature (T_g), cold crystallization temperature (T_{cc}) and melting temperature (T_m) were determined.

2.13 Thermogravimetric analysis (TGA)

TGA were performed using a TGA 4000 Perkin Elmer instrument; tests were conducted in air on samples weighting from 5 to 10 mg each, with a program that provides a single heating cycle from 30 °C to 650 °C at 10 °C/min.

2.14 Fourier transform infrared spectroscopy (FT-IR)

FT-IR Spectrometer (Spectrum 100, PerkinElmer) with an attenuated total reflection (ATR) was used to register spectra for all samples.

2.15 ^{1}H NMR analyses

^{1}H NMR spectra were registered with a Bruker Ultrashield 400 MHz. The chemical shifts are reported in ppm and referred to TMS as internal standard. All samples were prepared by dissolving 6–8 mg of material into 1 mL of deuterated solvent.

3. Results and discussion

3.1 Synthesis of monomers

L-MalOCA (**4**) was synthesized following the reactions reported in **Scheme 1**.

Starting from L-malic acid, the protection reaction (***a***) proceeded smoothly in high yield, following the literature procedure. Steps ***b*** and ***c*** gave also the expected products in good yields. Given the inherent instability of compound **4**, the last step (***d***) was necessarily performed immediately before the polymerization reaction.

L-LacOCA (*5*) was synthesised according to the literature, starting from enantiopure L-(+) Lithium lactate. The reaction can be performed also by using L-lactic acid as starting material, but it is less efficient and it needs the presence of activated charcoal, in order to promote the formation of *5*.

3.2 General polymerization procedures

L-MalOCA (**4**) and L-LacOCA (*5*) homopolymerization reactions were performed according to conditions reported in the Experimental Section, affording samples HOMO1 and HOMO2 respectively.

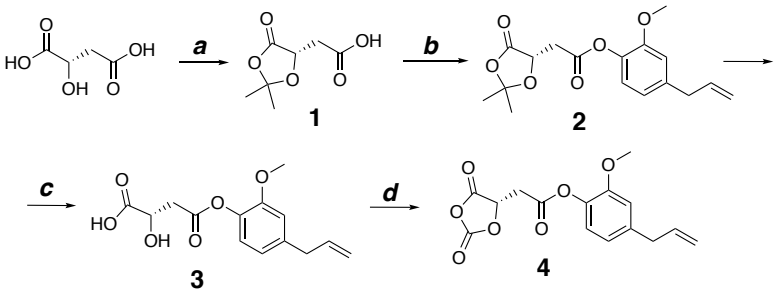

Scheme 1: Reagents and conditions: **a)** 2,2-dimethoxy propane, p-TSA, r.t., overnight. **b)** Eugenol, DIPEA, EDC·HCl, HOBt, DMAP, DCM, 0 °C to r.t., overnight. **c)** 1M aq HCl, THF, r.t., overnight. **d)** diphosgene, THF, activated charcoal, 0 °C to r.t., overnight.

Scheme 2: Reagents and conditions: **a)** 2,2-dimethyl-1-propanol, p-methoxy pyridine, DCM, r.t., 24 h.

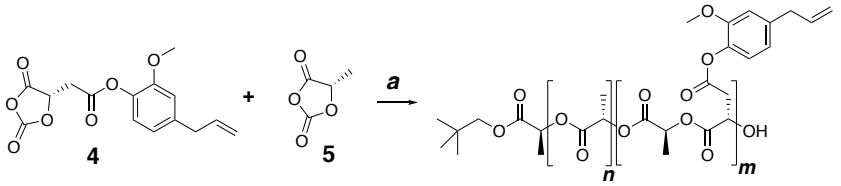

Two L-MalOCA /L-LacOCA copolymerizations were performed as reported in **Scheme 2**, varying the relative ratios between the two monomers. Samples COP1 (2 mol% **4**) and COP2 (10 mol% **4**) were obtained.

3.3 Reaction kinetics studies

One of the most important parameters in OCAs polymerization is the choice of a proper catalyst. The catalyst nature not only determines the feasibility of the reaction depending on OCA structure, but also its basicity has to be considered in order to avoid epimerization phenomena at the stereogenic centre. For these reasons it is difficult to properly tune reaction conditions for the copolymerization of OCAs with significantly different structures. To this regard, the great structural difference between monomers **4** and ***5*** could in principle act as an obstacle for their copolymerization. Studies concerning their homopolymerization kinetics were therefore needed, in order to determine the feasibility of a copolymerization reaction.

3.3.1 Homopolymerization reactions

Regarding L-MalOCA monomers, malic acid pyridinium salts and 4-methoxy pyridine are currently reported as suitable catalytic systems for polymerization reactions. Pyridinium salts can act both as catalysts and initiators and also ensure control over the product stereochemistry.[34] On the other hand, among basic organocatalysts, 4-methoxy pyridine shows the most satisfactory balance of stereochemical control and activity, also compared to differently substituted pyridines.[22]

With the aim of investigating the applicability of acid/base ion pairs to homopolymerization reactions, the synthesis of pyridinium salt of α-hydroxy acid **3** was addressed. Despite it was achieved in low yield, likely due to extensive hydrolysis of the phenolic ester moiety, the obtained salt was tested as catalyst. However, low control over the polymerization was observed, resulting in oligomeric products only. Given the poor results, the synthesis and use of pyridinium salts as catalysts was abandoned.

Turning our attention to 4-methoxy pyridine, homopolymerization of **4** was performed with a 20 : 1 : 1 monomer to initiator to catalyst ratio, with 2,2-dimethyl-1-propanol as initiator (see Experimental Section). Reaction was conducted at room temperature for 24 hours using DCM as solvent and with sampling from the reaction in order to follow the kinetics. Samples were analysed through ^{1}H NMR and SEC, to follow both the monomer consumption with time as well as the growth of the molecular weight.

Stacked ^{1}H NMR spectra relative to reaction sampling (**Figure 1**), show that all the monomer has consumed after just 30 minutes, as evidenced by the disappearance of the H_1 methyne proton signal, centered at 5.24 ppm in the spectrum of the starting material, and by the appearance of a broad signal at 5.79 ppm in the spectrum of the polymerization

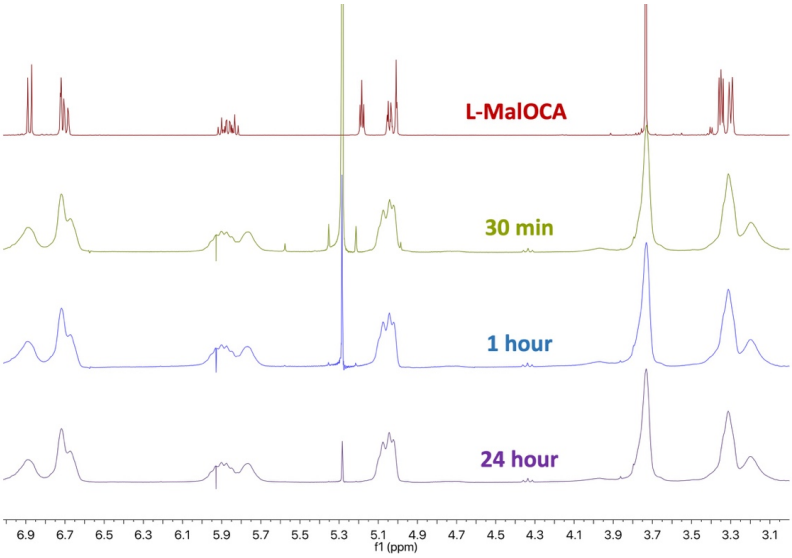

Figure 1: stacked ^{1}H NMR spectra relative to **4** homopolymerization reaction sampling.

Figure 2: ^{1}H NMR spectrum of HOMO1 purified product after 24 h.

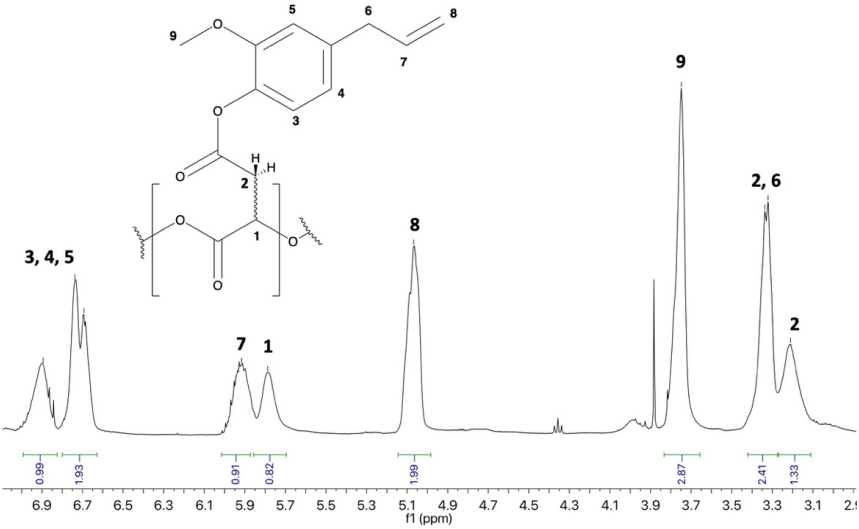

product (HOMO1).

A full 1D and 2D NMR characterization on a purified sample of HOMO1 was carried out, allowing a complete 1H signals attribution, as reported in **Figure 2**.

In particular, from 2D NMR spectra (^{1}H-^{1}H-COSY and ^{13}C-^{1}H-HSQC, see Supporting Information), the co-presence of two distinct ABX spin systems, related to protons 2-H_2 and H_1, was clearly assessed. Likely, these two systems derive from the partial epimerization of H_1, during the polymerization. Signals related to the first of these systems were centered at 3.21 (2-H_2) and 5.76 (H_1) ppm respectively, while signals relative to the second spin system fall to about 3.34 (2-H_2) and 5.95 (H_1) ppm respectively. The broadness of the signals and the partial superimpositions of the peaks make difficult to measure proper integration values, but it is still possible to estimate the quantity of epimerized product variable from 15% after 30 minutes of reaction up to a maximum of about 30% after 24 hours.

SEC traces confirmed that the final molecular weight was reached in 30 minutes. Traces relative to all samples are reported in SI file, while related molecular weight at 30 min and 24 h are reported in **Table 1**.

Table 1: molecular weight data relative to **4** hompolymerization reaction sampling.

Sample	$\overline{M_n}$ (g mol^{-1})[a]	$\overline{M_w}$ (g mol^{-1})[a]	$\overline{M_p}$ (g mol^{-1})[a]	Đ
30 min	3200	3800	3600	1.2
24h	3200	3800	3800	1.2

[a] The molecular weight was determined against PS calibration.

Relying again on 4-methoxy pyridine as catalyst, homopolymerization of ***5*** was performed in the same conditions used for monomer **4**, namely with a 20 : 1 : 1 monomer to initiator to catalyst ratio for 24 hours at room temperature, employing 2,2-dimethyl-1-propanol as initiator and DCM as solvent. Sampling of the reaction was performed within the 24 hours, in order to follow the reaction kinetics. The homopolymerization product (HOMO2) was characterized through NMR and SEC. Stacked ^{1}H NMR spectra for samples relative to ***5*** homopolymerization are reported in **Figure 3**.

The doublet relative to the methyl group shifts from 1.72 ppm in the L-LacOCA spectrum, to 1.52 ppm in the HOMO2 spectrum. NMR data show that the reaction was completed after just 30 minutes, given the complete absence of monomer signals.

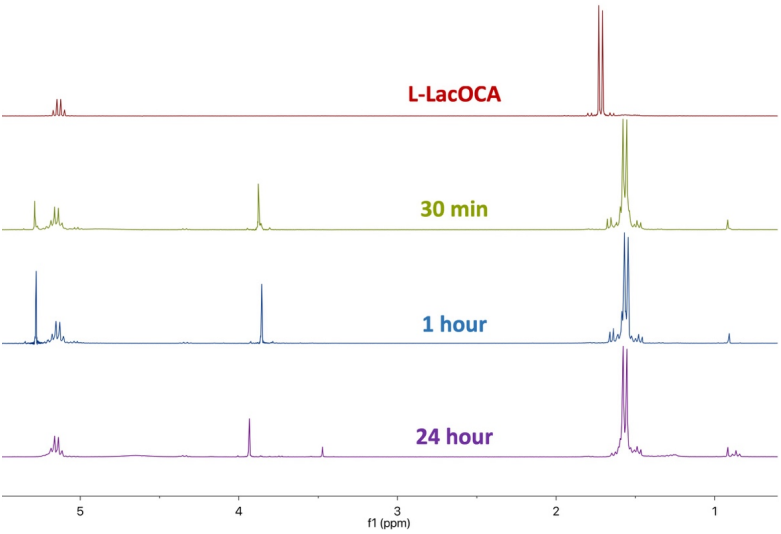

Figure 3: stacked ^{1}H NMR spectra relative to ***5*** homopolymerization reaction sampling.

It is worth noticing that the signal relative to the methyne proton does not show any significant difference in chemical shift between the L-LacOCA and the HOMO2 product. This observation is in contrast with what was described for L-MalOCA homopolymeryzation. To this regard, the occurrence of epimerization described for HOMO1 can be explained by taking into account the higher acidity of the methyne proton in the product, which makes it more sensitive to the basic catalyst. The reason for this increased acidity of the methyne proton in HOMO1 is not very clear. It is reasonable to assume that it can derive from conformational, rather than electronic reasons, in the sequence of malic acid-derived repeating units. Concerning stereochemistry, the sharpness of signals in the ^{1}H NMR of HOMO2 is a good indication of the retained configuration at the stereogenic centre in the product. Further confirmation was given by the ^{1}H NMR decoupled spectrum reported in the SI file.

SEC traces relative to all samples of ***5*** homopolymerization are reported in SI file, while related molecular weight at 30 min and 24 h are reported in **Table 2**. As already described for HOMO1 polymerization, SEC data confirmed the final molecular weight was reached after 30 minutes.

Table 2: molecular weight data relative to ***5*** hompolymerization reaction sampling.

Sample	$\overline{M_n}$ (g mol^{-1})[a]	$\overline{M_w}$ (g mol^{-1})[a]	$\overline{M_p}$ (g mol^{-1})[a]	Đ
30 min	2400	2600	2800	1.1
24h	2300	2500	2600	1.1

[a] The molecular weight was determined against PS calibration.

3.3.2 Copolymerization reactions

Having ascertained that monomers **4** and ***5*** can be reacted under similar polymerization conditions, two different copolymerization tests were performed. Different L-MalOCA/L-LacOCA ratios were tested, namely 2% and 10% mol of **4** with respect to ***5***, following the procedure described in the Experimental Section. Reactions were kept running for 24

Figure 4: ^{1}H NMR spectrum of COP1. Signals for L-malic acid-based repeating units are indicated in red, signals for L-lactic acid-based repeating units are indicated in green.

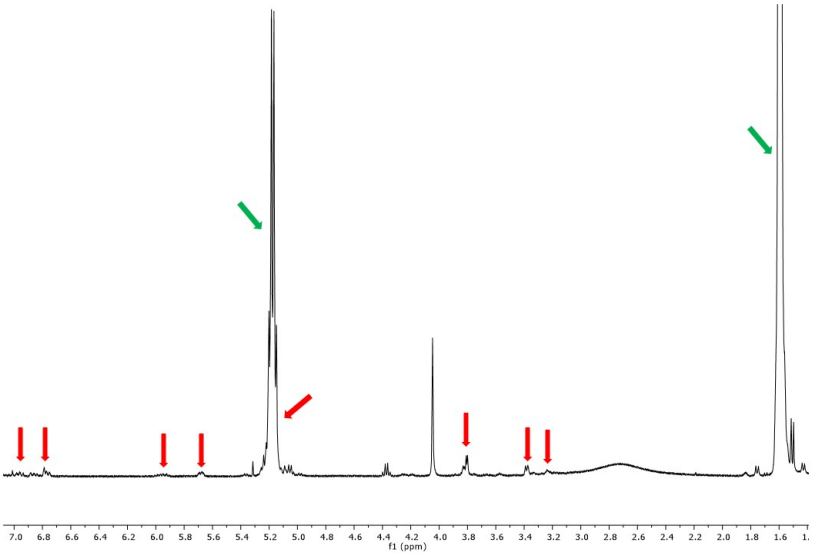

Figure 5: ^{1}H NMR spectrum of COP2. Signals for L-malic acid-based repeating units are indicated in red, signals for L-lactic acid-based repeating units are indicated in green.

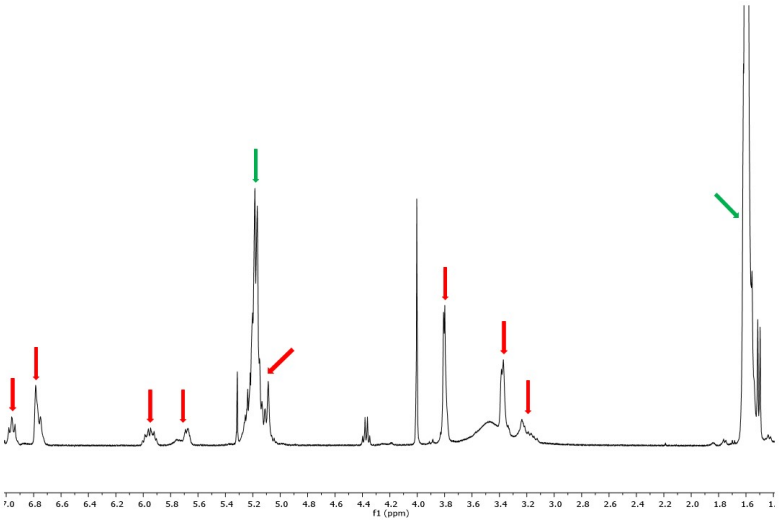

hours, yielding products COP1 and COP2 respectively. COP1 and COP2 were characterized through ^{1}H NMR and SEC, in order to assess the actual occurrence of copolymerization. ^{1}H NMR spectra relative of COP1 and COP2 are reported in **Figure 4** and **Figure 5** respectively.

Considering the integrations of signals relative to eugenol-derived methoxy group and lactic acid-derived methyl group, we could compare the starting L-MalOCA/L-LacOCA ratio with the actual occurrence of L-malic acid- and L-lactic acid-based repeating units in the final material. As data in **Table 3** show, consistent values were obtained both for COP1 and COP2, demonstrating the almost complete incorporation of L-MalOCA in the final product and therefore the promising tuning that can be achieved through this protocol.

Table 3: starting L-MalOCA/L-LacOCA ratio vs L-malic acid-based/L-lactic acid-based repeating units in the final product.

Reaction	% mol L-MalOCA/L-LacOCA starting monomers	% mol L-malic acid-based units/L-lactic acid-based repeating units[a]
COP1	2	1.4
COP2	10	10

[a]Estimated by ^{1}H NMR (integration values for OMe and Me groups).

Finally, a comparison of the ^{1}H NMR spectra in the 5.40 to 6.20 ppm region for all malic acid-based polymerization products is reported in **Figure 6**, in an attempt to shed further light on the copolymerization mode.

The signal related to the proton ***b*** in HOMO1 is centered at 5.76 ppm. This same signal is detectable for COP2 product only, suggesting the possible presence of malic acid-derived blocks, even if in low concentration. On the other hand, a signal at 5.69 ppm is present in both COP1 and COP2 spectra, likely referring to proton ***a***, belonging to isolated malic acid-derived repeating units.

The self-consistency of signals integration in the C□-H region, evaluated in comparison with that of the allyl proton at 5.95 ppm, suggests that no epimerization in the malic acid-derived unit occurred, neither in COP1 nor in COP2.

The partial epimerization observed in HOMO1 (see above) could therefore be ascribed to the highly hindered structure of the homopolymer. However, such phenomenon becomes irrelevant in materials that are characterized by a very low concentration of malic acid-derived blocks.

SEC analyses of COP1 and COP2 are reported in **Figure 7**. Analyses were run using a double wavelength detector, at 230 and 280 nm. In both samples, the two curves are perfectly superimposable, confirming the presence of a unimodal distribution of species carrying both L-lactic and L-malic acid-based repeating units.

COP1 and COP2 molecular weight data are reported in **Table 5**, in comparison with those obtained for HOMO1 and HOMO2.

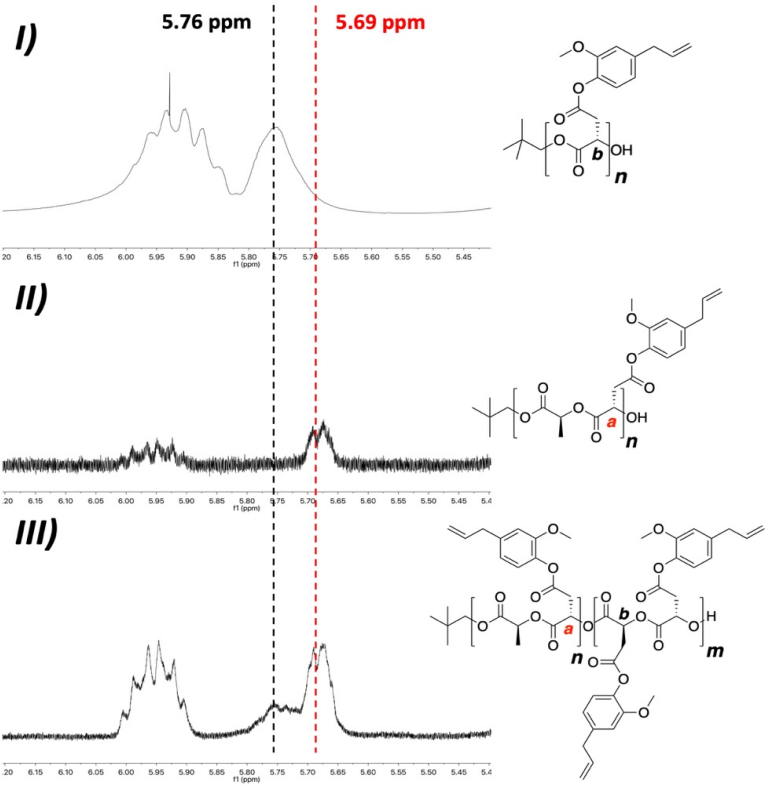

Figure 6: comparison of the spectra in the 5.4 to 6.2 ppm region for **I)** HOMO1, **II)** COP1 and **IV)** COP2.

Figure 7: a) COP1 SEC chromatograms registered at 230 and 280 nm and **b)** COP2 SEC chromatograms registered at 230 and 280 nm.

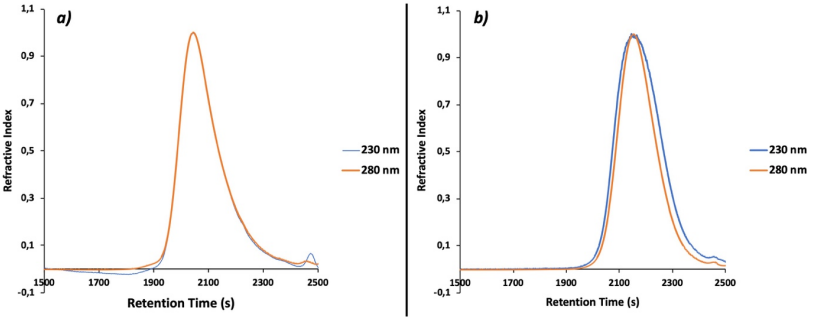

Table 5: molecular weight data relative to both homo- and copolymers.

Sample	$\overline{M_n}$ (g mol^{-1})[a]	$\overline{M_w}$ (g mol^{-1})[a]	$\overline{M_p}$ (g mol^{-1})[a]	Đ
HOMO1	3200	3800	3800	1.1
HOMO2	2300	2500	2600	1.2
COP1	3300	3800	4300	1.2
COP2	2100	2500	2700	1.2

[a] The molecular weight was determined against PS calibration.

3.4 Thermal analysis

3.4.1 DSC analyses

Samples were characterized through DSC analyses, in order to determine their thermal properties, in particular highlighting the effect that eugenol-derived bulky aromatic side chains have on PLA-based materials. DSC thermograms are reported in SI file.

Glass transition temperature (T_g) for HOMO1 was detected at 27 °C during the first heating scan. The following endotherm transition accounts for partial thermal degradation, as further confirmed by TGA analyses (see below). The complete disappearance of glass transition during the second heating scan can be explained by taking into account the possible occurrence of crosslinking phenomena at high temperature, as already shown in our previous work.[25]

HOMO2 shows a T_g at 19 °C. Cold crystallization (T_{CC}) and melting (T_m) can be also detected. However, all transitions take place at lower temperatures than those expected for standard PLA, probably due to HOMO2 low molecular weight. Thermal transitions for COP1 closely resemble those detected for HOMO2, even if they occur at higher temperatures. In particular, T_g increases by almost 30 °C. To this regard, it is reasonable to think that the higher molecular weight of COP1 with respect to HOMO2 is the main responsible for this shift in thermal transitions temperatures. Both HOMO2 and COP1 samples present a double melting peak, denouncing the presence of two distinct crystalline phases. However, in COP1 sample this second phase is much more significant. This behaviour can be attributed to the effect of aromatic side groups that make more difficult the formation of perfectly ordered α-crystals, favouring the formation of more disordered α'-crystals.

COP2 appears to be completely amorphous, with neither crystallization nor melting transitions. Only a glass transition can be spotted during the first heating scan, while two T_gs are present during the second heating. As discussed for HOMO1 product, also in this case it is reasonable to assume the occurrence of partial crosslinking at high temperature, at the end of the first heating scan. These crosslinking reactions could be responsible for the formation of a distinct, more rigid phase, having a glass transition at higher temperature.

3.4.2 TGA analyses

TGA analyses were performed in order to determine the thermal stability of both homo- and copolymers. All analyses were carried out in nitrogen atmosphere, running a heating scan from 30 to 650 °C at 20 °C/min. TGA curves are reported in **Figure 8**.

The products show significantly different degradation profiles. Temperatures corresponding to 5% weight loss ($T_{5\%}$), 50 % weight loss ($T_{50\%}$) and residual weight at 650 °C are reported in **Table 6**.

Figure 8: TGA degradation curves for all samples.

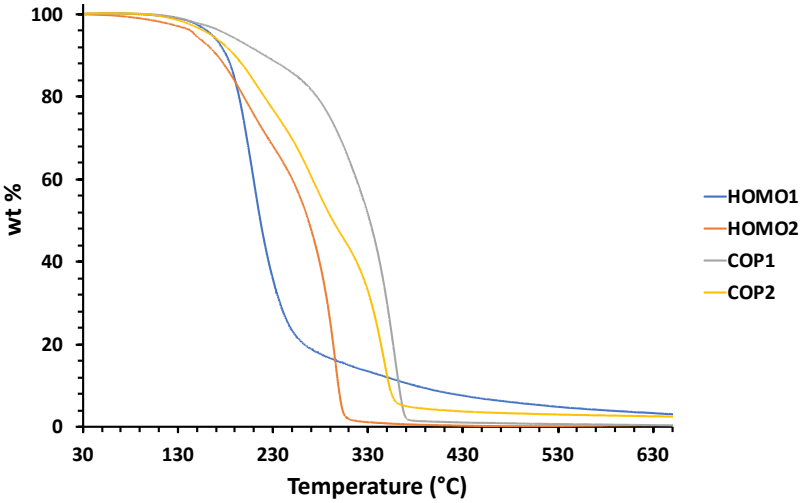

Both homopolymers show faster degradation with respect to copolymers. In particular, considering 5% weight loss as the beginning of degradation, HOMO1 shows higher thermal stability than HOMO2, while 50 % weight loss occurs at significantly higher temperatures for HOMO2 with respect to HOMO1. Regarding copolymers, they both exhibit a two-step degradation profile, which can be attributed to the degradation of the two different repeating units.

Furthermore, they both appear to have higher thermal stability with respect to HOMO1 and HOMO2, with COP1 showing both the highest $T_{5\%}$ and the highest $T_{50\%}$. Regarding residual weight, it increases proportionally to L-MalOCA concentration.

Sample	$T_{5\%}$	$T_{50\%}$	Residual weight
HOMO1	166.1	217.2	3.0%
HOMO2	148.6	267.8	0%
COP1	182.6	332.1	0.4%
COP2	165.1	292.7	2.4%

Table 6: thermal degradation data.

Based on our previous results,[25] occurring of crosslinking reactions with heating must be taken into account for eugenol-based monomers. These would eventually end up in non-degraded residues even at high temperatures.

3.5 FT-IR analyses

FT-IR spectra for all products are reported in **Figure 9**, with magnification of the region of interest.

All products show an intense carbonyl stretching band centred around 1750 cm^{-1}. While in COP1 and HOMO2 this band is sharp, it broadens for HOMO1 and COP2, due to the co-presence of both aliphatic and phenolic esters carbonyls.

In particular, the presence of phenolic esters is highlighted by the increasing intensity of a shoulder at 1730 cm^{-1}, which is the typical stretching wavelength for phenolic esters carbonyls. Furthermore, HOMO1, COP1 and COP2 samples show a peak at 1268 cm^{-1}, typical by C-O bond stretching in phenolic esters. The intensity of this band increases with increasing concentration of malic acid-derived repeating unit in the product.

More interestingly, **Figure 9** highlights two bands (at 1604 cm^{-1} and 1510 cm^{-1} respectively) that are detectable only in samples containing malic acid-derived units, namely HOMO1,

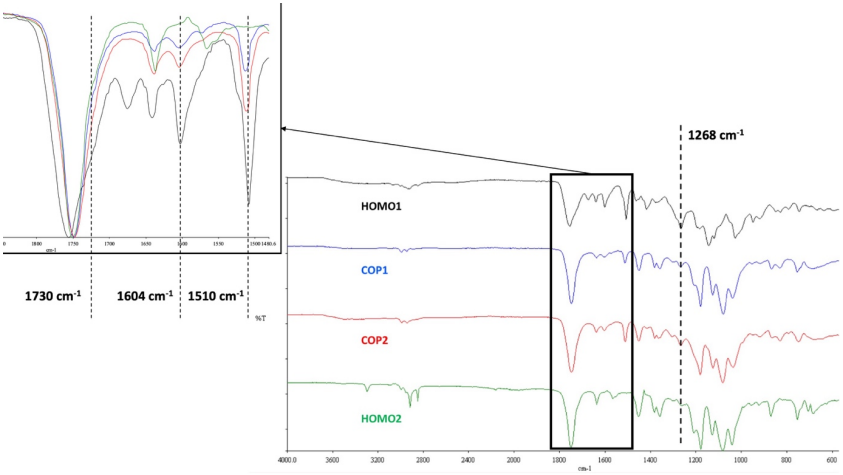

Figure 9: FT-IR spectra, with magnification of the area of interest.

COP1 and COP2. Such bands, whose intensity increases going from COP1 to COP2 and finally to HOMO1, can be likely attributed to eugenol double bonds.

3.6 Antimicrobial activity

HOMO1, COP1 and COP2 were tested for antimicrobial activity, against common food-related bacteria, namely *E. coli*, *P. aeruginosa*, *S. aureus* and *B. cereus*.[35] Only HOMO1 showed antibacterial activity against *S. aureus and B. cereus*, and, at a minor extent, against *P. aeruginosa*. No inhibition halo was detected instead against *E. coli*. Data relative to the inhibition halos of HOMO1 are reported in **Table 7**, while pictures are reported in **Figure 10**.

Microorganism	Inhibition zone (mm)
E. coli ATCC25922	<6
P. aeruginosa DSM22644	6.55±0.07
S. aureus ATCC25923	8.25±0.35
B. cereus DSM31	10.50±0.71

Table 7: inhibition halo of HOMO1 against tested microorganisms.

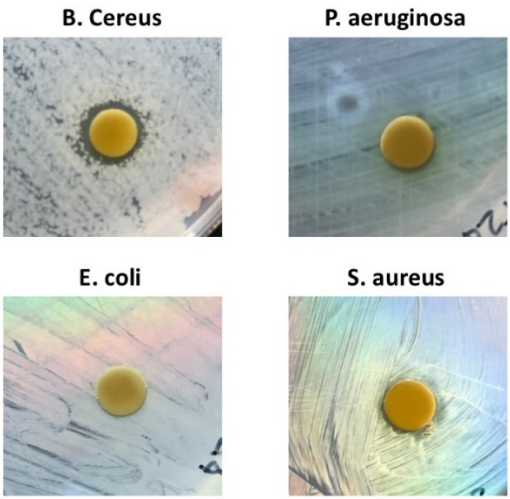

Figure 10: inhibition halo of HOMO1 against tested microorganisms.

4. Conclusions

The synthesis and characterization of innovative highly functionalized polyester-based materials was demonstrated. Taking advantage of OCAs polymerization chemistry, a tailored, monomer bearing naturally occurring phenol was synthesized, starting from enantiopure, naturally occurring L-malic acid. The monomer was homo- and copolymerized, together with well-known L-lactic acid-derived OCA monomer. Kinetics for the two homopolymerization reactions were studied and products characterized. Copolymerization reactions were then carried out, with varying relative concentrations of the two monomers. The actual occurrence of copolymerization was demonstrated by NMR and SEC analysis. Product were characterized and thermal properties evaluated and compared with the ones of homopolymers. The antimicrobial properties given by eugenol were finally tested and demonstrated for the L-MalOCA-derived homopolymer.

References

1. Alexandra Munoz-Bonilla, Maria L. Cerrada and Marta Fernandez-Garcia. Introduction to Antimicrobial Polymeric Materials. *RSC Polymer Chemistry Series* **2014**, Chapter 1.

2. Chen, J.; Wei, D.; Gong, W.; Zheng, A.; Guan, Y. Hydrogen-Bond Assembly of Poly(vinyl alcohol) and Polyhexamethylene Guanidine for Nonleaching and Transparent Antimicrobial Films. *ACS Appl. Mater. Interfaces* **2018**, Just Accepted Manuscript.

3. Li, Z.; Chen, J.; Cao, W.; Wei, D.; Zheng, A.; Guan, Y. Permanent antimicrobial cotton fabrics obtained by surface treatment with modified guanidine. *Carbohydrate Polymers*. **2018**, Accepted Manuscript.

4. Konai, M. M.; Bhattacharjee, B.; Ghosh, S.; Haldar, J. Recent Progress in Polymer Research to Tackle Infections and Antimicrobial Resistance. *Biomacromolecules* **2018**, 19, 1888−1917.

5. Ergene, C.; Yasuharab, K; Palermo, E. F. Biomimetic antimicrobial polymers: recent advances in molecular design. *Polym. Chem.* **2018**, 9, 2407-2427.

6. Santos, M. R. E.; Mendonça, P. V.; Almeida, M. C.; Branco, R.; Serra, A. C.; Morais, P. V.; Coelho, J. F. J. Increasing the antimicrobial activity of amphiphilic cationic copolymers by the facile synthesis of high molecular weight stars by SARA ATRP. *Biomacromolecules* **2018** Ahead of Print.

7. Khaneghaha, A. M.; Hashemib, S. M. B.; Limbo, S. Antimicrobial agents and packaging systems in antimicrobial active food packaging: An overview of approaches and interactions. *Food and Bioproducts Processing* **2018**, 111, 1-19.

8. Babu, R. P.; O'Connor, K.; Seeram, R. Current progress on bio-based polymers and their future trends. *Progress in Biomaterials* **2013**, 2, 1-16.

9. Cui, H.; Li, W.; Li, C.; Vittayapadung, S; Lin, L. Liposome containing cinnamon oil with antibacterial activity against methicillin-resistant Staphylococcus aureus biofilm. *Biofouling* **2016**, 32, 215-225.

10. Tunç, S.; Duman, O. Preparation of active antimicrobial methyl cellulose /carvacrol/ montmorillonite nanocomposite films and investigation of carvacrol release. *LWT - Food Science and Technology* **2011**, 44, 465-472.

11. Hossain, M.M.; Maisuria, J.L.; Effects of organic phase, fermentation media, and operating conditions on lactic Acid extraction *Biotechnol Prog.* **2008**, 24, 757–765.

12. Grizzi, I.; Garreau, H.; Li, S.; Vert, M. Hydrolytic degradation of devices based on poly(dl-lactic acid) size-dependence *Biomaterials* **1995**, 16, 305–311.

13. Da Silva, D.; Kaduri, M.; Poley, M.; Adir, O.; Krinsky, N.; Shainsky-Roitman, J.; Schroeder, A. Biocompatibility, biodegradation and excretion of polylactic acid (PLA) in medical implants and theranostic systems. *Chem. Eng. J.* **2018**, 340, 9–14.

14. Auras, R.; Harte, B.; Selke, S. An overview of polylactides as packaging materials. *Macromol. Biosci.* **2004**, 4, 835–864.

15. Turalija, M.; Bischof, S.; Budimir, A.; Gaan S. Antimicrobial PLA films from environment friendly additives. *Composites Part B* **2016**, 102, 94-99.

16. Guo, M.; Jin, T. Z.; Yang R. Antimicrobial Polylactic Acid Packaging Films against Listeria and Salmonella in Culture Medium and on Ready-to-Eat Meat. *Food Bioprocess. Technol.* **2014**, 7, 3293-3307.

17. Scaffaro, R.; Lopresti, F.; Marino, A.; Nostro, A. Antimicrobial additives for poly(lactic acid) materials and their applications: current state and perspectives. *Applied Microbiology and Biotechnology* **2018**.

18. Samsudina, H.; Auras, B.; Mishra, D.; Dolan, K.; Burgess, G.; Rubino, M.; Selke, S.; Soto-Valdez, H. Migration of antioxidants from polylactic acid films: A parameter estimation approach and an overview of the current mass transfer models. *Food Research International* **2018**, 103, 515–528.

19. Vaca, B. M.; Bourissou, D. O-Carboxyanhydrides: Useful Tools for the Preparation of Well- Defined Functionalized Polyesters. *ACS Macro Lett.* **2015**, 4, 792−798.

20. Kricheldorf, H. R.; Jonté, J. M. New Polymer Syntheses. 8. Synthesis and Polymerization of L-LacticAcidO-Carboxyanhydride (5-MethyI-Dioxolan-2,4-dione). *Polymer Bulletin*, **1983**, 9, 276-283.

21. Buchard, A.; Carbery, D. R.; Davidson, M. G.; Ivanova, P. K.; Jeffery, B. J.; Kociok-Kohn, G. I.; Lowe, J. P. Preparation of Stereoregular Isotactic Poly(mandelic acid) through Organocatalytic Ring-Opening Polymerization of a Cyclic O-Carboxyanhydride. *Angew. Chem. Int. Ed.* **2014**, 53, 13858 –1386.

22. Pounder, R. J.; Fox, D. J.; Barker, I. A.; Bennison M. J.; Dove, A. P. Ring-opening polymerization of an O-carboxyanhydride monomer derived from L-malic acid. *Polym. Chem.* **2011**, 2, 2204-2212.

23. Thillaye du Boullay, O.; Bonduelle, C.; Vaca, B. M.; Bourissou, D. Functionalized polyesters from organocatalyzed ROP of gluOCA, the O-carboxyanhydride derived from glutamic acid. *Chem. Commun.* **2008**, 1786–1788.

24. Sun, Y.; Jia, Z.; Chen, C.; Cong, Y.; Mao, X.; Wu, J. Alternating Sequence Controlled Copolymer Synthesis of α-Hydroxy Acids via Syndioselective Ring-Opening Polymerization of O-Carboxyanhydrides Using Zirconium/Hafnium Alkoxide Initiators. *J. Am. Chem. Soc.* **2017**, 139, 10723−10732.

25. Gazzotti, S.; Hakkarainen, M.; Adolfsson, K. H.; Ortenzi, M. A.; Farina, H.; Lesma, G.; Silvani, A. One-Pot Synthesis of Sustainable High-Performance Thermoset by Exploiting Eugenol Functionalized 1,3-Dioxolan-4-one. *ACS Sustainable Chem. Eng.* **2018**, Just Accepted Manuscript.

26. Yoshimura, T.; Shimasaki, T.; Teramoto, N.; Shibata, M. Bio-based polymer networks by thiol–ene photopolymerizations of allyl-etherified eugenol derivatives. *European Polymer Journal* **2015**, 67, 397–408.

27. Harvey, B. G.; Guenthner, A. J.; Yandek, G. R.; Cambrea, L. R.; Meylemans, H. A.; Baldwin, L. C.; Reams, J. T. Synthesis and characterization of a renewable cyanate ester/polycarbonate network derived from eugenol. *Polymer* **2014**, *55*, 5073-5079.

28. Cheng, C.; Li, J.; Yang, F.; Li, Y.; Hu, Z.; Wang, J. Renewable eugenol-based functional polymers with self-healing and high temperature resistance properties. *Journal of Polymer Research* **2018**, *25*, 1-13.

29. Torpol, K; Wiriyacharee, P.; Sriwattana, S.; Sangsuwan, J.; Prinyawiwatkul, W. Antimicrobial activity of garlic (Allium sativum L.) and holy basil (Ocimum sanctum L.) essential oils applied by liquid vs. vapour phases. *International Journal of Food Science and Technology* **2018**, 1-10.

30. Phanthonga, P.; Lomarata, P.; Chomnawangb, M. T.; Bunyapraphatsara, N. Antibacterial activity of essential oils and their active components from Thai spices against foodborne pathogens. *ScienceAsia* **2013**, 39, 472–476.

31. Hu, Q.; Zhou, M.; Wei, S. Progress on the Antimicrobial Activity Research of Clove Oil and Eugenol in the Food Antisepsis Field. *Journal of Food Science* **2018**, 83, 1476-1483.

32. Pounder, R. J.; Dove, A. P. Synthesis and Organocatalytic Ring-Opening Polymerization of Cyclic Esters Derived from L-Malic Acid. *Biomacromolecules* **2010**, 11, 1930–1939.

33. Thillaye du Boullay, O.; Marchal, E.; Vaca, B. M.; Cossìo, F. P.; Bourissou, D. An Activated Equivalent of Lactide toward Organocatalytic Ring-Opening Polymerization. *J. Am. Chem. Soc.* **2006**, 128, 16442–16443.

34. Bexisa, P.; De Winterb, J.; Coulembier, O.; Dove, A. P. Isotactic degradable polyesters derived from O-carboxyanhydrides of L-lactic and L-malic acid using a single organocatalyst/initiator system. *European Polymer Journal* **2017** 95 660–670.

35. Matuschek, E.; Brown, D. F. J.; Kahlmeter, G. Development of the EUCAST disk diffusion antimicrobial susceptibility testing method and its implementation in routine microbiology laboratories. *Clin. Microbiol. Infect.* **2014**, *20*, 255–266.

Supporting information

Eugenol-grafted aliphatic polyesters: towards inherently antimicrobial PLA-based materials through OCAs copolymerization

NMR characterization

4-allyl-2-methoxyphenyl (L)-2-(2,2-dimethyl-5-oxo-1,3-dioxolan-4-yl)acetate (2)

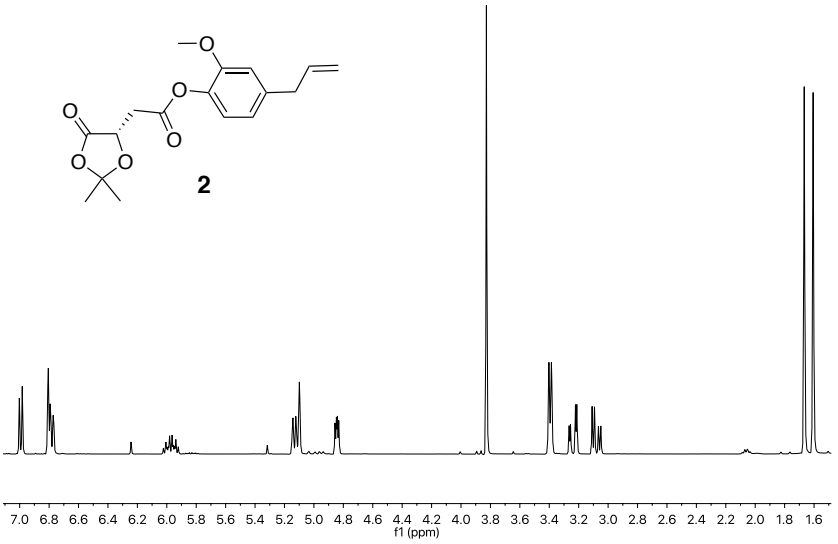

Figure S1: ^{1}H NMR spectrum for 2.

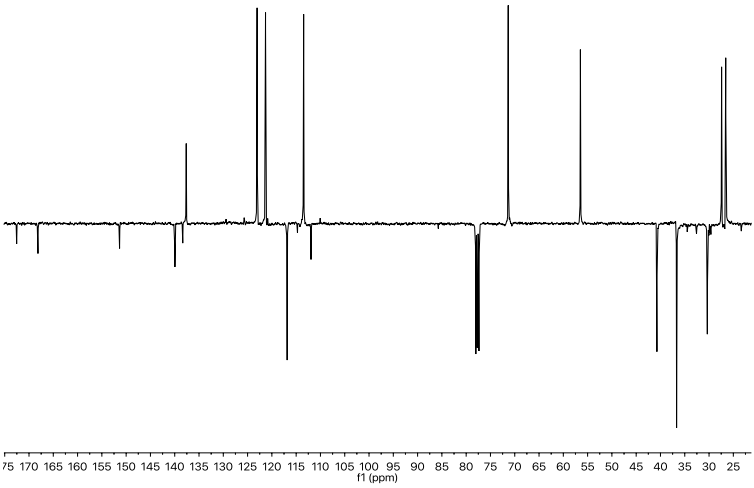

Figure S2: ^{13}C NMR spectrum for **2**.

(L)-4-(4-allyl-2-methoxyphenoxy)-2-hydroxy-4-oxobutanoic acid (3)

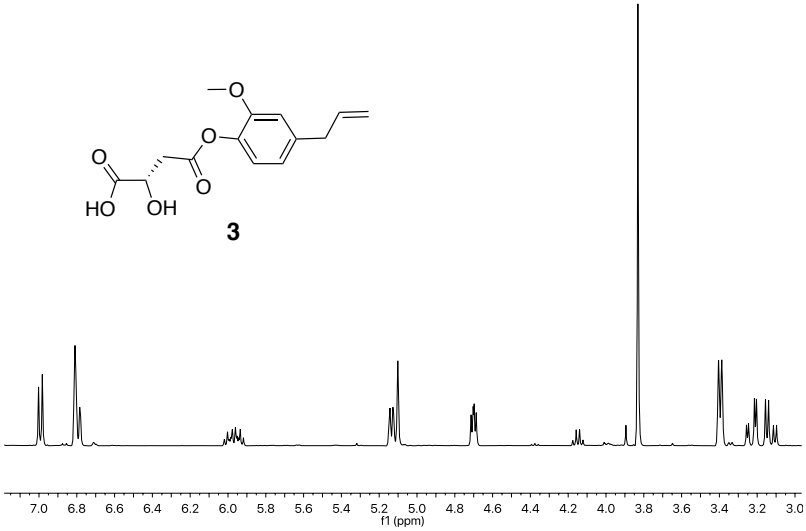

Figure S3: ^{1}H NMR spectrum for **3**.

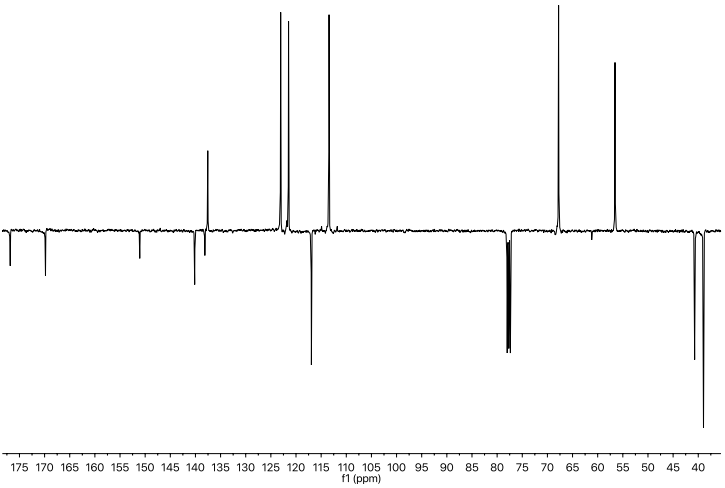

Figure S4: ^{13}C NMR spectrum for **3**.

4-allyl-2-methoxyphenyl (L)-2-(2,5-dioxo-1,3-dioxolan-4-yl)acetate (L-MalOCA, 4)

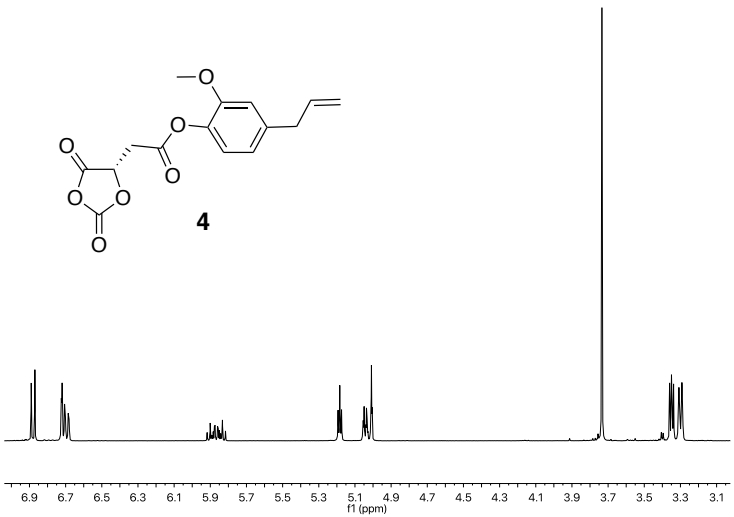

Figure S5: ^{1}H NMR spectrum for L-MalOCA (**4**).

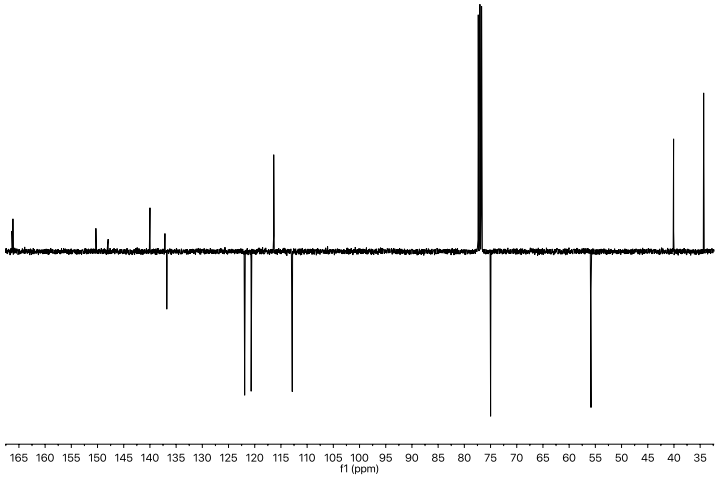

Figure S6: ^{13}C NMR spectrum for L-MalOCA (**4**).

HOMO1 polymerization product

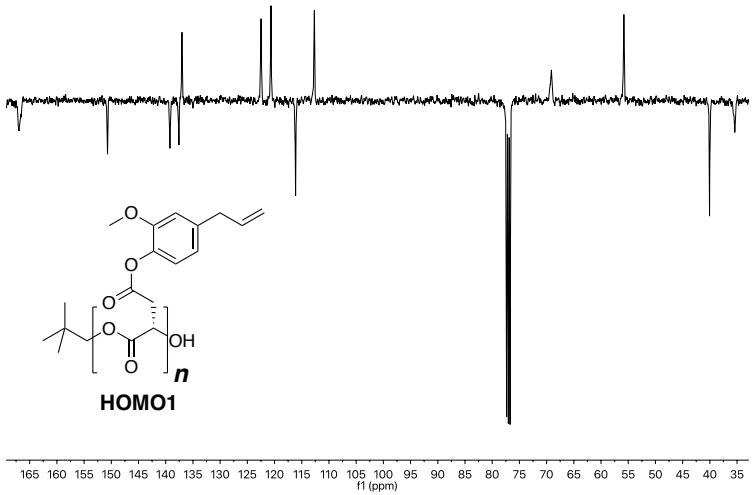

Figure S7: ^{13}C NMR spectrum for HOMO1.

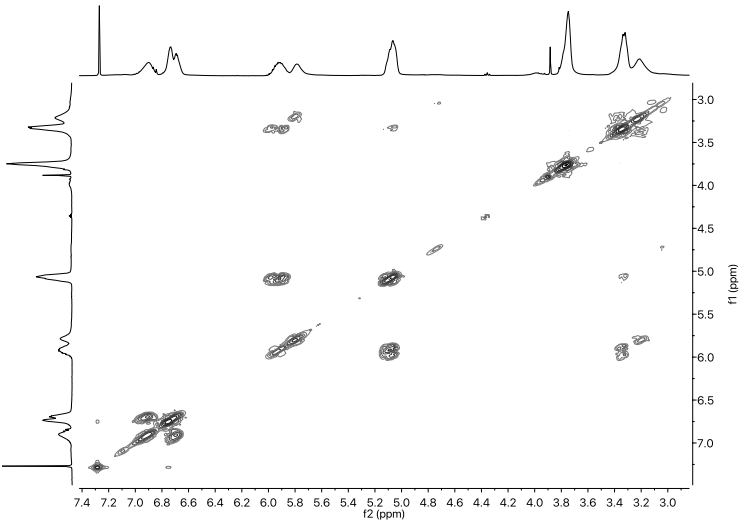

Figure S8: ^{1}H-^{1}H COSY spectrum for HOMO1.

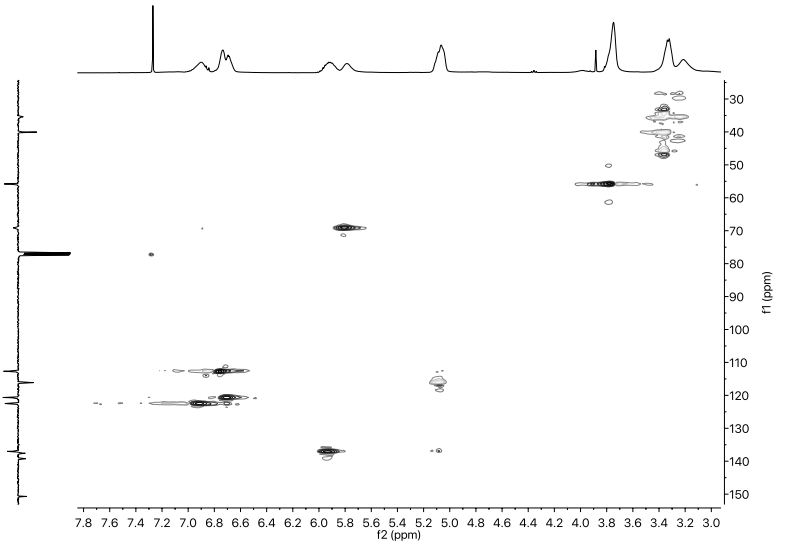

Figure S9: ^{1}H-^{13}C HSQC spectrum for HOMO1.

HOMO2 polymerization product

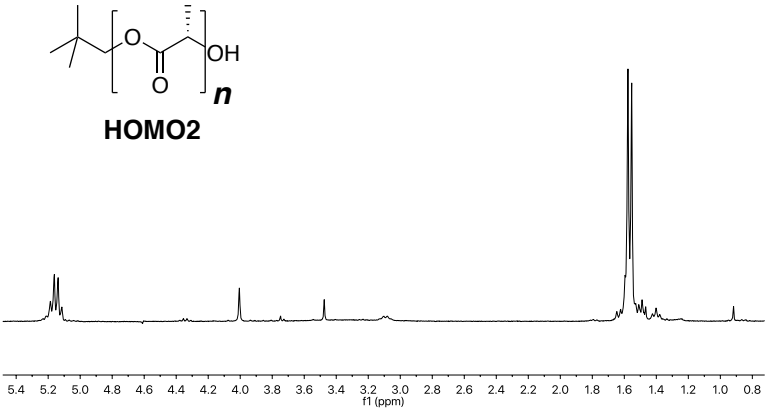

Figure S10: ^{1}H NMR spectrum for HOMO2.

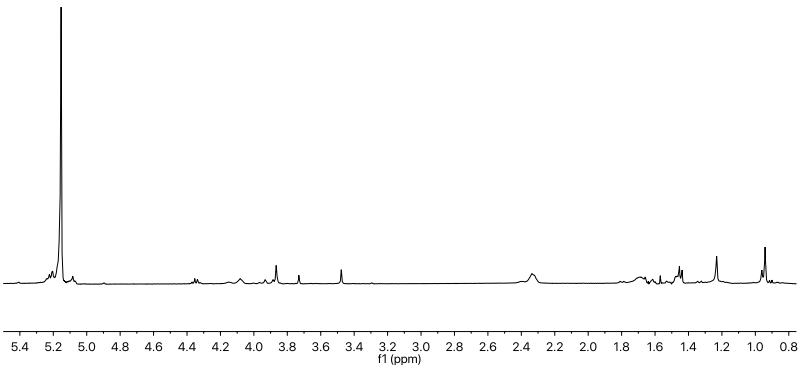

Figure S11: ^{1}H NMR decoupled spectrum for HOMO2.

SEC analyses

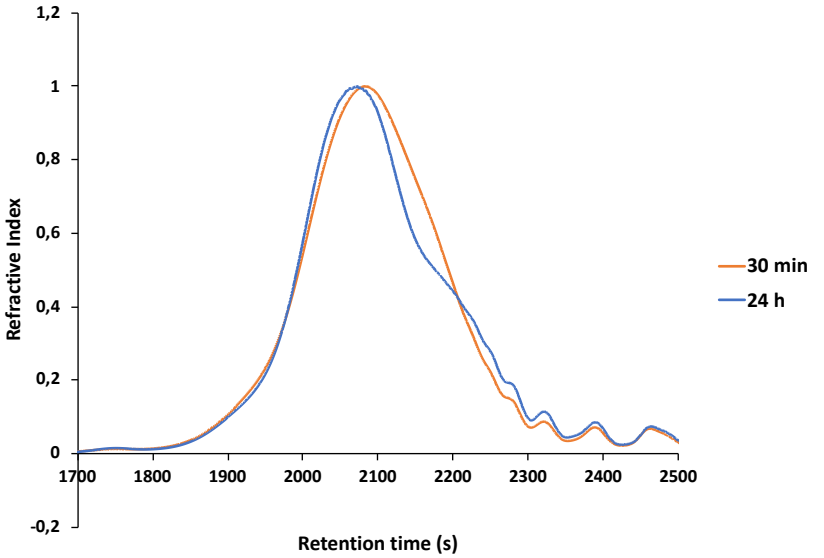

Figure S12: superimposed SEC traces relative to **4** homopolymerization reaction sampling.

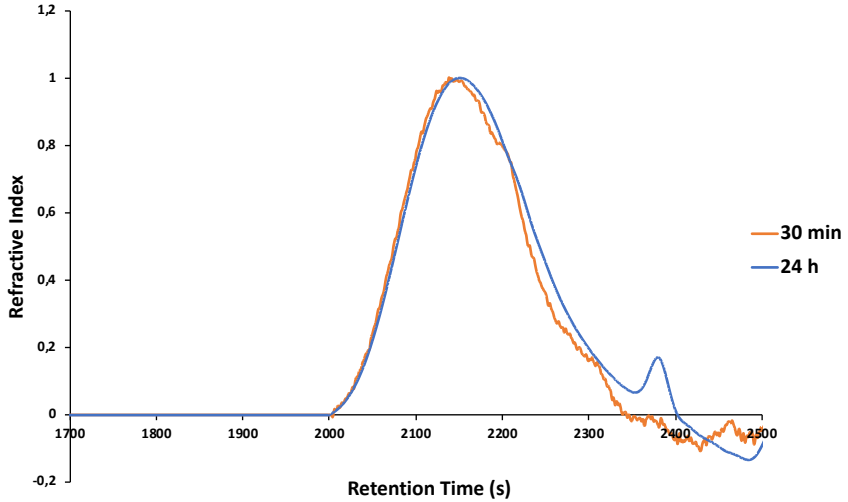

Figure S 13: superimposed SEC traces relative to ***5*** homopolymerization reaction sampling.

DSC analyses

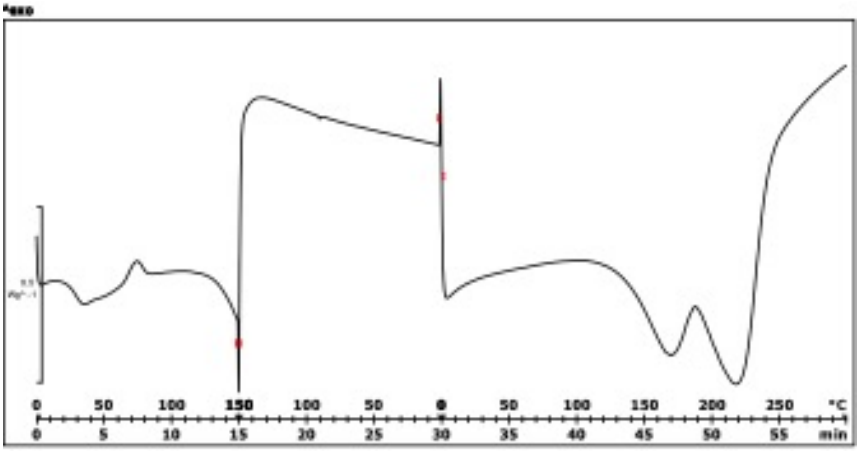

Figure S14: DSC thermogram for HOMO1 product.

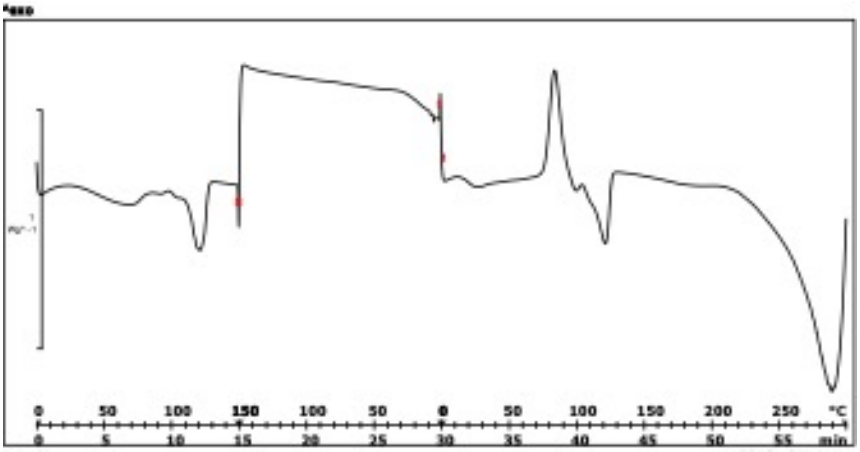

Figure S15: DSC thermogram for HOMO2 product.

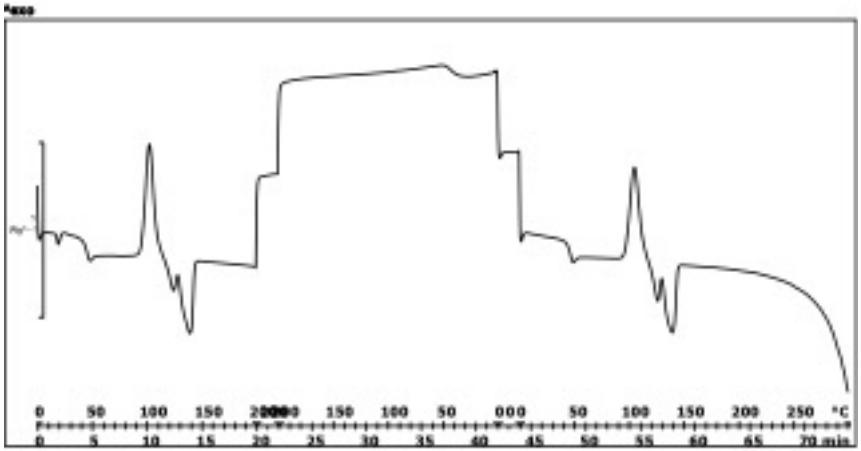

Figure S16: DSC thermogram for COP1 product.

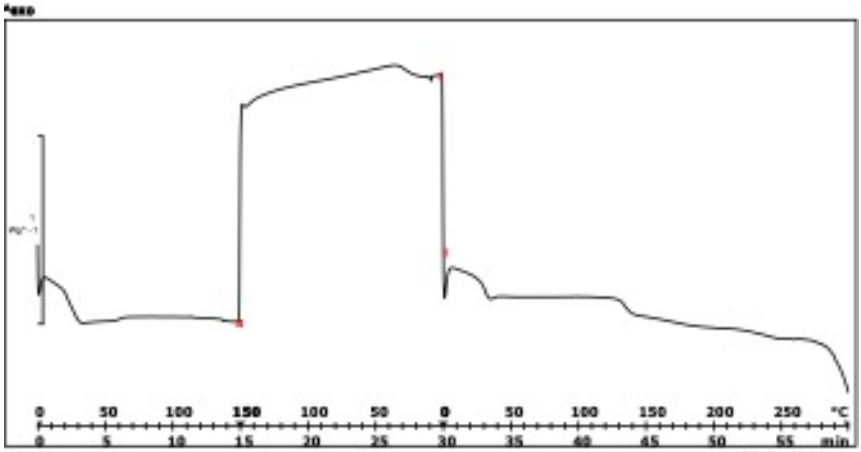

Figure S17: DSC thermogram for COP2 product.

1,3-dioxolan-4-ones as promising monomers for aliphatic polyesters: metal-free, in bulk preparation of PLA

The first example of organocatalyzed, solvent-free, polymerization of 1,3-dioxolan-4-ones, as easily accessible monomers for a green preparation of PLA, is here described. A screening of reaction conditions has been conducted, from which p-toluensulfonic acid emerges as the most efficient Brønsted acid catalyst. Reaction kinetics has been investigated, following the reaction conversion through ^{1}H NMR and the growth of the molecular weight through SEC analysis. A plausible polymerization mechanism has been proposed, explaining the key role of the acid catalyst. The obtained polymer shows complete retention of stereochemistry as well as good polydispersity and good thermal properties.

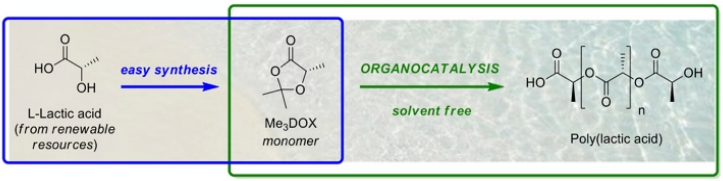

Work still in progress

1. Introduction

Following the ever-increasing manufacturing of plastic-made commodities, in recent years research efforts have been aimed towards the possibility of replacing traditional polymers based on petrochemical sources with more eco-friendly materials. Among them, polylactic acid (PLA) is one of the most intriguing, thanks to its derivation from renewable sources and, at the same time, to its good biodegradability.[1,2] Preparation of PLA relies either on polycondensation of lactic acid under azeotropic distillation conditions[3] or, more commonly, on ring-opening polymerization (ROP) of lactide, both routes typically involving appropriate catalysis. ROP is usually preferred, since it allows an optimal control over both molecular weight and stereochemistry, affording polymers with controlled properties.[4] L-lactide bulk ROP, generally running under the catalysis of tin(II) 2-ethylhexanoate (Sn(Oct)2), is at present the most common and industrially applied methodology for the preparation of PLA.[5]

While lactide ROP is extremely effective, the synthesis of precursory lactide monomers suffers from some drawbacks. Lactides can be prepared either through cracking of oligomers under metallic catalysis or through the dehydrative cyclization of α-hydroxy acids.[6] Thermal cracking requires a high thermal stability of the starting material and gives rise to non-negligible epimerization, offering scarce possibilities for what regards the functionalization and chemical modification of the lactide monomer. The dehydrative cyclization of α-hydroxy acids requires high dilutions and long reaction times, affording product in moderate yield. Aiming to tune and to broaden the properties of PLA-type materials, cyclization strategies have been developed for the preparation of lactides featuring functional groups, starting from variously substituted α-hydroxy acids and α-haloacyl chlorides. These reactions proved however to be troublesome, since oligomerization competes seriously with the desired formation of the six-membered ring.[7]

Given the intrinsic complexity in the synthesis of lactide monomers, together with the weak driving force for lactide ROP, brought by the relief of a six-membered ring strain,[8] alternative heterocyclic monomers have been proposed (**Figure 1**). The idea of increasing the ROP driving force brought to the development of 1,3-dioxolane-2,4-diones, also known as O-Carboxy Anhydrides (OCAs).[9,10] Polymerization of OCAs is indeed very fast thanks to the liberation of CO_2 and it well tolerates structural modification, allowing use of functionalized OCAs and hence introduction of functional groups along the polyester backbone.[11] A main

Figure 1: State of art for PLA synthesis.

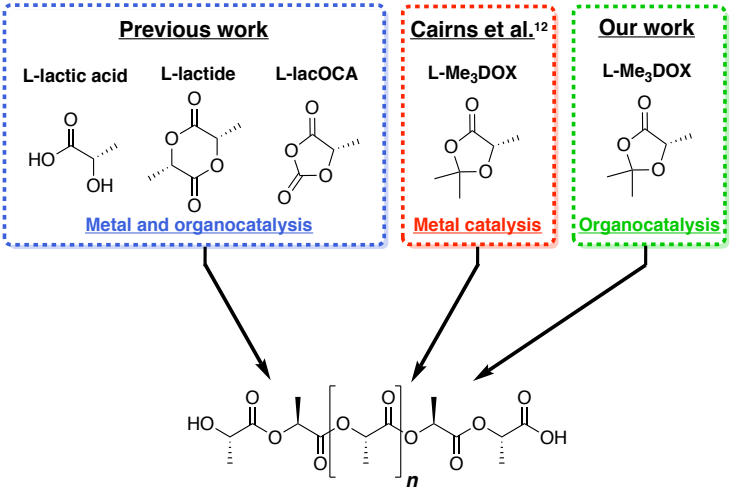

drawback is the use of phosgene or its equivalents for the synthesis of OCAs, resulting in high cost and severe toxicity problems. In addition, OCAs are very unstable and cannot be stored for a long time. Going forward with the idea of taking advantage from release of a small molecule in order to increase the driving force of the polymerization, quite recently Cairns and coworkers reported a promising example of ROP driven by the elimination of formaldehyde or acetone.[12] The strategy exploits 1,3-dioxolan-4-ones (DOX) as versatile and stable monomers deriving from sustainable and inexpensive resources,[13] and a salen supported aluminium complex as suitable Lewis acid catalyst for DOX polymerization.

In addition to research on new monomers, in recent years intensive efforts have been directed towards making the synthesis of PLA more 'green', by replacing toxic and polluting heavy metal catalysts with organocatalysts.[14, 15] Up to now, various metal-free systems have been developed for the polymerization of both lactide and OCAs. However their application in bulk remains a major challenge, preventing for the moment the transition to the industrial scale.[16] Basic organocatalysts for lactide ROP under solvent-free conditions have been widely investigated with several serious drawbacks, such as their low thermal stability and racemization of L-lactide.[17] In contrast, acids have been poorly explored until now, with only two recent studies in bulk, employing respectively triflic acid (TfOH)[18] and diphenylphosphate (DPP)[19, 20] as Brønsted acid catalysts.

Continuing our interest in the synthesis of PLA-based polymers,[21, 22, 23] we looked at DOX as promising monomers for a green PLA-production.[24] We here describe a mild DOX-polymerization procedure, employing an easily available and low-cost acid organocatalyst, in bulk at 100 °C. After screening of the reaction conditions, the obtained material was characterized, showing high retention of stereochemistry, good dispersity of molecular weights and good thermal properties, comparable to those reported for standard PLA.[25, 26]

2. Experimental section

2.1 Chemicals and materials

All reagents have been purchased by Sigma Aldrich and used as received. L-(+)-Lactic acid, ≥ 98 %; Paraformaldehyde, reagent grade, crystalline; *p*-Toluenesulfonic acid monohydrate, ≥ 98 %; Toluene, ≥ 99.7 %; Acetone ≥ 99.5 %; Magnesium sulfate, anhydrous, ≥ 99.5 %; Trifluoromethanesulfonic acid, 98 %; Trifluoroacetic acid, 99 %; Diphenyl phosphate, 99 %; (±)-Camphor-10-sulfonic acid, 98 %; Neopentanol, 99 %.

2.2 Synthesis of 1,3-dioxolan-4-one (MeDOX)

L-lactic acid (5 g, 55.5 mmol), para-formaldehyde (4.17 g, 138.8 mmol) and *p*-toluensulfonic acid (5.36 mg, 0.03 mmol) were dissolved in toluene (150 mL) and refluxed for 6h using a Dean-Stark apparatus to periodically remove water. The reaction was then cooled and the solvent evaporated. The residue was dissolved into CH_2Cl_2 (50 mL) and washed with sodium bicarbonate aqueous solution (3x25 mL) and brine (3x25 mL). The organic layer was dried with sodium sulfate and the solvent was evaporated to obtain the product as a colorless oil (yield 70%). ^{1}H NMR (400 MHz, $CDCl_3$) δ 5.55 (s, 1H), 5.42 (s, 1H), 4.30 (q, 1H, J = 6.0 Hz), 1.49 (d, 3H, J = 6.0 Hz).

2.3 Synthesis of 2,2,5-trimethyl-1,3-dioxolan-4-one (Me_3DOX)

L-lactic acid (5 g, 55.5 mmol) and *p*-toluensulfonic acid (212 mg, 1.23 mmol) were dissolved in a 1:1 acetone:toluene mixture (300 mL) and refluxed for 6h with a Dean-Stark apparatus to periodically remove water. The reaction was then cooled and solvent evaporated. The residue was dissolved into CH_2Cl_2 (50 mL) and washed with sodium bicarbonate aqueous solution (3x25 mL) and brine (3x25 mL). The organic layer was dried with sodium sulfate and the solvent was evaporated. The product was dried over CaH_2 overnight yielding a colorless oil (yield 58%). ^{1}H NMR (400 MHz, $CDCl_3$) δ 4.47 (q, 1H, J = 6.8 Hz), 1.60 (s, 3H), 1.53 (s, 3H), 1.47 (d, 3H, J = 6.8 Hz).

2.4 General polymerization procedure

Monomer, acid catalyst, initiator and $MgSO_4$ were mixed under nitrogen atmosphere, without solvent. Polymerization reaction was conducted at 100 °C up to 48h. The reaction mixture was dissolved into CH_2Cl_2 (20 mL) and washed with sodium bicarbonate aqueous solution (3x15 mL) and brine (3x15 mL). The organic layer was dried over sodium sulfate and the solvent evaporated, to obtain a yellowish solid. This was then dissolved in CH_2Cl_2 and precipitated in MeOH, to obtain the product as white solid. ^{1}H NMR (400 MHz, $CDCl_3$): δ 5.15 (q, 1H, J = 4.0 Hz), 1.57 (d, 3H, J = 4.0 Hz).

2.5 Size exclusion chromatography (SEC)

Molecular weights and dispersities of the polymers were evaluated using a SEC system having Waters 1515 Isocratic HPLC pump and a four Waters Styragel columns' set (HR3-HR4-HR5-HR2) with an UV detector Waters 2487 Dual λ Absorbance Detector set at 230 nm, using a flow rate of 1 mL min^{-1} and 60μL as injection volume. Samples were prepared dissolving 50 mg of polymer in 1 mL of anhydrous CH_2Cl_2 and filtering the solution on 0.45 μm filters.

Given the relatively high loading, a check was performed using lower concentration of polymer (5 mg mL^{-1}), in order to ensure no column overloading. Anyway, higher loadings were preferred as UV signal of PLA is relatively weak.

Molecular weight data are expressed in polystyrene (PS) equivalents. The calibration was built using monodispersed PS standards having the following nominal peak molecular weight.

(Mp) and molecular weight distribution (D): Mp = 1,600,000 Da (D ≤ 1.13), Mp = 1,150,000 Da (D ≤ 1.09), Mp = 900,000 Da (D≤1.06), Mp=400,000Da (D≤1.06), Mp=200,000Da (D≤1.05), Mp=90,000Da (D≤1.04), Mp=50,400Da (D=1.03), Mp=30,000Da (D=1.06), Mp=17,800Da (D=1.03), Mp=9730Da (D=1.03), Mp=5460Da (D=1.03), Mp=2032Da (D=1.06), Mp=1241Da (D=1.07), Mp=906Da (D=1.12), Mp=478Da (D=1.22); Ethyl benzene (molecular weight = 106 g mol^{-1}). For all analyses, 1,2-dichlorobenzene was used as the internal reference.

2.6 ^{1}H NMR analyses

^{1}H NMR spectra were registered with a Bruker Ultrashield 400 MHz. The chemical shifts are reported in ppm and referred to TMS as internal standard. All samples were prepared by dissolving 6–8 mg of polymer into 1 mL of $CDCl_3$.

2.7 DSC analysis

DSC analyses were conducted using a Mettler Toledo DSC1, on sample weighting from 5 to 10 mg. Melting and crystallization temperatures were measured using the following temperature cycles:

1. Heating from 25 °C to 190 °C at 10 °C/min;
2. 5 min isotherm at 190 °C;
3. Cooling from 190 °C to 25 °C at 10 °C/min;
4. 2 min isotherm at 25 °C;
5. Heating from 25 °C to 190 °C at 10 °C/min.

The first two cycles were run to eliminate residual internal stresses deriving from the synthesis and workup procedures. Glass transition temperature (T_g), cold crystallization temperature (T_{cc}) and melting temperature (T_m) were determined during the second heating scan.

2.8 MALDI-ToF

Mass spectrum was registered on a Bruker Autoflex MALDI-ToF spectrometer. MALDI-ToF samples were prepared using 2-(4-Hydroxyphenylazo)benzoic acid matrix and potassium trifluroacetate as the ionisation source.

2.9 TGA analysis

TGA was performed using a TGA 4000 Perkin Elmer instrument; test was conducted in nitrogen atmosphere, with a program that provides a single heating cycle from 30 °C to 500 °C at 10 °C/min.

3. Results and discussion

3.1 Polymerization reaction of 1,3-dioxolan-4-one

We started our investigation selecting 1,3-dioxolan-4-one (MeDOX), 1 as monomer, known to be able to undergo polymerization releasing volatile formaldehyde. MeDOX was synthesized as reported in **Scheme 1a**, applying a slightly modified literature protocol.[12]

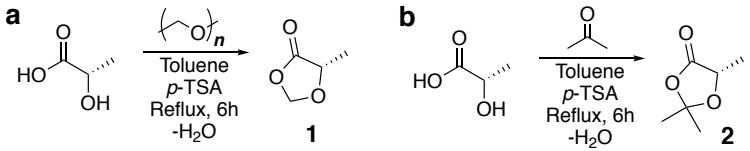

Scheme 1: (**a**) Synthesis of 1,3-dioxolan-4-one (MeDOX) **1**, 70%. (**b**) Synthesis of 2,2,5-trimethyl-1,3-dioxolan-4-one (Me_3DOX) **2**, 58%.

The first attempt for the polymerization of **1** was carried out using neopentanol as initiator and TfOH as organocatalyst (1:10:200 initiator:catalyst:monomer molar ratio). The reaction was conducted without solvent, at 100 °C, sampling from the mixture at different times - namely 2, 4.5, 23, 48h - in order to follow the reaction kinetics. Chromatograms from SEC analyses of all samplings are reported in **Figure 2a**.

The reaction took about 48h to reach full conversion, with a significant growth in terms of molecular weights only after about 20h of reaction, according to SEC traces.

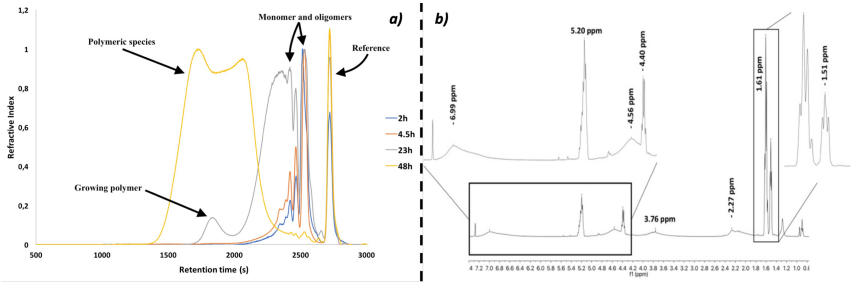

Figure 2: (**a**) SEC chromatograms of samples taken from the MeDOX polymerization reaction. (**b**) ^{1}H NMR spectrum of the MeDOX polymerization products.

The trace relative to the 48h sampling possesses a quite uncommon bimodal shape. Indeed, the corresponding ^{1}H NMR spectrum (**Figure 2b**) demonstrated the presence of a complex mixture of species, some of which are reported in **Figure 3**. The signal centered at 5.20 ppm is typical for the **a** proton in linear isotactic PLA. However, in highly stereoregular PLA, this signal appears as a sharp quartet. The broad appearance of this signal could possibly indicate some degree of irregularity along the chain. In addition, the possible occurrence of epimerization phenomena and the participation of formaldehyde in polymerization reaction must also be taken into account.

To this regard, the co-existence of structures like **II**, **III** and **IV** would broaden the signal centered around 5.20 ppm, relative to **c** protons, because of the increased mobility of the chains given by the acetal bridges. The presence of entities like **II**, **III** and **IV** can also explain the irregular appearance of the signal at 1.61 ppm, relative to the **d** methyl groups and the presence of broad signals centered at 6.99 and 4.56 ppm, likely attributable to **e**, **f** and **g** methylene groups. A more regular structure such as **V** could be also present, accounting for the sharp quartet centered around 4.40 ppm (**h** proton) and for the broad signal at 3.76 (**j** CH_2).

The statistical introduction of esteracetal bridges along polyester chains has been already reported by Martin and coworkers.[13] They recently described the synthesis of marine-degradable PLA, proving that the introduction of esteracetals significantly changes the properties of the material, enhancing in particular its degradation in aqueous media.

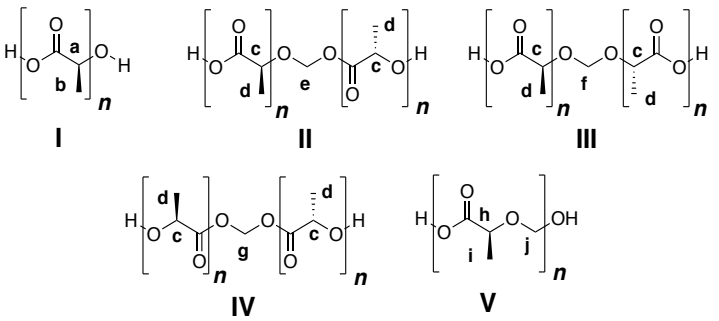

Figure 3: Plausible molecular entities present in the MeDOX polymerization mixture.

3.2 Polymerization reaction of 2,2,5-trimethyl-1,3-dioxolan-4-one

2,2,5-Trimethyl-1,3-dioxolan-4-one (Me3DOX, **2**) was then considered as an alternative monomer. Its synthesis is shown in Scheme 1b. The first polymerization reactions were carried out overnight using the same conditions described above for MeDOX, namely a 1:10:200 initiator:catalyst:monomer molar ratio, without solvent. Again, neopentanol was the initiator and TfOH the catalyst of choice. In the ^{1}H NMR spectrum of the product no signals denouncing the possible insertion of acetone seem to be present. However, since from SEC analysis only oligomeric species appear to have formed, a screening of polymerization conditions was conducted, aimed to increase the molecular weight of the products.

3.2.1 Catalyst screening

A series of protic organic acids were evaluated as possible organocatalysts. All reactions were conducted in bulk, at 100 °C under N_2 atmosphere for 16h. Again, a 1:10:200 initiator:catalyst:monomer molar ratio was chosen. Results are expressed in terms of molecular weight of the final product, determined through SEC analysis (**Table 1**). Except for TfOH (entry 1), a correlation between the acidity of the catalyst and the efficacy of the polymerization reaction can be argued, namely as the acidity of the catalyst increases, the results in terms of molecular weight improve. In the case of the extremely acid TfOH, the effective protonation of the monomer is likely accompanied by the increasing role of the TfO- counterion as chain initiator, thus affecting the final molecular weight of the product.

Table 1: Screening of acid catalysts.[31-34]

Entry	Acid	M_n (PS equivalents) [gmol^{-1}]	pK_a
1	Triflic acid (TfOH)	1300	-14.7
2	*p*-Toluensulfonic acid (*p*-TSA)	7700	-6.7
3	Trifluoroacetic acid (TFA)	7000	0.5
4	Camphorsulphonic acid (CSA)	6900	1.2
5	Diphenylphosphate (DPP)	956	3.9

Similar peculiar behavior for TfOH has been already described in the ROP of lactide.[27] Reaction catalysed by DPP (entry 5) resulted in the product with the lowest molecular weight, possibly indicating an insufficient activation of the monomer by the acid catalyst. Since *p*-toluensulfonic acid (*p*-TSA) (entry 2) afforded the best result in terms of final molecular weight of the product, it was selected for further optimization of the reaction conditions.

Neopenatnol was chosen as initiator of choice for further investigations, given the ease in detecting its *t*-butyl moiety through NMR. The chain-end incorporation of the alcohol is indeed demonstrated through ^{1}H NMR (see spectral expansion in SI).

Entry	*p*-TSA loading (m/m %)	M_n (PS equivalents) [gmol^{-1}]
2a.1	5%	7700
2a.2	2%	7100
2a.3	0.5%	Oligomers

Table 2: Screening of p-TSA catalyst loading.

3.2.2 Catalyst loading

Two further reactions were conducted lowering the quantity of the *p*-TSA catalyst, as reported in **Table 2**. Besides the starting 5 m/m % concentration (200:10 monomer:initiator molar ratio), two lower catalyst concentrations were tested, namely 2 and 0.5 m/m %. While the reduction to 2% has low influence on the outcome of the reaction in terms of molecular weight of the product, the reduction to 0.5% only leads to oligomeric species, disclosing a limit value for catalyst concentration.

3.2.3 Kinetic studies

The reaction kinetics was studied employing neopentanol as initiator and *p*-TSA as catalyst, with a 1:10:200 initiator:catalyst:monomer molar ratio.

Samples were taken from the reaction at 1, 2, 4, 6 and 24h, following the change of molecular weight through SEC analysis and the reaction conversion through ^{1}H NMR (**Figure 4**).

From SEC chromatograms (see SI), it appears that the formation of polymeric species already starts after two hours. The peak profile slightly changes its shape at longer reaction times and after 24h it slightly broadens. In ^{1}H NMR spectra, the quartet centered at 4.47 ppm (labeled as **1**) can be followed, in order to observe the decrease in monomer concentration. Starting from 1h reaction time, a quartet centered at 5.15 ppm, increasing its intensity over reaction time, can be observed, likely attributable to the correspondent proton (labeled as **2**) in the developing PLA chains. Conversion becomes quantitative within 6h. Released acetone is well visible at 2.17 ppm, and other products deriving from its self-condensation are visible at around 2.5 ppm and 5.3 ppm, especially at higher reaction times.

In **Table 3**, molecular weights are reported in comparison to increasing conversion. It appears that monomer fully reacts after 6h, but after only 2h the molecular weights are already similar to the ones obtained at higher reaction times.

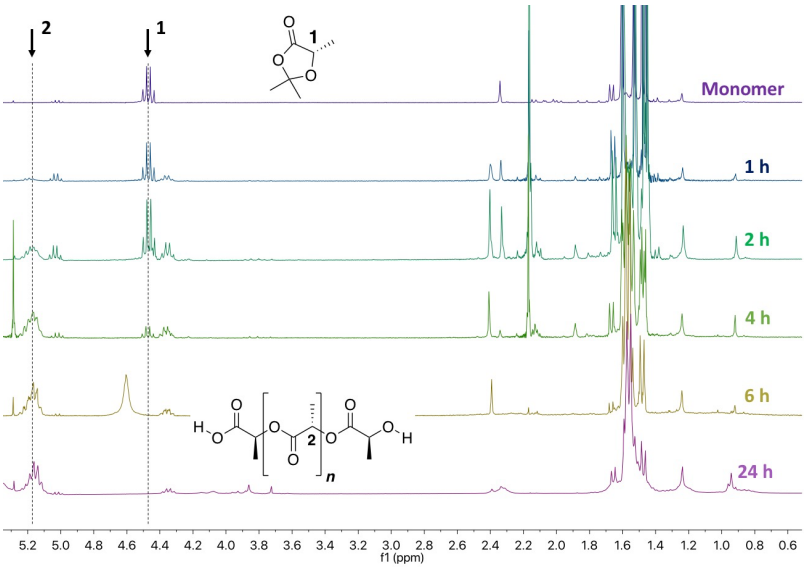

Figure 4: Stacked ^{1}H NMR spectra of samples taken from the Me$_3$DOX polymerization reaction, compared with the monomer's ^{1}H NMR spectrum.

Table 3: Data relative to kinetic studies of Me3DOX (**2**) polymerization.

Sample	Conversion[a]	M_P (PS equivalents) [$gmol^{-1}$]	Đ
1h	25%	Oligomers	//
2h	41%	7600	1.3
4h	84%	7500	1.4
6h	100%	7400	1.3
24h	100%	7400	1.5
Purified	//	7200	1.1

[a]Conversion was calculated through NMR, following the decrease of monomer signal (quartet centered at 4.47 ppm).

SEC traces in the higher molecular weights region of the crude samplings at 2, 4, 6, 24h are shown and discussed in SI. The dispersity index was also calculated, as a measure of the distribution of molecular masses in 2, 4, 6 and 24 h samples. Given the presence of a high number of oligomers and acetone self-condensation by-products, peak molecular weight was considered as being more reliable. In addition, the presence of these byproducts results in an increase of the polydispersity in the crude samples with respect to the purified product. A merging of data from SEC and ^{1}H NMR analyses indicates 6h as the optimal reaction time, when the best combination of conversion, molecular weight and dispersity is reached. The SEC chromatogram of the sample after purification is shown in **Figure 5**, molecular weight data reported in **Table 3**. The chromatogram shows a curve having a shoulder at higher retention times, indicating that probably two different macromolecular species are present in the mixture. Full description of the species involved was possible thanks to MALDI-ToF as discussed later. Considering that typical dispersities vary based on the mechanism of polymerization, a reaction mechanism for the *p*-TSA-catalyzed polymerization of Me3DOX is proposed (**Scheme 2**). As for the well-assessed mechanism of the DMAP-catalyzed polymerization of OCAs, also in this case the reaction proceeds with elimination of a small molecule and a presumable double activation by the organocatalyst, reconfirming once again the well-known ability of sulfonic acids to work through double activation mechanisms.[28, 29]

Figure 5: SEC trace relative to the purified product. Polymer peak and reference peak are highlighted.

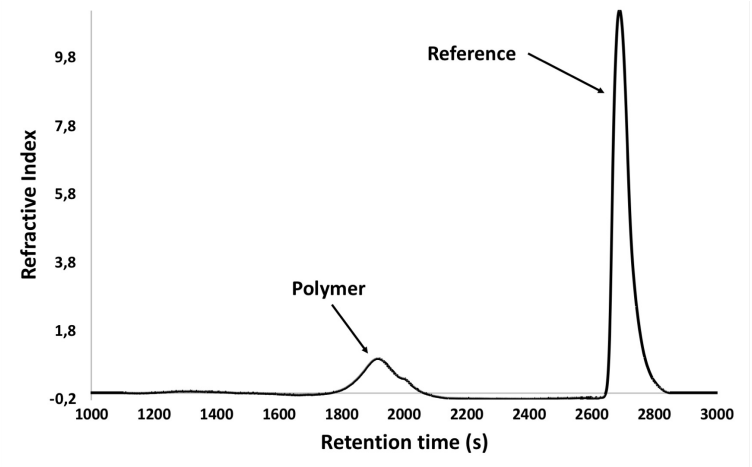

At this stage it is also worth mentioning that the experimental values for the molecular weights are far from the theoretical ones, as already described.[12] Further studies will be therefore needed, in order to fully disclose and avoid possible competing initiation reactions.

3.2.4 Thermal analyses

The DSC analysis was performed on the purified product in order to assess the thermal behaviour of the synthesized material (for the DSC thermogram, see SI). A semi-crystalline behavior was observed, with a cold crystallization temperature of 100 ° C and a melting peak (T_m) at 125 ° C. Glass transition temperature (T_g) has been registered at 36 ° C. While the cold crystallization temperature is close to that reported for PLA, T_g and T_m are quite low, possibly denouncing the overall moderate molecular weight of the product.[30]

TGA analysis was performed, in order to study the thermal stability of the purified product (TGA curve reported in the SI). It appears that the degradation profile is pretty regular, even if the degradation starts at low temperatures. This behavior could be due both to the evaporation of water absorbed and to the overall low molecular weight as well as the presence of different species as highlighted by both SEC and MALDI-ToF.

Scheme 2: Proposed polymerization mechanism for Me3DOX, compared with that for LacOCA.

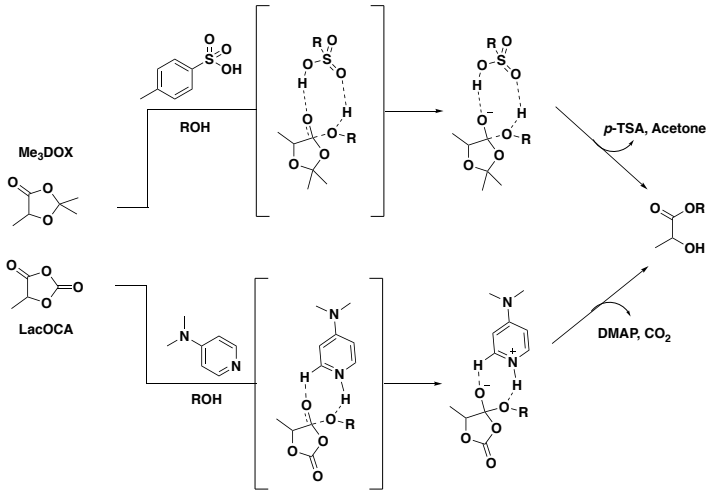

3.2.5 ^{1}H NMR analysis

^{1}H NMR analysis was useful in order to determine the stereoregularity of the product. Decoupled spectrum of the purified product was recorded and reported in **Figure 6**. The spec-

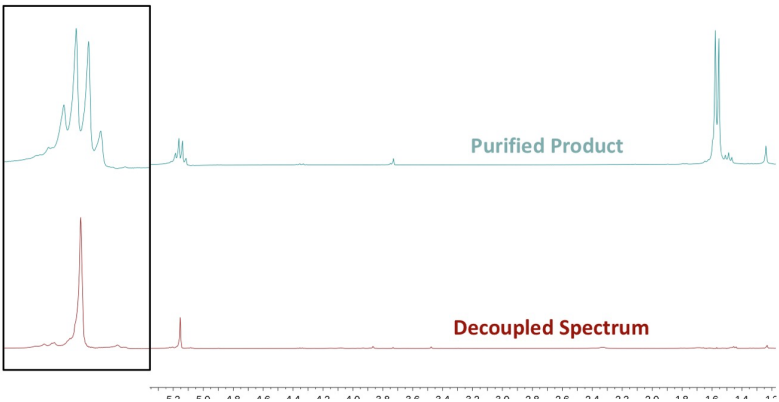

Figure 6: ^{1}H NMR spectrum of purified product (comparison between standard ^{1}H NMR and decoupled ^{1}H NMR). Spectral expansion of the region of interest reported in the black box.

trum shows a sharp singlet centered at 5.15 ppm, indicating an optimal retention of configuration in the product and therefore allowing to confirm the absence of epimerization phenomena during the reaction.

3.2.6 MALDI-ToF

MALDI-ToF experiment was performed in order to fully describe the structure of the product. Spectrum is reported in **Figure 7**. Two distributions are present and highlighted, with related structures reported. The main distribution can be referred to a PLA chain grown starting from neopentanol. To explain the presence of the minor polymeric species, it is reasonable to assume that, as the polymeric chain grows, acetalic bridges can statistically form. This event likely occurs mostly at late reaction stages, when the monomer concentration decreases. As acetal bridges form, the chain growth significantly slows down, giving as a result structures like the one shown in **Figure 7**. It has to be pointed out that the occasional formation and subsequent decomposition of acetal bridges in the early reaction stages can severely affect the reaction kinetics and mechanism. The occurrence of this kind of side reactions, proved by MALDI-ToF, can explain the discrepancy in terms of theoretical and experimental molecular weight of the product.

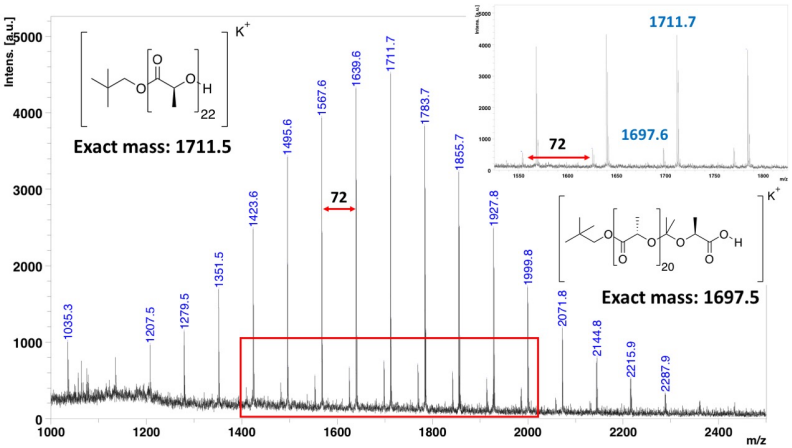

Figure 7: MALDI-ToF spectrum of the product with expansion and related structures.

4. Conclusions

In conclusion, polymerization of DOX monomers through an organocatalyzed protocol has been achieved for the first time. While MeDOX proved to be not suitable as monomer, because of the insertion of formaldehyde in the product's chains, Me$_3$DOX turned out to be more promising. A screening of organic acid catalysts was performed for Me$_3$DOX polymerization, disclosing a dependence of the molecular weights from both the acidity and the loading of the catalyst. Reaction kinetics highlighted the complete conversion of the monomer after only 6h, resulting in highly stereoregular PLA product with good dispersity. A plausible reaction mechanism is also proposed, closely resembling the one described for polymerization of OCAs.

Work is underway for the further optimization of the reaction conditions, with the aim of improving the molecular weight of the final polymer. Copolymerization reactions with DOX monomers bearing different side groups will be also considered in the due time, in order to exploit the green potential of this protocol for more focused applications.

References

1. R. Datta and M. Henry, *J. Chem. Technol. Biotechnol.*, **2006**, 81, 1119-1129.
2. S. Inkinen, M. Hakkarainen, A. Albertsson and A. Sodegard, *Biomacromolecules*, **2011**, 12, 523-553.
3. K. Enomoto, M. Ajioka, A. Yamaguchi, *Chem. Abstr.*, **1994**, 120, 9195.
4. O. Dechy-Cabaret, B. Martin-Vaca, and D. Bourissou, *Chem. Rev.*, **2004**, 104, 6147-6176.
5. P. Degée, P. Dubois, R. Jerome, S. Jacobsen and H. G. Fritz, *Macromol. Symp.*, **1999**, 144, 289.
6. T. L. Simmons and G. L. Baker, *Biomacromolecules*, **2001**, 2, 658.
7. M. Leemhuis, C. F. van Nostrum, J. A. W. Kruijtzer, Z. Y. Zhong, M. R. ten Breteler, P. J. Dijkstra, J.Feijen and W. E. Hennink, *Macromolecules*, **2006**, 39, 3500-3508.
8. Y. Wang and M. A. Hillmyer, *Macromolecules*, **2000**, 33, 7395.

9. O. Thillaye du Boullay, E. Marchal, B. Martin-Vaca, F. P. Cossío and D. Bourissou, *J. Am. Chem. Soc.*, **2006**, 128, 16442.

10. B. Martin Vaca and D. Bourissou, *ACS Macro Lett.*, **2015**, 4, 792-798.

11. A. Buchard, D. R. Carbery, M. G. Davidson, P. K. Ivanova, B. J. Jeffery, G. I. Kociok-Köhn and J. P. Lowe, *Angew. Chem. Int. Ed.*, **2014**, 53, 13858.

12. S. A. Cairns, A. Schultheiss and M. P. Shaver, *Polym. Chem.*, **2017**, 8, 2990-2996.

13. R. T. Martin, L. P. Camargo and S. A. Miller, *Green Chem.*, **2014**, 16, 1768-1773.

14. N.E. Kamber, W. Jeong, R.M. Waymouth, R.C. Pratt, B.G.G. Lohmeijer and J.L. Hedrick, *Chem. Rev.*, **2007**, 107, 5813-5840.

15. F. Nederberg, E. F. Connor, M. Moller, T. Glauser and J. L. Hedrick, *Angew. Chem., Int. Ed.*, **2001**, 40, 2172.

16. D. Bourissou, S. Moebs-Sanchez and B. Martin-Vaca, *C. R. Chimie*, **2007**, 10, 775-794.

17. R. J. Pounder, D. J. Fox, I. A. Barker, M. J. Bennison and A. P. Dove, *Polym. Chem.*, **2011**, 2, 2204-2212.

18. M. Bednarek, M. Basko, T. Biedron, E. Wojtczak and A. Michalski, *Eur. Polym. J.*, **2015**, 71, 380-388.

19. T. Saito, Y. Aizawa, K. Tajima, T. Isono and T. Satoh, *Polym. Chem.*, **2015**, 6, 4374-4384.

20. D. Delcroix, A. Couffin, N. Susperregui, C. Navarro, L. Maron, B. Martin-Vaca and D. Bourissou, *Polym. Chem.*, **2011**, 2, 2249.

21. S. Gazzotti, H. Farina, G. Lesma, R. Rampazzo, L. Piergiovanni, M. A. Ortenzi and A. Silvani, *Eur. Polym. J.*, **2017**, 94, 173-184.

22. L. Basilissi, G. Di Silvestro, H. Farina, M. A. Ortenzi, *J. App. Polym. Sci.*, **2013**, 128, 1575-1582.

23. V. Sabatini, H. Farina, L. Basilissi, G. Di Silvestro and M.A. Ortenzi, *J. Nanomater.*, **2015**, 1-16.

24. L. Mezzasalma, A. P. Dove and O. Coulembier, *Eur. Polym. J.*, **2017**, 95, 628-634.

25. T. Kawai, N. Rahman, G. Matsuba, K. Nishida, T. Kanaya, M. Nakano, H. Okamoto, J. Kawada, A. Usuki, N. Honma, K. Nakajima and M. Matsuda, *Macromolecules,* **2007**, 40, 9463.

26. M. Cocca, M.L. Di Lorenzo, M. Malinconico and V. Frezza, *Eur. Polym. J.*, **2011**, 47, 1073–1080.

27. M. Basko and P.Kubisa, *J. Polym. Sci. Part A: Polym. Chem.*, **2008**, 46, 7919-7923.

28. N. Susperregui, D. Delcroix, B. Martin-Vaca, D. Borissou and L. Maron, *J. Org. Chem.*, **2010**, 75, 6581-6587.

29. D. Bourissou, B. Martin-Vaca, A. Dumitrescu, M. Graullier and F. Lacombe, *Macromolecules*, **2005**, 38, 9993-9998.

30. J. Ambrosio-Martin, M. J. Fabra, A. Lopez-Rubio and J.M. Lagaron, *J. Mater. Sci.*, **2014**, 49, 2975-2986.

31. A. Pascual, J. R. Leiza, D. Mecerreyes, *European Polymer Journal,* **2013**, 49, 1601–1609.

32. V. Thomas, P. Maurer and R. Iftimie, *J. Phys. Chem. B*, **2010**, 114, 8147–8155.

33. D. C. French and D. S. Crumrine, *J. Org. Chem.*, **1990**, 55, 5494-5496. P. Christ, A. G. Lindsay, S. S. Vormittag, J. M. Neudorfl, A. Berkessel, and A. C. O'Donoghue, *Chem. Eur. J.*, **2011**, 17, 8524 – 8528.

Supporting Information

1,3-dioxolan-4-ones as promising monomers for aliphatic polyesters: metal-free, in bulk preparation of PLA

NMR Characterization

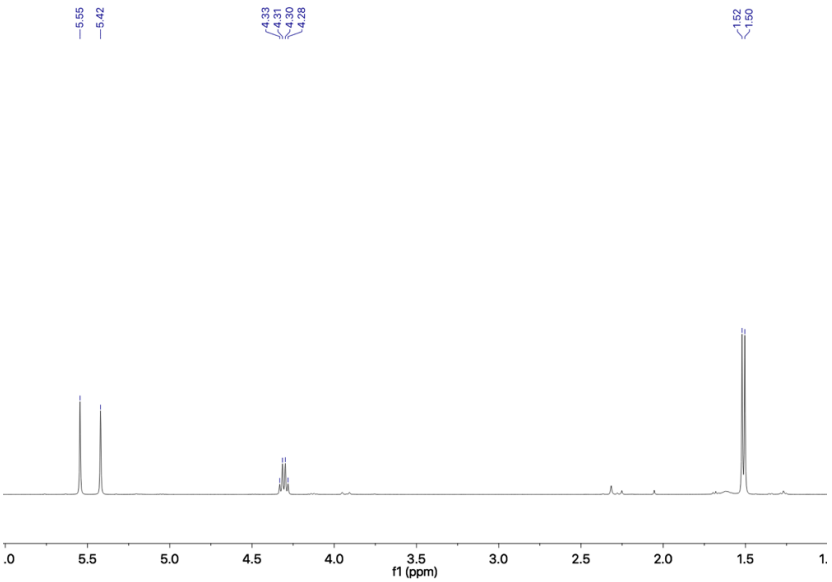

Figure S1: ^{1}H NMR spectrum of 1,3-dioxolan-4-one (MeDOX)

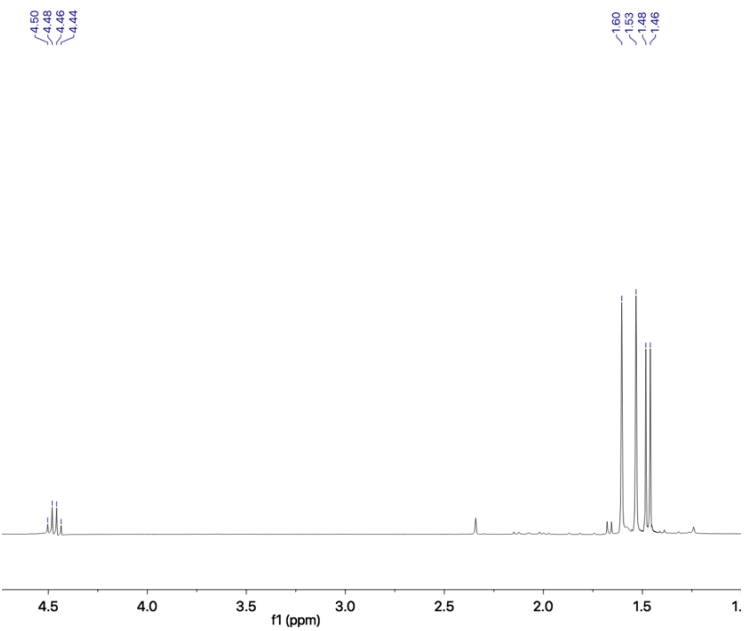

Figure S2: ^{1}H NMR spectrum of 2,2,5-trimethyl-1,3-dioxolan-4-one (Me3DOX).

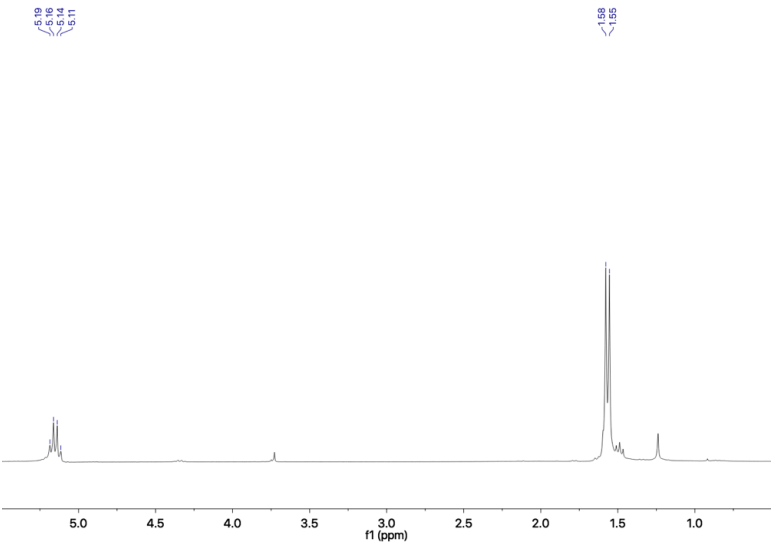

Figure S18: ^{1}H NMR spectrum purified polymerization product.

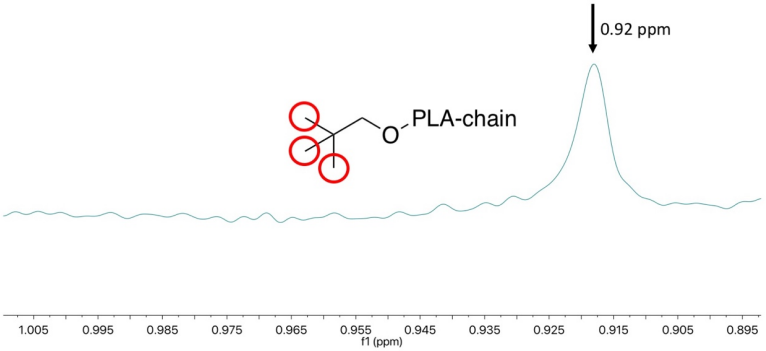

Figure S19: ^{1}H NMR spectrum expansion. t-Butyl signal relative to neopentanol initiator highlighted.

DSC analysis

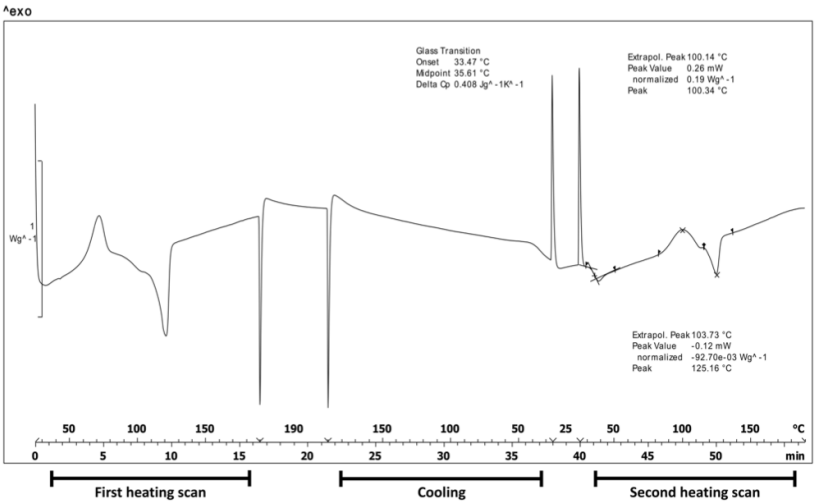

Figure S20: DSC thermogram for Me3DOX polymerization product.

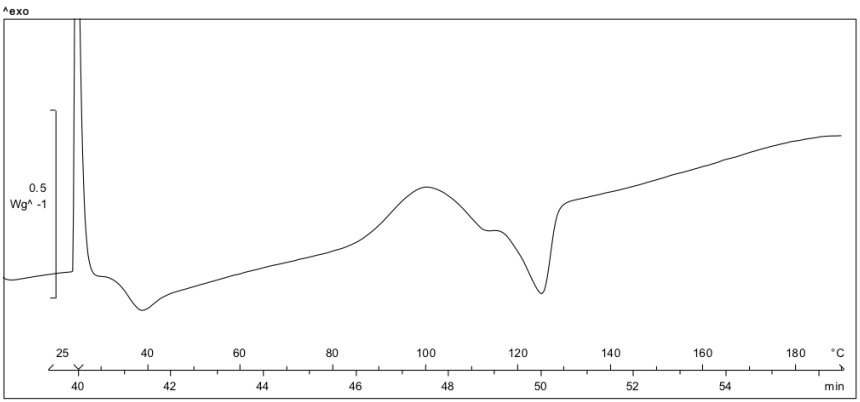

Figure S21: Magnification of the second heating scan in the DSC thermogram.

TGA analysis

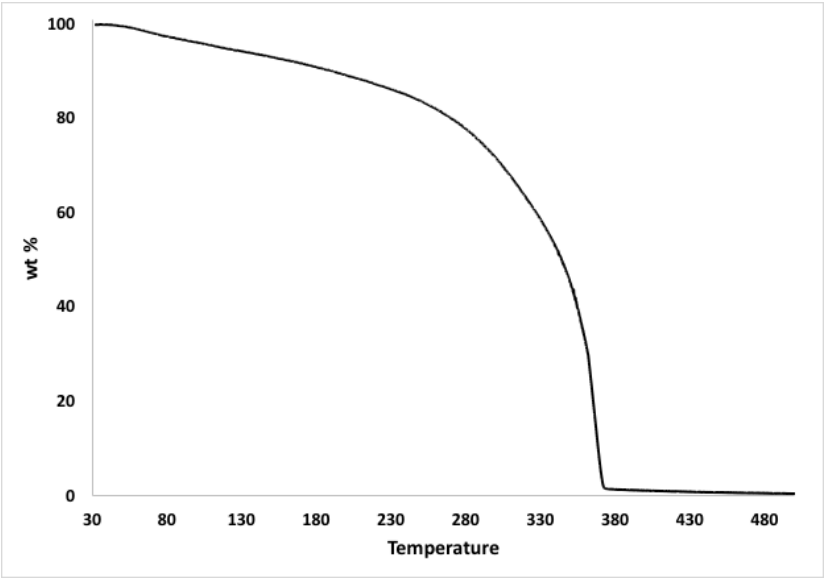

One-pot synthesis of sustainable high-performance thermoset by exploiting eugenol functionalized 1,3-dioxolan-4-one

1,3-dioxolan-4-one (DOX) chemistry was explored for production of "one-pot" biobased polyester thermosets. DOX monomer was first functionalized by naturally occurring eugenol to introduce a structural element, which could induce crosslinking reaction through cationic polymerization of the double bond. The feasibility of polymerizing DOX monomers bearing bulky side groups was proved by model phenol-substituted DOX monomer (PhDOX). Once the reaction was shown to be effective, the same protocol was applied to eugenol-substituted monomer (EuDOX). A brief screening of the optimal catalyst concentration was performed, to obtain a highly crosslinked product. The synthesized thermoset showed good thermal resistance and high mechanical strength probably due to the rich aromatic content. The obtained thermoset was further subjected to microwave-assisted hydrothermal degradation test, which demonstrated complete recyclability to water or methanol soluble products. NMR and MALDI-MS analysis of the obtained degradation products unveiled the structure of the thermoset strongly indicating that the polymerization of eugenol functionalized DOX monomer resulted in polylactide-like chains connected with aromatic-aliphatic segments resulting from the reaction of the eugenol double bonds. The presence of free hydroxyl and carboxyl groups shed light to the mechanism behind the observed shape-memory and self-healing properties.

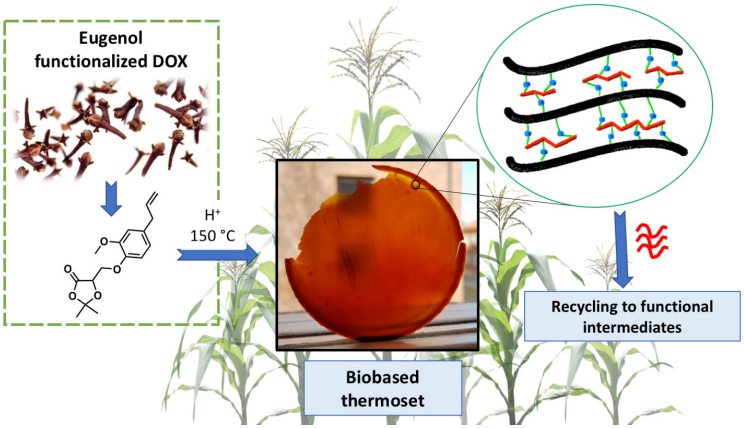

ACS Sustainable Chem. Eng. DOI: 10.1021/acssuschemeng.8b03655

1. Introduction

Thermoset resins have been widely used in many different fields of application, ranging from coatings to adhesives, electronics and many others. Considering their wide applicability and high industrial value, research efforts have targeted the development of novel biobased[1-6] and recyclable[7-9] thermosets with the aim to replace the mostly used petroleum-based and not easily recyclable counterparts. A thermoset resin able to conjugate both these features (i.e. renewability and recyclability) can be considered as the best target possible from a sustainability point of view. The preparation of polylactic acid (PLA)-based thermosets appears as a suitable strategy to achieve this result,[10-13] taking into account that PLA is a well-known biobased, biodegradable and biocompatible polyester.[14,15] However, it's use as thermosetting resin is currently accomplished only through post-modification reactions.[16-19] In addition the properties and mechanical strength at not good enough for many thermoset applications.

Compared to the multi-step approach, the use of a tailor-made monomers that enable one-pot PLA-like thermoset synthesis appears valuable from an industrial point of view, reducing the synthetic steps needed for obtaining the final product. To this regard, however, the reduced monomer scope in classical PLA synthetic methodologies (i.e. ring opening polymerization and polycondensation) stands as a major limitation. The use of recently described O-carboxyanhydrides (OCAs)[20,21] and 1,3-dioxolan-4-ones (DOXs)[22] monomers can significantly broaden the functionalization possibilities towards highly substituted PLA-based materials. In particular, while OCAs synthesis relies on highly toxic reagents and results into highly unstable products, DOX monomers can be prepared starting from safer precursors and stored for long periods of time.[23] The straightforward synthesis of DOX monomers also allows the easy introduction of a wide range of side groups, which can be exploited for the fine tuning of the material's final properties.

Within this context, eugenol-derived side group could be a valuable option providing additional functionality as well as renewability. Eugenol can be extracted from clove oil and lignin and it is very well known for its antifungal and antimicrobial properties.[24] In addition, the co-presence of a phenol moiety together with an allyl group makes it attractive from a chemical point of view, opening the possibility for many different synthetic approaches and improvement of materials properties such as mechanical strength.[25] To this regard, several examples have been reported in literature showing the use of eugenol as building block for

the preparation of different kinds of high performances thermosets with, for example, great heat resistance, low permittivity and low flammability.[26-28]

Following our interest in DOXs polymerization chemistry, we aimed to synthesize a novel eugenol-bearing 1,3-dioxolan-4-one monomer and to utilize it for one-pot preparation of a high performing thermoset. It was hypothesized that this monomer could react or polymerize through two mechanisms resulting in polylactide-like chains connected with aromatic-aliphatic hydrocarbon segments formed by reaction of the eugenol double bonds. The aromatic group of eugenol unit is also expected to enhance the mechanical properties of the resulting thermoset as compared to previous fully aliphatic polylactide-based thermosets. Addressing the concept of circular chemistry and manufacturing, we also evaluated the possibility to recycle the obtained thermoset back to functional intermediates through microwave-assisted hydrothermal reaction.

2. Experimental section

2.1 Chemicals and materials

All reagents were purchased by Sigma Aldrich and used as received. (±)-3-Chloro-1,2-propanediol, 98 %; HNO_3, ≥ 65 %; Eugenol, ≥ 98 %; HCl, ≥ 37 %; Ethyl Acetate (AcOEt), H_2SO_4, 95-97 %; *p*-Toluene sulfonic acid monohydrate (*p*-TSA), ≥ 98.5 %; Phenol, ≥ 99.5 %; Methanol (MeOH); 2,5-Dihydroxybenzoic acid (DHB), ≥ 99.5 %; Potassium trifluoroacetate, 98%; Dimethyl sulfoxide-d^6 (DMSO-d^6) minimum deuteration degree 99.8 %; Chloroform-d ($CDCl_3$), minimum deuteration degree 99.8 %.

2.2 Synthesis of 3-chloro-2-hydroxypropanoic acid (1)

According to literature procedure.[29]

2.3 Synthesis of 3-(4-allyl-2-methoxyphenoxy)-2-hydroxypropanoic acid (2)

Eugenol (4.75 g, 28.98 mmol) and sodium hydroxide (2.64 g, 66 mmol) were added to a dispersion of **1** (2 g, 16.1 mmol) in 20 mL of water. The reaction mixture was heated to reflux and left under stirring for 2 hours. The solution was then acidified to pH 1 with conc. HCl and extracted with AcOEt (4x10 mL), to obtain a mixture of product **2** and unreacted eugenol. The organic phases were collected and extracted with saturated aqueous $NaHCO_3$ solution (4x10 mL) in order to isolate the pure product. The aqueous phases were also collected, acidified with conc. H_2SO_4 to reach pH 1 and finally extracted with AcOEt (4x10 mL). The organic phases were collected, dried over Na_2SO_4 and the solvent was evaporated under reduced pressure, to obtain **2** as dark orange viscous oil (3.00 g, 74% yield). ^{1}H (NMR 400 MHz, DMSO-d^6) δ 6.90 (d, J = 8.1 Hz, 1H), 6.79 (d, J = 2.0 Hz, 1H), 6.68 (dd, J = 8.1, 2.0 Hz, 1H), 5.95 (ddt, J = 16.8, 10.0, 6.7 Hz, 1H), 5.12 – 4.98 (m, 2H), 4.31 (dd, J = 5.7, 3.5 Hz, 1H), 4.08 (m, 2H), 3.73 (s, 3H), 3.30 (d, J = 6.7 Hz, 2H). ^{13}C NMR (101 MHz, DMSO-d_6) δ 173.76, 149.56, 146.79, 138.37, 133.40, 120.80, 115.99, 114.66, 113.42, 71.65, 69.91, 56.06, 56.02. ^{1}H and ^{13}C NMR spectra of **2** are reported in Figure S1 and S2 in supporting information.

2.3 Synthesis of 5-((4-allyl-2-methoxyphenoxy)methyl)-2,2-dimethyl-1,3-dioxolan-4-one (EuDOX, 3)

2 (1.50g, 5.96 mmol) was dissolved in acetone (50 mL). The solution was cooled to -10 °C and then concentrated sulfuric acid was added dropwise (2.5 mL). Reaction was left under stirring for 4 hours. $NaHCO_3$ was then added until pH 8 was reached. Solid was filtered off and solvent removed under reduced pressure to obtain **3** as an orange solid (1.33 g, 76% yield). ^{1}H NMR (400 MHz, $CDCl_3$) 6.87 (d, J = 7.8 Hz, 1H), 6.72 (d, J = 7.9 Hz, 2H), 5.97 (ddt, J = 16.9, 10.2, 6.7 Hz, 1H), 5.13 – 5.05 (m, 2H), 4.79 (dd, J = 4.5, 2.5 Hz, 1H), 4.32 (qd, J = 10.9, 3.6 Hz, 2H), 3.84 (s, 3H), 3.35 (d, J = 6.7 Hz, 2H), 1.75 (s, 3H), 1.63 (s, 3H). ^{13}C NMR (101 MHz, $CDCl_3$) δ 170.63, 149.97, 146.18, 137.51, 134.45, 120.57, 115.72, 115.16, 112.98, 111.89, 74.41, 68.82, 55.94, 39.82, 26.88, 26.71. ^{1}H and ^{13}C NMR spectra of **3** are reported in Figure S3 and S4 in supporting information.

2.4 Synthesis of 2-hydroxy-3-phenoxypropanoic acid (4)

Phenol (2.73 g, 28.98 mmol) and sodium hydroxide (2.64 g, 66 mmol) were added to a dispersion of **1** (2 g, 16.1 mmol) in 20 mL of water. The reaction mixture was heated to reflux and left under stirring for 2 hours.

The solution was then acidified to reach pH 1 with conc. HCl and extracted with AcOEt (4x10 mL). The organic phases were collected and extracted with a saturated $NaHCO_3$ solution (4x10 mL). The aqueous phases were then collected, acidified with H_2SO_4 to reach pH 1 and finally extracted with AcOEt (4x10 mL). The organic phases were collected, dried over Na_2SO_4 and the solvent was evaporated under reduced pressure, to obtain **4** as a pale brown solid. (2.32 g, 79 % yield). ^{1}H and ^{13}C NMR data were in agreement with the literature.[30]

2.5 Synthesis of 2,2-dimethyl-5-(phenoxymethyl)-1,3-dioxolan-4-one (PhDOX, 5)

4 (1.50 g, 5.96 mmol) was dissolved in acetone (50 mL). The solution was cooled to -10 °C and then concentrated sulfuric acid was added dropwise (2.5 mL). Reaction was left under stirring for 4 hours. $NaHCO_3$ was then added until pH 8 was reached. Solid was filtered off and solvent removed under reduced pressure to obtain **5** as a pale brown solid (1.43 g, 51

% yield). ^{1}H NMR (400 MHz, $CDCl_3$) δ 7.31 (dd, *J* = 8.8, 7.4 Hz, 2H), 7.01 (tt, *J* = 7.3, 1.1 Hz, 1H), 6.95 (dd, *J* = 8.8, 1.1 Hz, 2H), 4.78 (dd, *J* = 4.2, 2.4 Hz, 1H), 4.39 – 4.24 (m, 2H), 1.72 (s, 3H), 1.64 (s, 3H). ^{13}C NMR (101 MHz, $CDCl_3$) δ 170.41, 158.17, 129.52, 121.61, 114.79, 111.78, 74.25, 66.96, 27.06, 26.68. ^{1}H and ^{13}C NMR spectra of ***5*** are reported in Figure S5 and S6 in supporting information.

2.6 2,2-dimethyl-5-(phenoxymethyl)-1,3-dioxolan-4-one (5) polymerization procedure.

5 (700 mg, 3.14 mmol) was introduced in a round bottomed flask. *p*-TSA (30 mg, 0.157 mmol) was added thereafter. The mixture was heated to 150 °C under nitrogen atmosphere for 3 hours to obtain a brown solid product.

2.6 EuDOX (3) polymerization.

3 (750 mg, 2.56 mmol) and *p*-TSA (24.4 mg, 0.128 mmol) were dissolved in 3 mL of AcOEt. As soon as both the monomer and the catalyst were completely dissolved they were poured in an aluminium mold and the solvent was left to evaporate overnight. The curing process was then performed, by heating at 150 °C for 3 hours, to obtain a dark orange transparent film.

2.7 Microwave degradation

Thermoset degradation was conducted in a microwave oven named flexiWAVE from Milestone Inc. Two solvents were tested as degradation medium: water and methanol. In addition to degradation in pure solvents, the effect of NaOH addition was evaluated (0.5 % w/w). Based on optimization of the general degradation conditions in earlier work with other aliphatic polyesters,[31] 200 mg of product was degraded by heating for 1 h either at 150 °C (water) or 110 °C (methanol). The degradation temperatures were reached after a ramp time of 3 min in both cases. Input irradiation power was varied automatically to reach and keep the specified temperatures.

2.8 Nuclear magnetic resonance (NMR)

400 MHz ^{1}H-NMR and 100 MHz ^{13}C-NMR spectra were recorded on a Bruker Advance 400 spectrometer at 298 K.

2.9 Matrix-assisted Laser desorption/ionization-Mass spectrometry (MALDI-MS)

For the measurements, a Bruker UltraFlex time-of-flight (TOF) mass spectrometer with a SCOUT-MTP ion source and equipped with a 337 nm nitrogen laser was used in reflector mode. Before analysis, the samples (1 mg/ml), the matrix, DHB (10 mg/ml) and the salt Potassium trifluoroacetate (1 mg/ml) solutions in MeOH were mixed and drop casted on a stainless steel MALDI plate in a volume of 8 µl.

2.10 Fourier transform infrared spectroscopy (FTIR)

FTIR was done on a Perkin Elmer Spectrum 100 with 16 scans from 4000 to 600 cm^{-1} through a resolution of 4 cm^{-1}. The golden gate was from Graseby Specac (Kent, UK) and the software PerkinElmer Spectrum was used to process the data.

2.11 Differential scanning calorimetry (DSC)

Mettler-Toledo 820 was utilized to conduct the measurements. 5 mg of each sample was placed in a 100 µl aluminium cup with a pinhole on the lid. The applied heating rate was 10 °C min^{-1} in a nitrogen atmosphere (rate 50 ml min^{-1}). Thermal behaviour was investigated using the following temperature cycles:

1. Heating from 25 °C to 200 °C.
2. 5 min isotherm at 200 °C.
3. Cooling from 200 °C to 25 °C.
4. 2 min isotherm at 25 °C.
5. Heating from 25 to 200 °C.

The first heating and cooling cycle was run to eliminate residual internal stresses deriving from the thermoset preparation.

2.12 Thermogravimetric analysis (TGA)

Mettler-Toledo TGA/SDTA 851e was utilized for thermal analysis. 5 mg of each sample was placed into a 70 µl alumina cup and heated at a rate of 10 °C min^{-1}. The measurements were performed under 80 ml min^{-1} nitrogen flow.

2.13 Size exclusion chromatography (SEC)

Verotech PL-GPC 50 Plus system equipped with a PL-RI Detector and two PLgel 5µm MIXED-D (300 x 7.5 mm) columns from Varian were employed for the measurements. Chloroform was used as the mobile phase (1 ml min^{-1}, 30 °C) and toluene as an internal standard to correct for flow rate fluctuations. The calibration was based on polystyrene standards with a narrow molecular weight ranging from 160 to 371 000 g/mol.

2.14 Gel Content Test

In order to determine the gel content ≈ 500 mg of the product was extracted with $CHCl_3$ (≈ 5 mL) for 24 h. The insoluble fraction was dried at 30 °C until constant weight was reached. Gel content was then calculated, following equation (1).

$$Gel\ content = \frac{m_{ae}}{m_{be}} \cdot 100\ \% \qquad (1)$$

Where m_{ae} indicates the sample weight after extraction and m_{be} the sample weight before extraction.

2.15 Tensile testing.

The testing was conducted on an INSTRON 5944 module equipped with pneumatic grips. A 500 N load cell was used for the measurements with a gauge length of 10 mm, and a crosshead speed of 5 mm/min was applied. The samples were cut into strips of width 0.5

cm with a thickness of an average of 0.1 mm. Before analysis, the test strips were preconditioned according to ASTM D618−96 (40 h at 50 % ± 5 % relative humidity and 23°C ± 1 °C).

2.16 Antimicrobial testing

The thermoset was crushed into pieces with mortar. Three different concentrations were tested: 1000 μg mL^{-1} and 2 dilution series -> 500 and 250 μg mL^{-1}. The thermoset at the highest concentration was compared with washed pieces of thermoset at the same concentration. The washing was performed in ethanol 70 % for 30 min. Thereafter, the ethanol was decanted off and the pieces was left to dry before testing was performed. The bacteria E-coli were harvested in mid-exponential phase and the tests were performed according to macrodilution in a bacteria concentration of 10^7 CFU mL^{-1}. 100 μL of bacteria suspension (107 CFU mL^{-1}) was transferred to 10 mL of LB broth. 2 mL of this suspension was then added into glass vials of three replicates. Bacteria suspensions were used as negative control and two types of antibiotics in tablet form with a loading of 10 μg were used as positive controls. The bacteria suspensions with and without material were placed in incubator with rpm 70 for 24 hours. At time 0, the suspensions were transparent and gave an OD value of 0.0467. Neither colour nor transparency was obviously changed when adding the materials. Then the OD were measured again after 12 h, 19 h and 24 h.

3. Results and discussion

Previously the efficacy of 1,3-dioxolan-4-one monomers (DOX) for the preparation of PLA materials has been highlighted.[22] Here the scope of DOX monomers was broadened to synthesis of high-performance polyester thermosets through functionalization by eugenol. Microwave-assisted hydrothermal degradation of the thermoset was also performed to obtain proof concerning the chemical structure and recyclability.

3.1 Synthesis of monomers

The two DOX monomers EuDOX, **3** and PhDOX, ***5*** were synthesized starting from 3-chloro-1,2-dihydroxypropanediol, through the common intermediate 3-chloro-2-hydroxy-propanoic acid **1 (Scheme 1)**. Compound **1** was then reacted with eugenol or phenol to obtain respectively the phenolic ethers **2** and **4**, achieved in high purity and in good yield. Subsequent α-hydroxy acid protection with acetone allowed obtaining the DOX monomers **3** and ***5***.

3.2 Proof of concept for polymerization of DOX with bulky side group: PhDOX polymerization

First polymerization of PhDOX was attempted, to prove the feasibility of the polyester formation from DOX monomers bearing a bulky side group. Since a rising difficulty has been

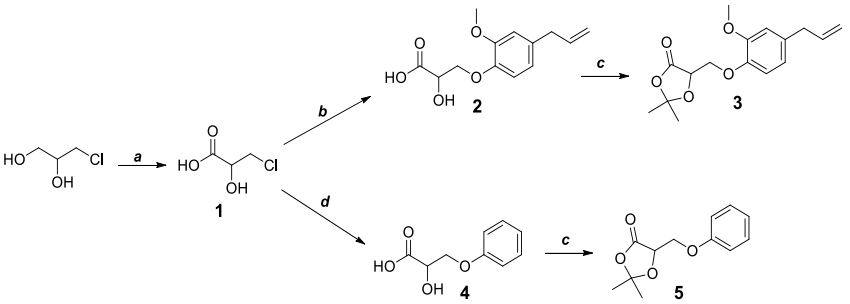

Scheme 3. Synthesis of the two DOX monomers including reagents and conditions, ***a)*** HNO_3, heating; ***b)*** eugenol, NaOH, H_2O, reflux, 2 h; ***c)*** acetone, H_2SO_4, 4h; ***d)*** phenol, NaOH, H_2O, reflux, 2 h.

Figure 1. ^{1}H NMR spectrum of the polymerization product of monomer ***5***.

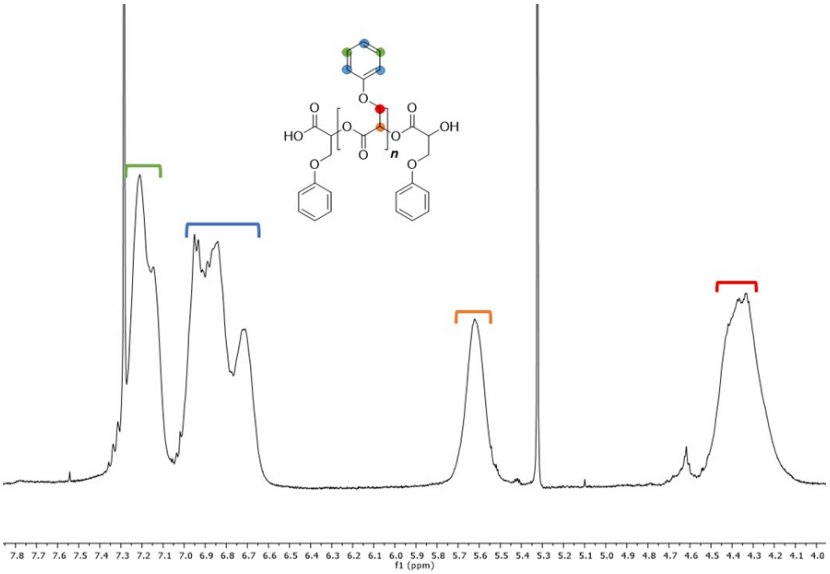

reported in aluminium salen-catalysed polymerization of 1,3-dioxolan-4-ones as the bulkiness of the side group increases,[22] we looked at a less cumbersome catalyst, namely Brønsted *p*-toluene sulfonic acid (*p*-TSA).

The polymerization reaction was firstly tested on PhDOX, utilized as a model monomer lacking additional reactive groups. Reaction was conducted in bulk, using *p*-TSA as catalyst with a 20:1 monomer to catalyst molar ratio (5 % m/m) at 150 °C for 3 hours under nitrogen atmosphere (**Scheme 2**). Reaction successfully yielded an oligomeric product (2000 g/mol according to SEC analysis). The ^{1}H NMR spectrum with peak assignments is shown in **Figure 1**.

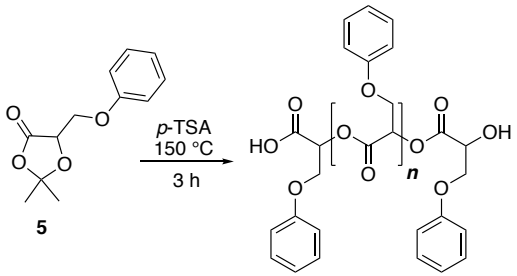

Scheme 2. Polymerization of monomer PhDOX.

3.3 EuDOX Polymerization

3.3.1 Catalyst to monomer ratio screening.

The same reaction protocol was then applied to EuDOX. This yielded an insoluble product, indicating that a crosslinking reaction likely occurred, resulting in a thermoset material. Encouraged by this outcome, the efforts were concentrated on screening the best reaction conditions and then evaluating the properties of the obtained eugenol-derived material.

First, a small survey on the optimal monomer to catalyst ratio was performed. Reactions were carried out varying the catalyst to monomer ratio, followed by determination of the gel content according to the procedure reported in the experimental section. The gel content of a thermoset is an important parameter that indicates the amount of crosslinked material in the product and therefore it can indicate the efficiency of the curing reaction.

Four different catalyst concentrations were tested and the respective gel content of the product was determined and reported in **Table 1**.

Table 1. Optimization of catalyst to monomer ratio and the resulting gel content.

Sample	Catalyst concentration (mol %)	Gel content (%)
TS0	0	0
TS1	1	31
TS5	5	89
TS10	10	90

As shown by the data in Table 1, there was a relationship between the catalyst concentration and the gel content. Starting from the TS0 sample, with 0 mol % catalyst concentration, no crosslinking reaction took place. By increasing the catalyst concentration to 1 mol %, some crosslinking took place, but the extent was low resulting in only 31 % gel content. Regarding the TS5 and TS10 samples with 5 or 10 mol % catalyst they both exhibited high and comparable gel content of around 90 %. Considering that no significant differences were registered between TS5 and TS10 samples, the lower catalyst concentration, i.e., 5 mol % was selected as the catalyst concentration for further studies and material production.

3.3.2 Film preparation

To obtain a film for evaluation of mechanical properties, an ethyl acetate solution of monomer and catalyst (5 % m/m loading) was prepared and poured into an aluminium mold, as shown in **Figure 2**. The solution was originally transparent (**Figure 2a**). The solvent was evaporated overnight at 30 °C in vacuum and the curing was then performed in an oven at 150 °C for 3 hours (**Figure 2b**). After curing the film was dark brown or orange due to the exposure to air at elevated temperature. The transparent and homogeneous film could then be removed from the mold (**Figure 2c**) and thin stripes were cut from the film, suited for tensile testing (**Figure 2d**).

3.3.3 Tensile testing

The mechanical properties of the cured thermoset were evaluated by tensile testing. The thermoset showed a tensile strength at break of 70.8 ± 0.7 MPa. This is a top end value among commercial polyester-based thermosets and previously described biobased thermos

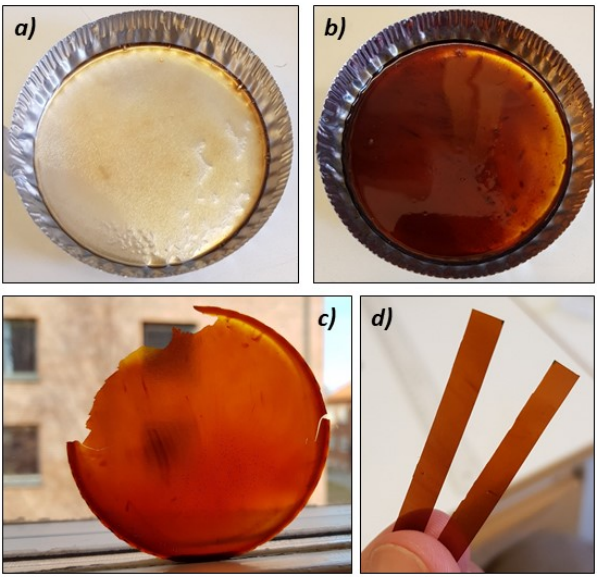

Figure 2. ***a)*** monomer/catalyst mixture after AcOEt overnight evaporation ***b)*** cured product ***c)*** cured film out of the mold ***d)*** stripes cut out of the cured film.

sets. The material proved to be extremely stiff, with a very low tensile strain (1.4 ± 0.2 %) and an extremely high Young's modulus (8.8 ± 0.2 GPa) probably due to the high aromatic content resulting from eugenol functionalization. **Table 2** reports these values (***a***) in comparison with those described for typical biobased thermosets.[6,17,32-34]

3.3.4 Microwave-assisted degradation of the thermoset

Due to the non-solubility of the thermoset materials it is generally difficult to prove their exact chemical structure.

Table 2. Comparison of the mechanical properties with previously reported biobased thermosets.

Thermoset	Young's Modulus (MPa)	Tensile strength at break (MPa)	Tensile strain (%)
a	8765±19	70.8 ± 0.7	1.4 ± 0.2
Itaconic acid-based[6]	398±6.6	15.0±3.0	6±1
PLA-based[17]	//	57.3±2.6	4.03±0.19
Natural triphenol-based[32]	//	80.0	2.68
Diphenolate ester-based[33]	1306±69	68.7±6.3	9.3±1.4
Cardanol-based[34]	//	73.2±1.4	10.7±0.3

In earlier work it was demonstrated that ester bonds in poly(3-hydroxybutyrate) can be effectively hydrolysed by microwave-assisted process.[31] The thermoset synthesized here was subjected to similar microwave-assisted process aiming to elucidate and shed light on its chemical structure. In addition, the degradability and potential recyclability of the thermosets to functional chemicals or intermediates for new material production is of high interest to move forward towards circular society and circular materials. Four different degradation tests were performed, respectively in water, methanol, alkaline water and alkaline methanol.

The microwave process in alkaline water and alkaline methanol resulted in complete degradation of the thermoset to water or methanol soluble products with no remaining solid residue. The thermoset degraded partially during the microwave-process in pure water or

methanol, but some non-degraded solid product remained. The alkaline solutions were acidified to pH 1 with sulphuric acid and extracted with AcOEt. After solvent evaporation the residues were characterized through ^{1}H NMR, MALDI-TOF and FT-IR.

3.3.5 ^{1}H NMR analysis of the degradation products from the microwave process.

The ^{1}H NMR spectrum for the degradation products after microwave processing in alkaline methanol was recorded (**Figure 3**). Even if an exhaustive interpretation of the spectrum was not possible given the complexity of the degradation mixture and hence of the signal patterns, the spectrum gives good indication of the occurred crosslinking and provides insights into the chemical structure of the thermoset.

First of all, both carboxylic –OH as well as alcoholic –OH signals can be detected at 12.5 and 5.5 ppm, respectively.

Free α-hydroxyl acid groups are therefore likely to be present after degradation. No signals for allyl groups are detectable, while signals are present in the high field aliphatic region (see expansions in **Figure 3**). The presence of olefinic proton singlets around the 6.2 ppm area

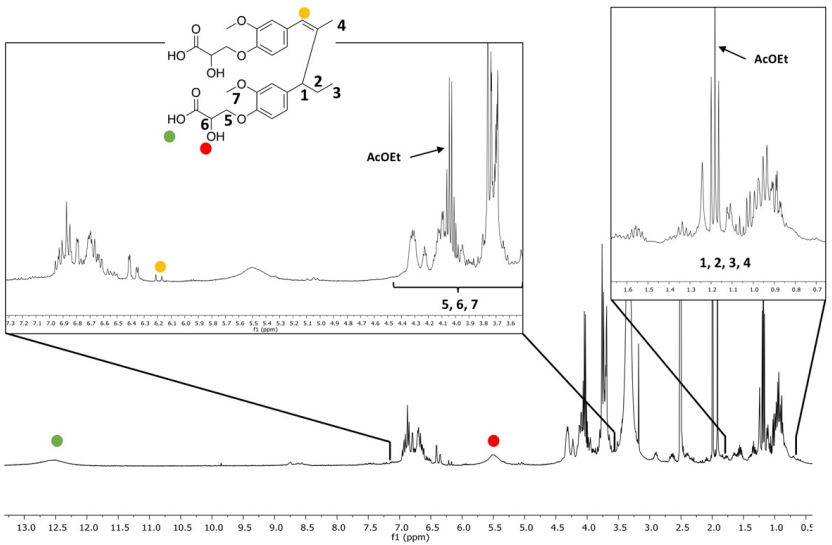

Figure 3. ^{1}H NMR spectrum of the degradation products after microwave processing in alkaline methanol with 0.5 % w/w NaOH/Methanol.

gives evidence for the actual occurrence of a reaction at the eugenol double bonds. In particular, a cationic polymerization mechanism can be hypothesized, starting from the protonation of the allylic double bond, to give the expected secondary carbocation, but also the rearranged benzylic one. Indeed, hydride shift is likely to take place in the reaction conditions, resulting in head-to-tail reaction, as the structure depicted in **Figure 3** illustrates. Termination through proton transfer then generates the terminal double bond. The ^{1}H NMR spectrum of the degradation products after microwave-assisted degradation in alkaline water does not show any significant differences with respect to the reported one. It is, however, reasonable to expect some methanolysis products after degradation in methanol. Signals relative to methyl esters or ethers would fall in the 3.5-4.5 ppm region, but the possible presence of these species cannot be safely disclosed.

3.3.6 MALDI-TOF analysis of the degradation products from the microwave process.

MALDI-TOF analysis confirmed extensive degradation by the exclusive appearance of compounds with very low overall molecular weights. The m/z value of the peaks with the highest intensity can be ascribed to dimer structures as those reported in **Figure 4**, confirming what was already hypothesised by NMR. Alongside this main series, the corresponding

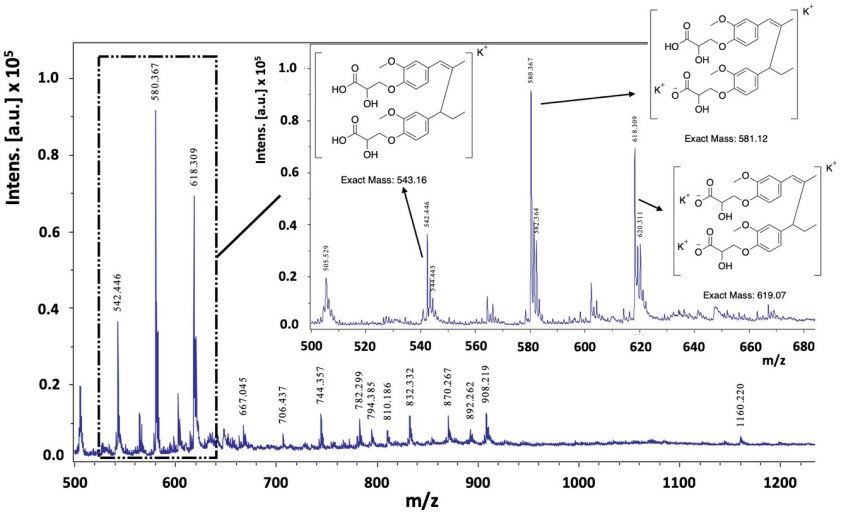

Figure 4. MALDI-TOF spectrum of degradation products after the microwave-assisted degradation in alkaline methanol.

trimers could be detected with m/z = 794, 832, 870 and 908, respectively. The formation of degradation products bearing free α-hydroxy acid groups supports the expected formation of polyester during the curing reaction, i.e., a structure that can be hydrolysed during the MW-assisted degradation. The crosslinking, likely occurring by the double bond polymerization, could lead to different C-C bonds, for instance through occurrence of allylic polymerization, affording degradation fragments that would fit with NMR and MALDI-TOF outputs. A possible structure for the thermoset is reported in **Figure 5**, taking into account all these reaction possibilities.

In order to fully demonstrate the reactivity of eugenol allyl moiety, a reaction of eugenol only in the same conditions was carried out. Also in this case the complete disappearance of double bonds is registered, with the formation of a great number of signals in the aliphatic region (^{1}H NMR spectrum of the obtained product is reported in Figure S7 and S8 in supporting information).

3.3.7 Analysis of the degradation products from the microwave process by *FT-IR*.

Further proof regarding the chemical structure of the thermoset came from FT-IR analyses. A comparison of the spectra for the monomer, the cured material and the degradation product is reported in **Figure 6**.

Both the thermoset and the degradation products showed a broad O-H stretching band, centred at 3440 cm^{-1}. In the case of the thermoset, it can be attributed to the presence of

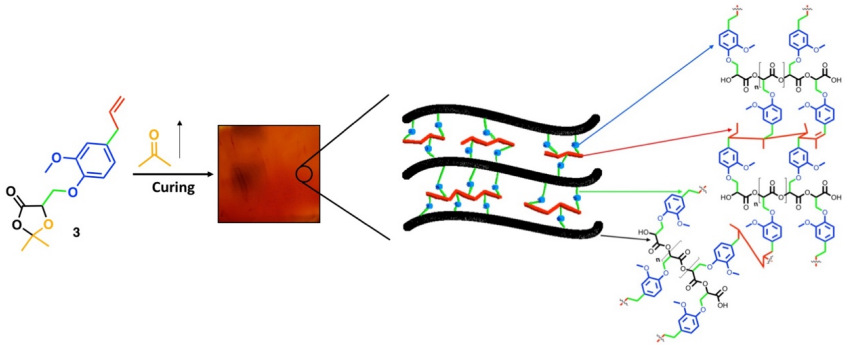

Figure 5. Proposed structure and schematic representation of the synthesized thermoset.

Figure 6. Comparison of the FTIR spectra of the monomer, thermoset and degradation products.

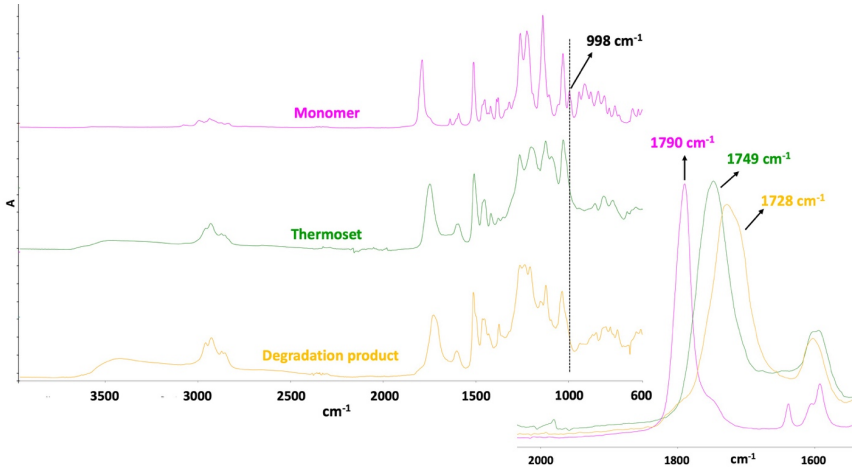

surface free hydroxyl and carboxyl groups. In the degradation product spectrum the same band is present, but with significantly greater intensity, due to the massive formation of free –OH and –COOH groups. In the 2000-1600 cm^{-1} region the shift of the C=O stretching peak gives confirmations about the reaction. While in the monomer it is sharp and centered at 1790 cm^{-1}, it shifts to 1749 cm^{-1} for the thermoset, confirming the formation of the polyester. Finally, after the degradation the carbonyl peak shifted further to 1728 cm^{-1}, as a result of the presence of carboxylic acid functional groups. In addition, in the monomer spectrum it is possible to highlight the peak relative to the terminal C-H bending for the allyl group at 1000 cm^{-1}. In both thermoset and degradation product spectra this peak cannot be detected, confirming the reaction of the double bond during the curing process.

3.3.8 Thermal Analyses

DSC analysis was performed in order to determine both the curing kinetics and the thermal properties of the thermoset. The curing reaction proceeded for 75 minutes after the temperature of 150 °C was reached. After 75 minutes a plateau region was observed indicating that the curing reaction was completed. DSC analysis was also run on the product cured in a mold, in order to determine its thermal behaviour. The related thermogram is reported

Figure 7. TGA curves showing the thermoset degradation in both nitrogen and oxygen atmosphere.

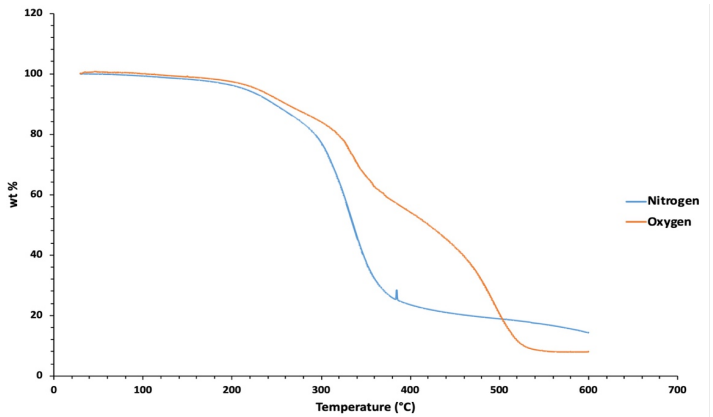

in SI file. The second heating scan shows a glass transition at 125 °C. Glass transition could also be detected during the cooling step. As expected and typical for thermosets, the material seemed completely amorphous and no melting peak was detected at least during heating up to 200 °C.

TGA curves relative to the degradations in both nitrogen and oxygen atmosphere are reported in **Figure 7**. Temperatures relative to 5 % weight loss ($T_{95\%}$), 50 % weight loss ($T_{50\%}$) as well as the weight residue at 600 °C are reported in **Table 3** for both experiments.

The two degradation curves have significantly different profiles. The TGA analysis run in nitrogen atmosphere shows a faster two-step weight loss at a relatively narrow temperature range, as well as a greater residue at the end of the analysis.

In the TGA analysis run in oxygen three-step degradation can be observed. Considering the 5 % weight loss as the beginning of the degradation, it can be argued that the thermoset showed higher thermal stability when the analysis was run in oxygen atmosphere. Furthermore, looking at $T_{50\%}$, a significant difference is present, with the thermoset losing 50 % of its mass at an 85 degrees higher temperature when the analysis was conducted in oxygen rather than in nitrogen atmosphere. The reason behind this behaviour could be found in the possible occurrence of oxygen-promoted reactions at high temperature. For instance, the possible formation of reactive species could lead to new crosslinking reactions, likely

resulting in a higher thermal resistance. This hypothesis seems reasonable also when looking at the degradation profiles, where the two first degradation steps seem to partially coinside irrespective whether the analysis was performed in nitrogen or oxygen atmosphere.

In both atmospheres, these two steps occur at very similar temperatures, namely at around 240 °C and 330 °C respectively. However, in relation to the weight loss observed, the second-step is much smaller when the degradation is performed in oxygen atmosphere. At the same time the process expands to somewhat higher temperature, which could indicate formation of more stable species during the degradation process. These species are finally degraded during the third step, occurring at 500 °C.

Gas	$T_{95\%}$ (°C)	$T_{50\%}$ (°C)	wt % residue at 600 °C
Nitrogen	213.9	335.6	14.2
Oxygen	227.3	420.6	8.0

Table 3. Degradation data from the thermogravimetric analysis in nitrogen and oxygen.

3.3.9 Shape memory and self-healing properties

Previous studies demonstrated that the presence of free surface carboxyl and hydroxyl functionalities can lead to shape memory and self-healing properties.[35,36] Therefore, the shape memory and self-healing properties of the synthesized thermoset were also evaluated.

First the thermoset was subjected to thermal treatment at 150°C. **Figure 8** shows how the planar and flexible thermoset film changed shape during the thermal treatment. The new shape was then retained when the material was cooled back to room temperature. However, when heated again the thermoset returned back to the original shape of planar film.

Finally, the self-healing capability of the thermoset was evaluated by scratching the surface and then subjecting the material to elevated temperature at 150°C to facilitate the chemical reactions leading to self-healing behaviour. **Figure 9** illustrates the scratched surface and the partially self-healed material after the thermal treatment. It can be observed that superficial scratches were repaired after 1 hour heating at 150 °C, while the deeper scratches partially remained.

Transesterification exchange reactions have been reported to bare the main responsibility for self-healing and shape memory properties of polyester-containing thermosets.[36]

Figure 8. Shape memory behaviour at high temperature.

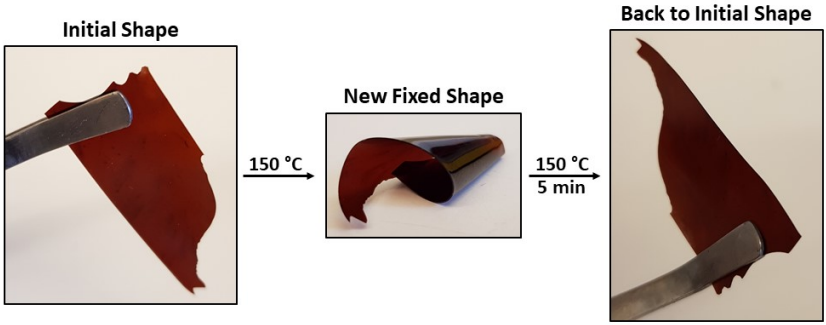

Due to the formation of potentially reversible links at high temperatures, the network structure can change while keeping the number of chemical bonds constant. Unlike many other polyester-based thermosets, the thermoset presented here can also benefit from the presence of short hydrocarbon segments or crosslinks that are stable at temperatures around 150°C. These non-affected bonds can give increased stability to the system and play a crucial role in the shape memory properties, helping the system to go back to the initial shape by acting as a stable frame. In addition, the greater flexibility of polyolefin structures with respect to the polyester backbone can allow easier structural rearrangement during the transesterification exchange reactions. On the other hand, the stability of these bonds and their inability to undergo transient reactions can restrict the self-healing properties.

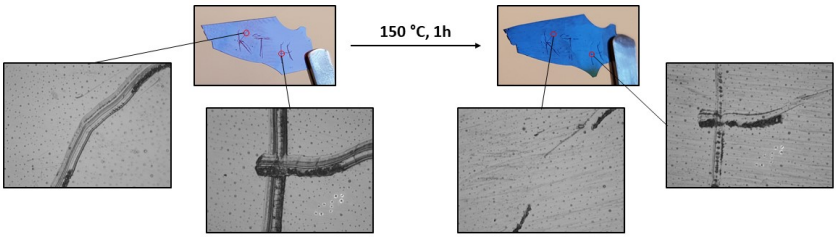

Figure 9. Self-healing properties tested by scratching the surface of the thermoset film followed by heating.

Figure 10: Schematic representation of possible mechanism behind the shape memory and self-healing capabilities.

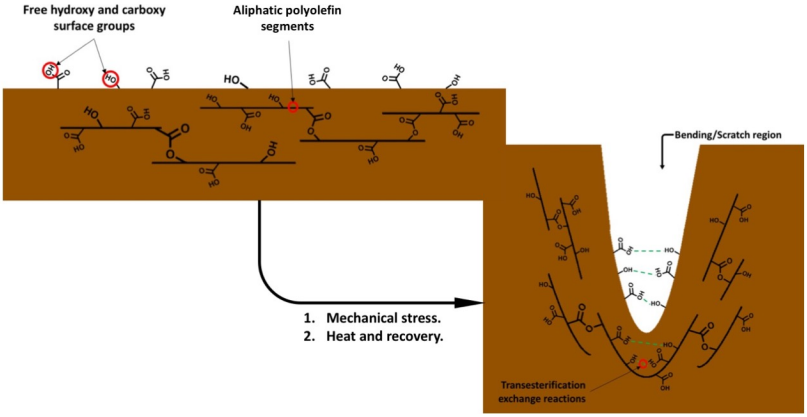

Figure 10 reports a schematic representation of the possible mechanism behind shape memory and self-healing properties of the prepared thermosets. Basically free hydroxy and carboxy surface groups can combine through transesterification exchange reactions at high temperatures, providing shape memory and self-healing capabilities. Aliphatic polyolefin segments can bend but not rearrange. This results in a tendency of the material to go back to the initial shape. At the same time it could hinder the recovery of deeper scratches, due to the reduced mobility given by both the aromatic rings and the shortness of these segments.

3.3.10 Antimicrobial testing

Given the well-known antimicrobial properties of eugenol,[37] as well as its successful incorporation in antimicrobial polymeric systems,[38] the antimicrobial activity of the thermoset was investigated. Antimicrobial activity against *E. coli* was tested, following the protocol reported in the experimental section. However, no significant inhibition was registered. The reason behind the loss of activity of eugenol once incorporated in the thermoset structure can be found in the loss of the allyl moiety after the crosslinking reaction. The allyl group is necessary for the interaction with microorganisms,[39] therefore its reaction inhibits its action.

4. Conclusion

The synthesis and characterization of innovative high-performance thermoset starting from renewable feedstocks was successfully demonstrated. Taking advantage of the emerging DOX polymerization chemistry, a tailored monomer functionalized by naturally occurring phenol, eugenol, was successfully synthesized. The monomer was further polymerized and cured in one-pot through the simultaneous polymerization of DOX and reaction through eugenol double bonds leading to crosslinked structure. The thermoset obtained proved to possess outstanding mechanical properties, and good thermal stability. Microwave-assisted hydrothermal degradation in alkaline water or methanol completely degraded the thermoset to water or methanol soluble low molecular weight products, showing recyclability back to functional intermediates. Structural investigation of the degradation products allowed envisioning the chemical structure of the thermoset indicating polylactide-like chains crosslinked with aromatic-aliphatic segments formed by reaction of the eugenol double bonds. The presence of free hydroxyl and carboxyl groups gives a plausible explanation to the disclosed shape memory and self-healing properties of the thermoset through transesterification.

References

1 Dumas, L.; Bonnaud, L.; Olivier, M.; Poorteman, M.; Dubois, P. Chavicol benzoxazine: Ultrahigh Tg biobased thermoset with tunable extended network. *Eur. Polym. J.* **2016**, (81), 337–346.

2 Namrata V. P.; Anil N. N. Nonedible Starch Based "Green" Thermoset Resin Obtained via Esterification Using a Green Catalyst. *ACS Sustainable Chem. Eng.* **2016**, 4, 1756−1764.

3 Wang, Z.; Yuan, L.; Ganewatta, M. S.; Lamm, M. E.; Rahman, M. A.; Wang, J.; Liu, S.; Tang, C. Plant Oil-Derived Epoxy Polymers toward Sustainable Biobased Thermosets. *Macromol. Rapid Commun.* **2017**, 38, 1700009.

4 Jahandideh, A.; Muthukumarappan, K. Synthesis, characterization and curing optimization of a biobased thermosetting resin from xylitol and lactic acid. *Eur. Polym. J.* **2016**, 83, 344–358.

5 Xu, Y.; Hua, G.; Hakkarainen, M.; Odelius, K. Isosorbide as Core Component for Tailoring Biobased Unsaturated Polyester Thermosets for a Wide Structure–Property Window. *Biomacromolecules* **2018**, 19, 3077-3085.

6 Barrett, D. G.; Merkel, T. J.; Luft, J. C.; Yousaf M. N. One-Step Syntheses of Photocurable Polyesters Based on a Renewable Resource. *Macromolecules* **2010**, 43, 9660–9667.

7 Ma, S.; Webster D. C.; Degradable thermosets based on labile bonds or linkages: A review. *Progr. Polym. Sci.* **2018**, 76, 65–110.

8 Buchwalter, S.L.; Kosbar, L. L. Cleavable epoxy resins: design for disassembly of a thermoset. *J. Polym. Sci. Part A Polym. Chem.* **1996**, 34, 249–260.

9 Harada, M.; Ando, J.; Yamaki, M.; Ochi, M. Synthesis, characterization, and mechanical properties of a novel terphenyl liquid crystalline epoxy resin. *J. Appl. Polym. Sci.* **2015**, 132, 41296.

10 Torpanyacharn, O.; Sukpuang, P.; Petchsuk, A.; Opaprakasit, P.; Opaprakasit, M. Curable precursors derived from chemical recycling of poly(ethylene terephthalate) and polylactic acid and physical properties of their thermosetting (co)polyesters. *Polym. Bull.* **2018**, 75, 395–414.

11 Sakai, R.; John, B.; Okamoto, M.; Seppala, J. V.; Vaithilingam, J.; Hussein, H.; Goodridge, R. Fabrication of Polylactide-Based Biodegradable Thermoset Scaffolds for Tissue Engineering Applications. *Macromol. Mater. Eng.* **2013**, 298, 45–52.

12 Zenkiewicz, M.; Malinowski, R.; Rytlewski, P.; Richert, A.; Sikorska, W.; Krasowska, K. Some composting and biodegradation effects of physically or chemically crosslinked poly(lactic acid). Polym. Test. 2012, 31, 83–92.

13 Tounthai, J.; Petchsuk, A.; Opaprakasit, P.; Opaprakasit M.; Curable polyester precursors from polylactic acid glycolyzed products. *Polym. Bull.* **2013**, 70, 2223–2238.

14 Datta, R.; Henry, M. Lactic acid: recent advances in products, processes and technologies – a review. J. Chem. Technol. *Biotechnol.* **2006**, 81, 1119–1129.

15 Albertsson, A.C.; Minna Hakkarainen, M. Designed to degrade. *Science* **2017**, 358 (6365), 872-873.

16 Jahandideh, A.; Muthukumarappan, K. Star-shaped lactic acid based systems and their thermosetting resins; synthesis, characterization, potential opportunities and drawbacks. *Eur. Polym. J.* **2017**, 87, 360–379.

17 Chang, S.; Zeng, C.; Lia, J.; Rena, J. Synthesis of polylactide-based thermoset resin and its curing kinetics. *Polym. Int.* **2012**, 61, 1492–1502.

18 Helminen, A.; Korhonen, H.; Seppala, J.V. Biodegradable crosslinked polymers based on triethoxysilane terminated polylactide oligomers. *Polymer* **2001**, 42, 3345-3353.

19 Meekum, U.; Kingchang, P. Peroxide/Silane Crosslinked Poly(lactic acid) Hybrid Biocomposite Reinforced with Empty Fruit Bunch and Cotton Fibers for Hot-Fill Food Packaging. *BioResources* **2017**, 12 (3), 5086-5101.

20 Thillaye du Boullay, O.; Marchal, E.; Martin-Vaca, B.; Cossio, F.P.; Bourissou, D. An Activated Equivalent of Lactide toward Organocatalytic Ring-Opening Polymerization. *J. Am. Chem. Soc.* **2006**, 128, 16442-16443.

21 Martin Vaca, B.; Bourissou, D. O-Carboxyanhydrides: Useful Tools for the Preparation of Well- Defined Functionalized Polyesters. *ACS Macro Lett.* **2015**, 4, 792−798.

22 Cairns, S.A.;Schultheiss, A.; Shaver, M.P. A broad scope of aliphatic polyesters prepared by elimination of small molecules from sustainable 1,3-dioxolan-4-ones. *Polym. Chem.* **2017**, 8, 2990–2996.

23 Martin, R.T.; Camargo, L.P.; Miller S.A. Marine-degradable polylactic acid. *Green Chem.* **2014**, 16, 1768-1773.

24 Almaroofa, A.; Niazib, S.A.; Rojoa, L.; Mannoccib, F.; Deba, S. Influence of a polymerizable eugenol derivative on the antibacterial activity and wettability of a resin composite for intracanal post cementation and core build-up restoration. *Dental Materials* **2016**, 32, 929–939.

25 Kaufman, T.S.; The Multiple Faces of Eugenol. A Versatile Starting Material and Building Block for Organic and Bio-Organic Synthesis and a Convenient Precursor Toward Bio-Based Fine Chemicals. *J. Braz. Chem. Soc.* **2015**, 26 (6), 1055-1085.

26 Liu, T.; Hao, C.; Wang, L.; Li, Y.; Liu, W.; Xin, J.; Zhang, J. Eugenol-Derived Biobased Epoxy: Shape Memory, Repairing, and Recyclability. *Macromolecules* **2017**, 50, 8588−8597.

27 Zhang, Y.; Li, Y.; Thakur, V.K.; Gao, Z.; Gua J.; Kessler, M.R. High-performance thermosets with tailored

28 properties derived from methacrylated eugenol and epoxy-based vinyl ester. *Polym. Int.* **2018**, 67, 544–549.

29 Faye, I.; Decostanzi, M.; Ecochard, Y.; Caillol, S. Eugenol bio-based epoxy thermosets: from cloves to applied materials. *Green Chem.* **2017**, 19, 5236–5242.

30 Zhang, X.; Dai, Y. A Functionalized Cyclic Lactide Monomer for Synthesis of Water-Soluble Poly(Lactic Acid) and Amphiphilic Diblock Poly(Lactic Acid). *Macromol. Rapid Commun.* **2017**, 38, 1600593.

31 Bredikhina, Z.A.; Pashagin, A.V.; Kurenkov, A.V.; Bredikhin, A.A. Synthesis of Enantiomerically Pure 3-Aryloxy-2-hydroxy- propanoic Acids, Intermediate Products in the Synthesis of cis-4-Aminochroman-3-ols. *Russ. J. Org. Chem.* **2014**, 50, 535–539.

32 Yang, X.; Odelius, K.; Hakkarainen, M. Microwave-Assisted Reaction in Green Solvents Recycles PHB to Functional Chemicals. *ACS Sustainable Chem. Eng.* **2014**, 2, 2198−2203.

33 Zhao, S.; Huang, X.; Whelton, A.J.; Mahdi M. Abu-Omar, M.M. Renewable Epoxy Thermosets from Fully Lignin-Derived Triphenols. *ACS Sustainable Chem. Eng.* **2018**, 6 (6), 7600–7608.

34 McMaster, M.S.; Yilmaz, T.E.; Patel, A.; Maiorana, A.; Manas-Zloczower, I.; Gross, R.; Singer, K.D. Dielectric Properties of Bio-Based Diphenolate Ester Epoxies. ACS Appl. Mater. *Interfaces* **2018**, 10, 13924−13930.

35 Ma, Z.; Liao, B.; Wang, K.; Dai, Y.; Huanga, J.; Pang, H. Synthesis, curing kinetics, mechanical and thermal properties of novel cardanol-based curing agents with thiourea. *RSC Adv.* **2016**, 6, 105744.

36 Berg, G.J.; McBride, M.K.; Wang, C.; Bowman, C.N. New directions in the chemistry of shape memory polymers. Polymer 2014, 55, 5849-5872.

37 Montarnal, D.; Capelot, M.; Tournilhac, F.; Leibler, L. Silica-Like Malleable Materials from Permanent Organic Networks. *Science* **2011**, 334 (6058), 965-968.

38 Phanida, P.; Pattamapan, L.; Mullika T. C.; Nuntavan, B. Antibacterial activity of essential oils and their active components from Thai spices against foodborne pathogens. *ScienceAsia* **2013**, 39, 472–476.

39 Rojoa, L.; Vàzquez, B.; San Romàn, J.; Debb, S. *Dental Materials* **2008**, 24, 1709–1716.

40 Hu, Q.; Zhou, M.; Wei, S. *Journal of Food Science* **2018**, 83 (6), 1476-1483.

Supporting Information

One-pot synthesis of sustainable high-performance thermoset by exploiting eugenol functionalized 1,3-dioxolan-4-one

NMR Characterization

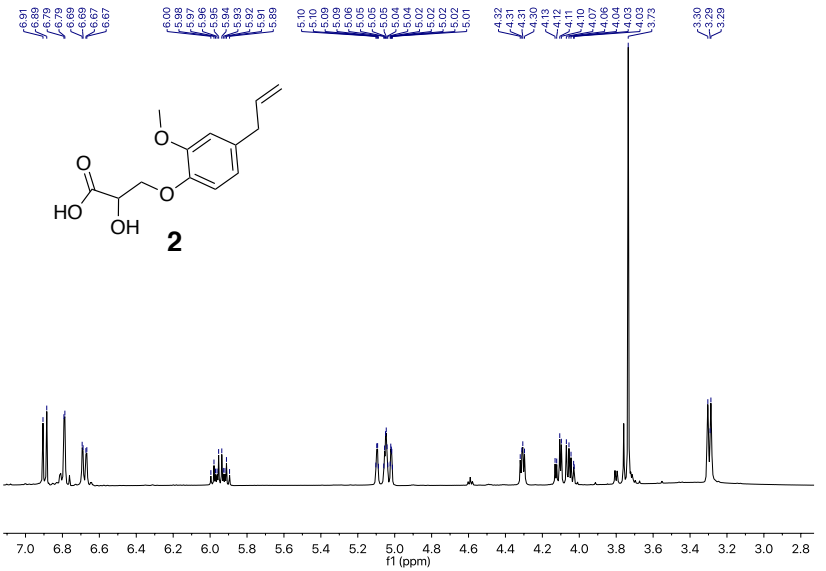

Figure S1. ^{1}H NMR spectrum of **2**.

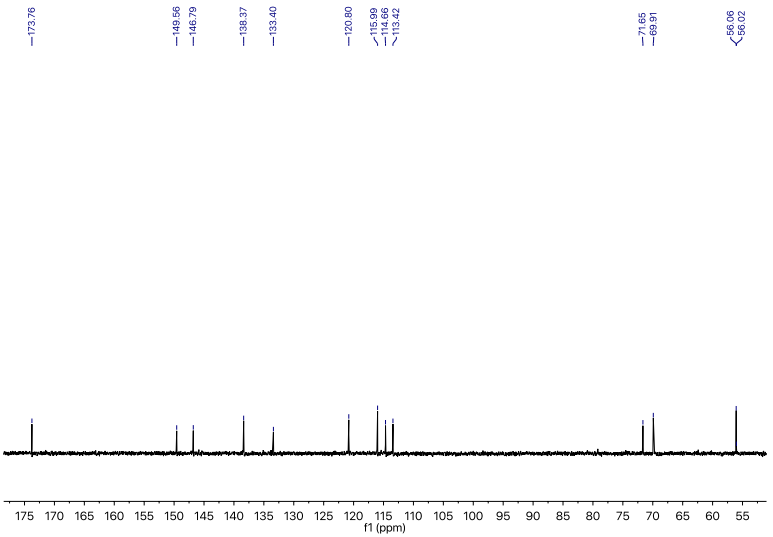

Figure S2. ^{13}C NMR spectrum of **2**.

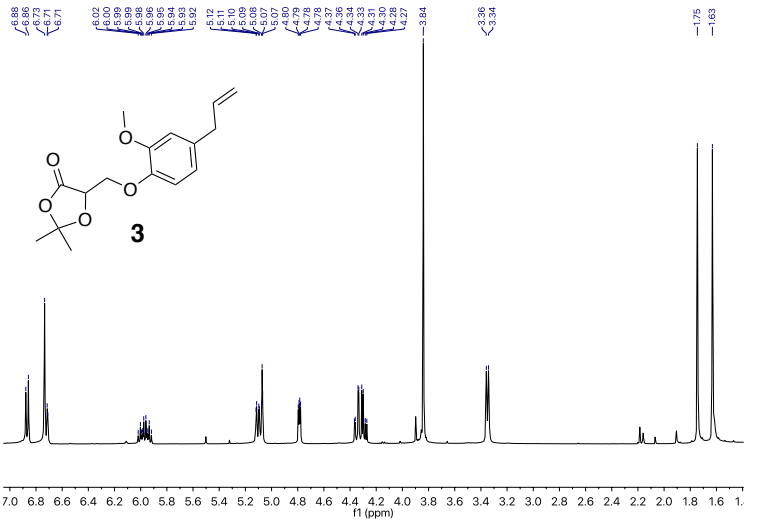

Figure S3. ^{1}H NMR spectrum of **3**.

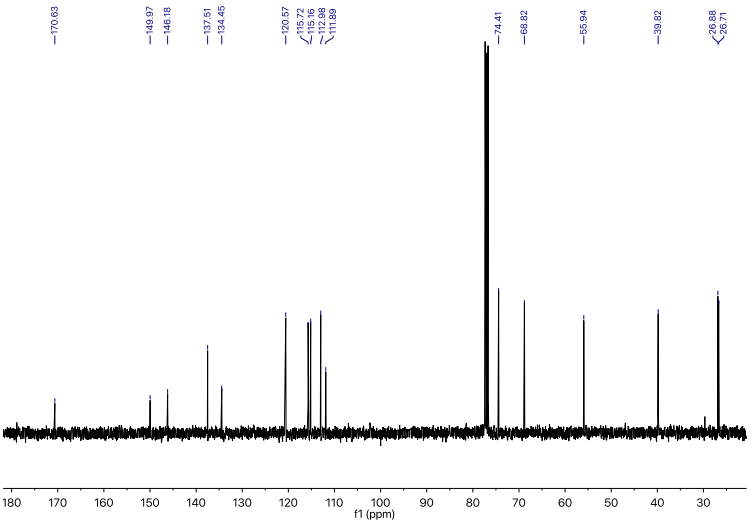

Figure S4. ^{13}C NMR spectrum of **3.**

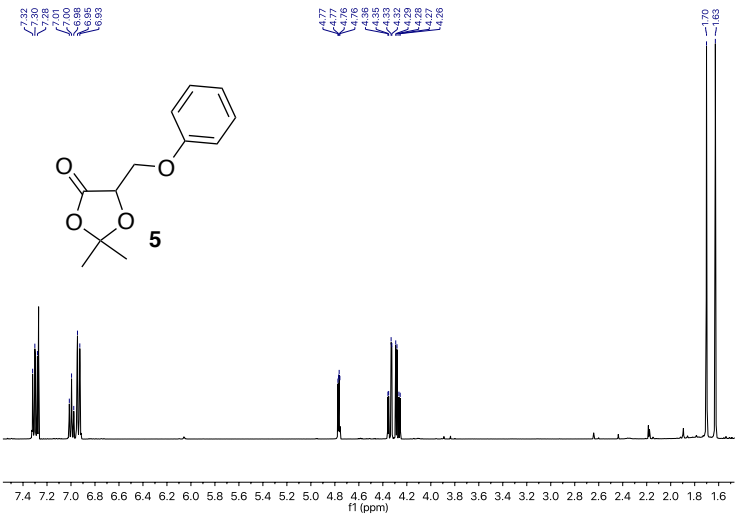

Figure S5. ^{1}H NMR spectrum of ***5***.

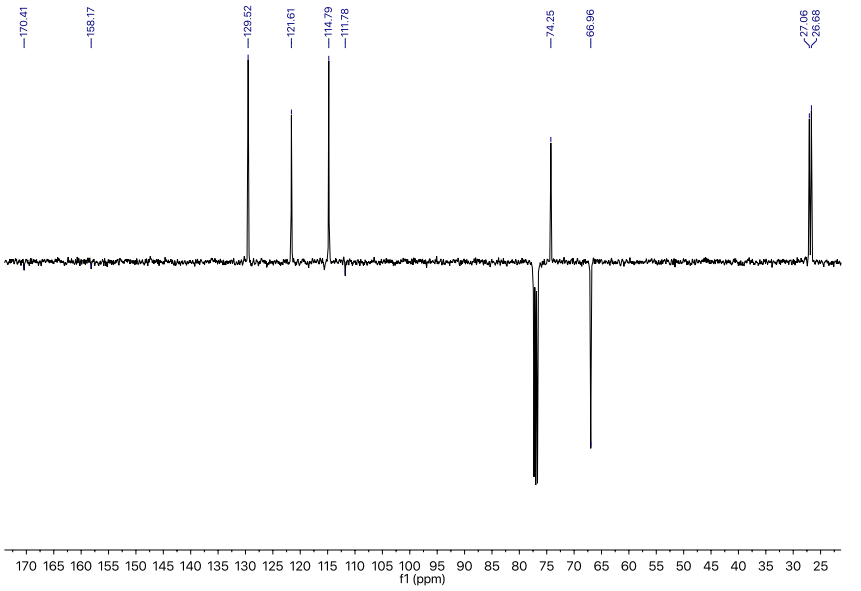

Figure S6. ^{13}C NMR spectrum of ***5***.

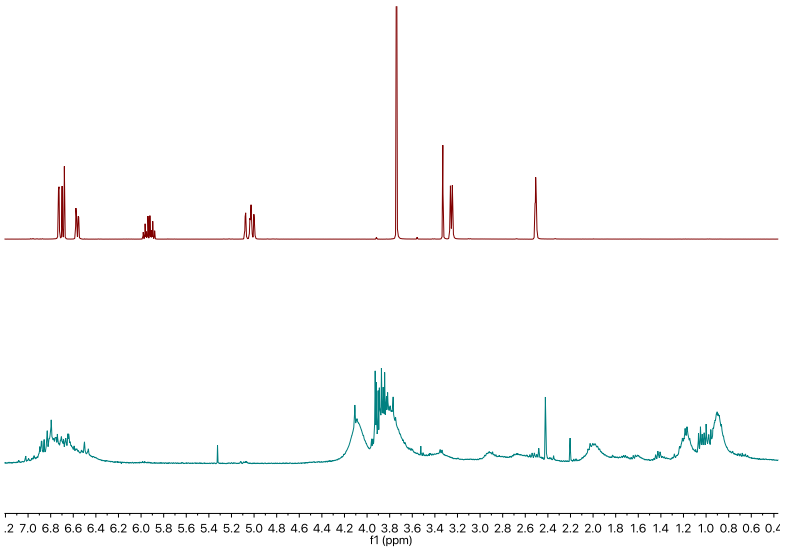

Figure S7. Comparison between ^{1}H NMR spectrum of eugenol (Top) and eugenol treated at 150 °C for 3 h with 5 mol % p-TSA catalysis (Bottom).

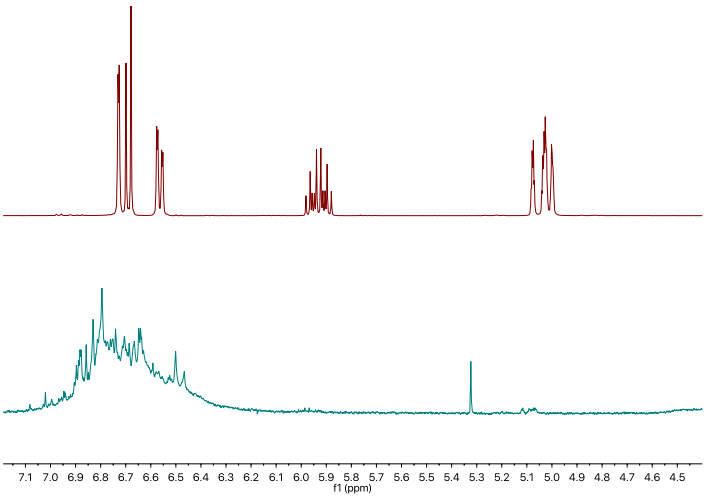

Figure S8. Magnification of the spectra reported in **Figure SI 7** in the olefin region**.**

DSC Characterization

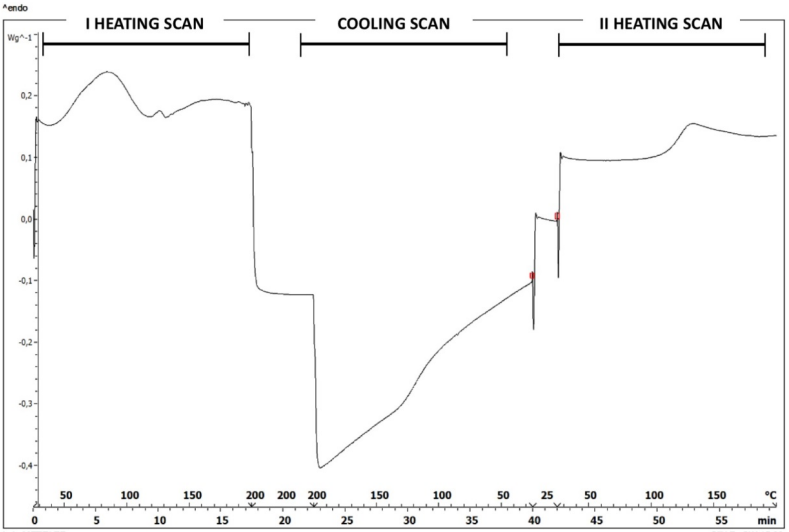

Figure S9: DSC thermogram for the thermoset.

General conclusions and future developments

The work that has been here presented found its origin in the expertise of my research group, namely the synthesis and characterization of polymers as well as the organic chemistry of natural and bioactive compounds. The merging of these two distinct worlds appeared, since the first results came to hand, as a powerful tool for the development of new products and materials.

The world of bioplastics and related research are living a true golden age whose limits are still far from to be reached. In particular, giving its promising properties, PLA stands well ahead of other known biopolymers. Clearly, its proper optimization for a true and wide industrial application hasn't been found yet, also because of its relatively recent discovery. For this reason, PLA-related research is commonly aimed at the improvement of material properties. As already discussed in the introductory section, a lot of different methodologies have been developed through years. Alongside the more industrially-driven solutions such as blending and compounding, chemically-sound strategies are much less investigated, given the inherently scarce monomer scope and functionalization possibilities.

Given these premises, the goal of this PhD thesis, namely the development of novel chemical approaches for PLA improvement, appeared challenging, yet promising. From one side, the preparation of cellulose-containing bionanocomposites showed great potentialities, resulting in materials with better properties with respect to standard polylactic acid. Moreover, the optimization of the *in situ* synthetic approach proved its effectiveness for the optimal dispersion of the nanofiller within the matrix.

On the other hand, novel synthetic methodologies towards new, highly functionalized polyester-based materials were investigated. Exploitation of O-Carboxyanhydrides chemistry, together with the introduction of natural products, allowed to obtain inherently antimicrobial polymers. Finally, pioneering studies on 1,3-dioxolane-4-ones as monomers resulted in the development of new metal-free polymerization conditions as well as new top-performing thermosets.

Results here presented were driven by the desire to find new routes and approaches in a continuously expanding field. For this reason, every chapter presents a different work that can be considered both as "standalone" as well as part of a wider research effort. Indeed, the strong interconnection existing between all projects has to be considered as a stimulus for future investigations and optimizations. In particular, the combination of different approaches will be deepened, for example through *in situ* synthesis of bionanocomposites exploiting OCAs or DOX chemistry. At the same time, the hope is that the reported academic achievements can open the path towards the development of focused applications, with the final aim of their industrial exploitation.